# Theoretical insights into oxygen defects on transition metal and rare earth oxide surfaces

M. Verónica Ganduglia-Pirovano

Institute of Catalysis and Petrochemistry, CSIC, Madrid, Spain

# Defects in bulk crystals

**No crystal of significance size is perfect !**

Types of Imperfections

| | | |
|---|---|---|
| ▪ 0D | Point Defect | Vacancies; Interstitials; Substitution |
| ▪ 1D | Line Defect | Dislocation |
| ▪ 2D | Planar Defect | Surface; Grain Boundary; Stacking Fault |

Point Defect

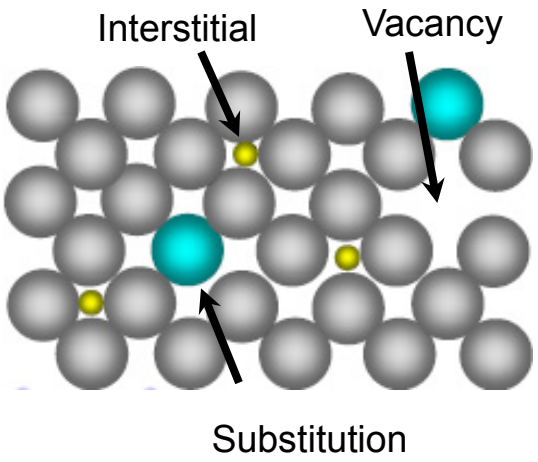


Line Defect

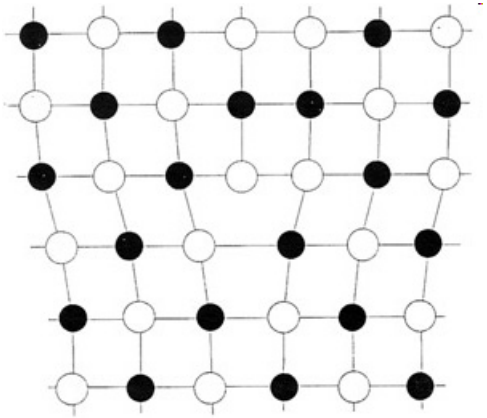

Planar Defect

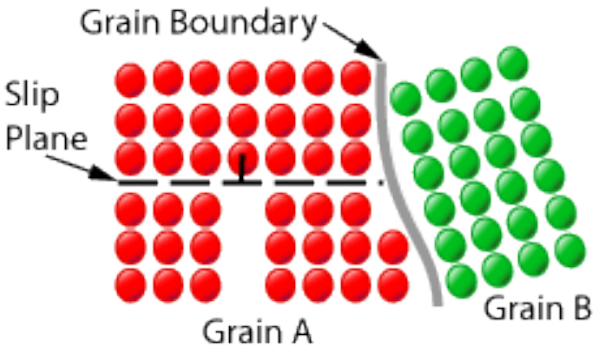

# Defects on surfaces: The example of NiO(111)

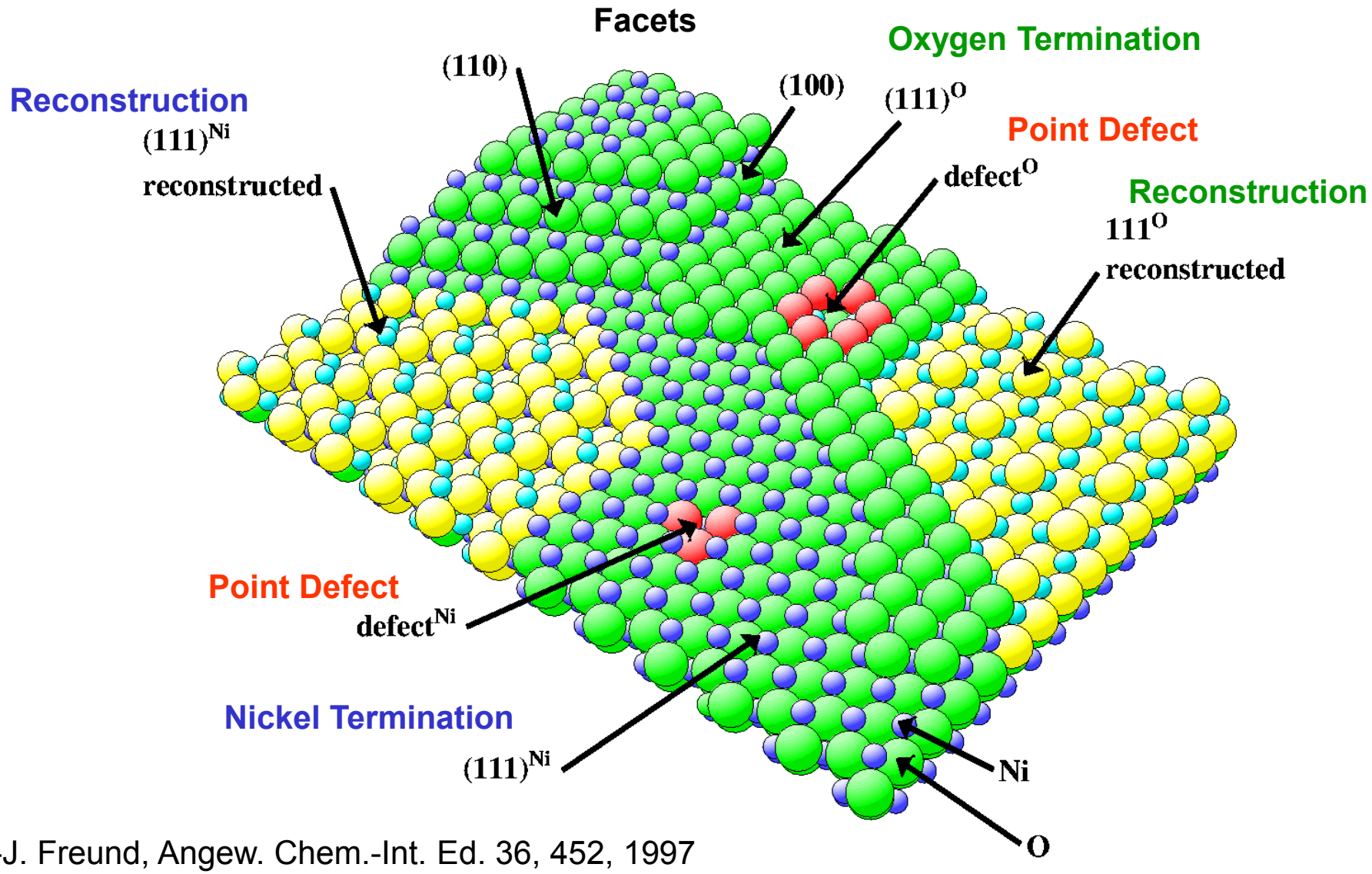


H.-J. Freund, Angew. Chem.-Int. Ed. 36, 452, 1997

# Defects in bulk and on surfaces of transition metal and rare earth oxides

Defects are always present in a real crystals due to thermodynamic reasons!

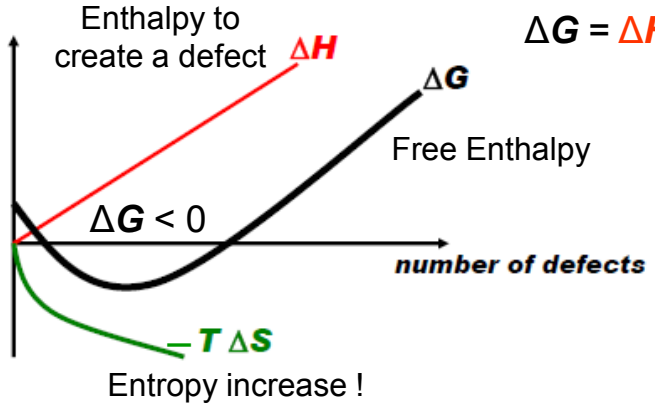


$\Delta G = \Delta H - T\Delta S$

Non-stoichiometry is common amongst transition metal and rare-earth compounds
e.g., $Fe_xO$ where $0.957 > x > 0.833$

Oxygen vacancies can be produced by

– irradiation of the sample
– thermal annealing

# The « beauty » of imperfection

Adding atoms to a semiconductor can improve its electronic properties. In an oxide, taking atoms away can have a similar electronic effect — one that could, it seems, be exploited in device applications.

Jochen Mannhart and Darrell G. Schlom, Nature **430**, 620 (2004)

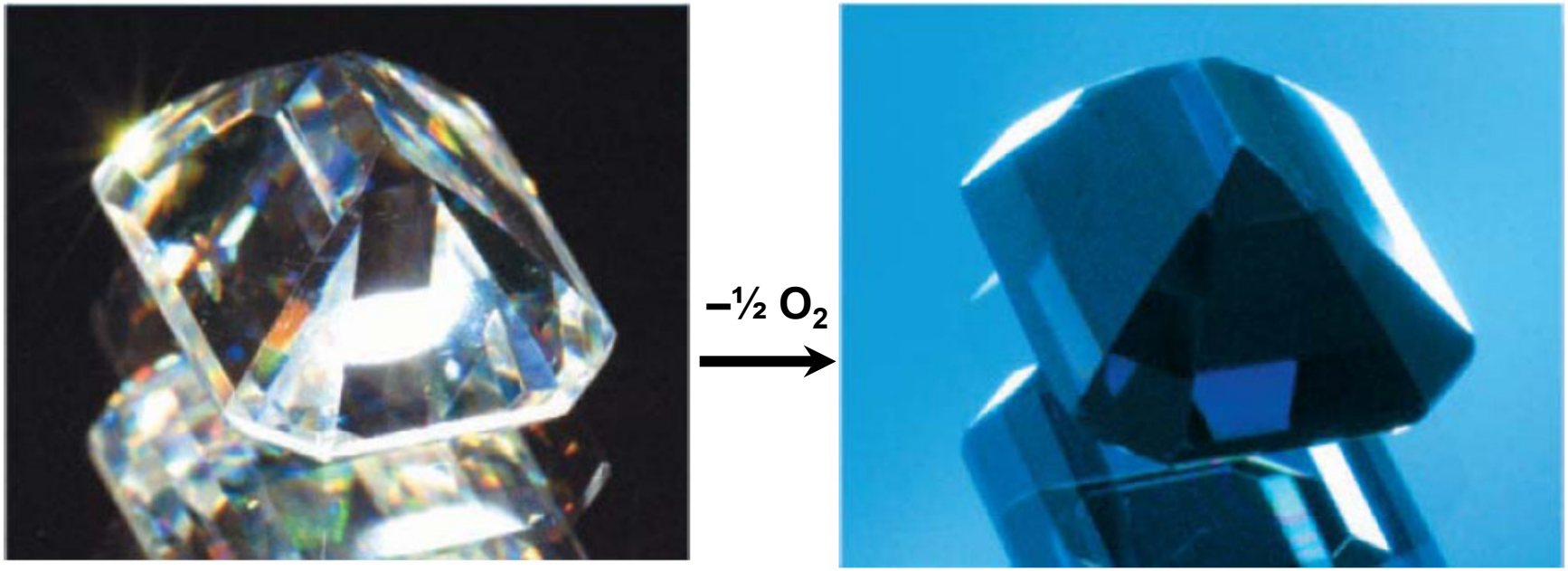


Figure 1 Now you see it, now you don't. These micrographs of a $SrTiO_3$ crystal show the effect of removing oxygen atoms, leaving vacancies in the crystal lattice: the glistening oxidized gem is transformed into a dull blue, conductive crystal .

# Scanning Tunneling Microscopy/Spectroscopy (STM/STS)

- Tunneling current between tip and sample

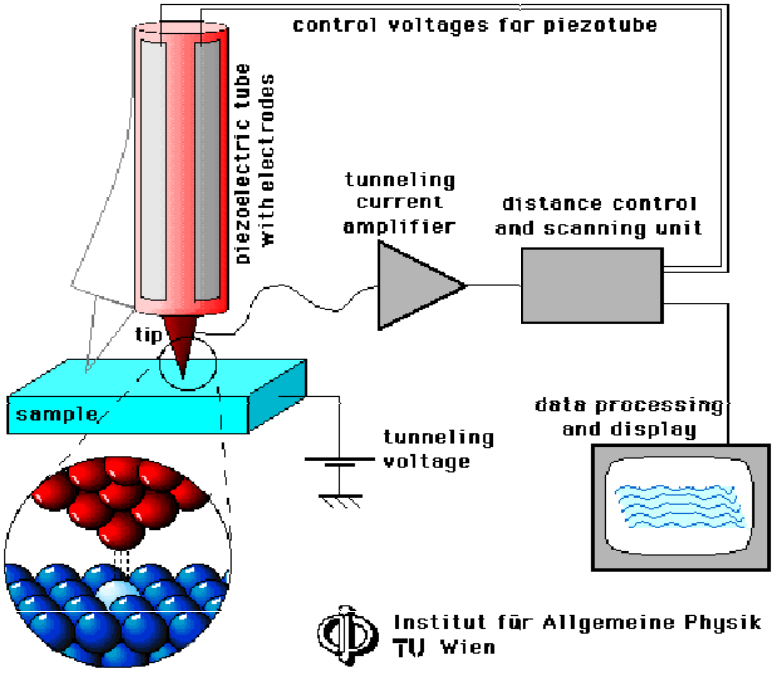


$$I \sim (V/s)\ \exp(-A\sqrt{\phi}\, z)$$

$\phi$.... Workfunction, typically 3-5 eV

z ... Tip-sample separation, 4-10 Å

Scanning mode → 2D atomic resolution images

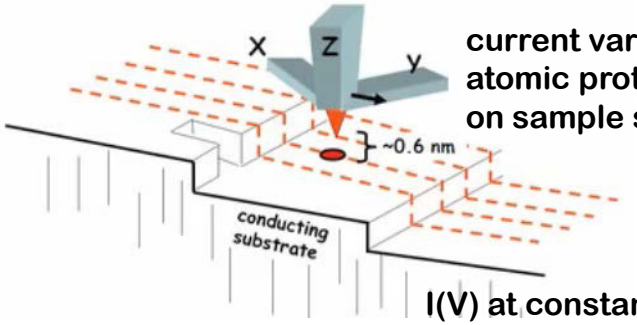


current varies as one scans atomic protuberances on sample surface

I(V) at constant z or variable z

In constant current mode uses feedback loop to control a voltage applied to piezo-scanner in order to continuously adjust the tip height, so that tunneling current is maintained→„topographic“ image

Mind: imaging of local electron density of states with atomic resolution

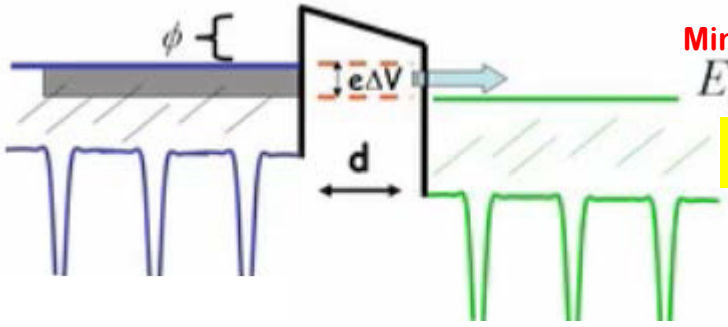


$$I \sim e\,\Delta V\, \rho(E_F - eV)\, e^{-2\alpha d}$$

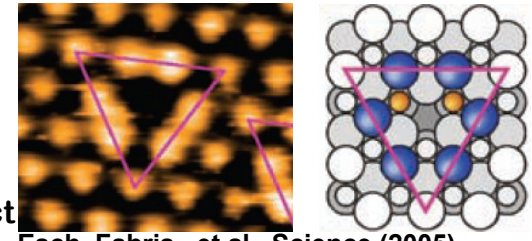

$CeO_2(111)$: surface O defect

Esch, Fabris, et al., Science (2005)

# Scanning Tunneling Microscopy/Spectroscopy (STM/STS)

**Spectroscopy mode → I–V profiling at specific sites (LDOS)**

$$I \sim e\,V\,\rho(E_F - eV)\,e^{-2\alpha d}$$

**probe V-dependent filled and empty states at each (x,y) point**

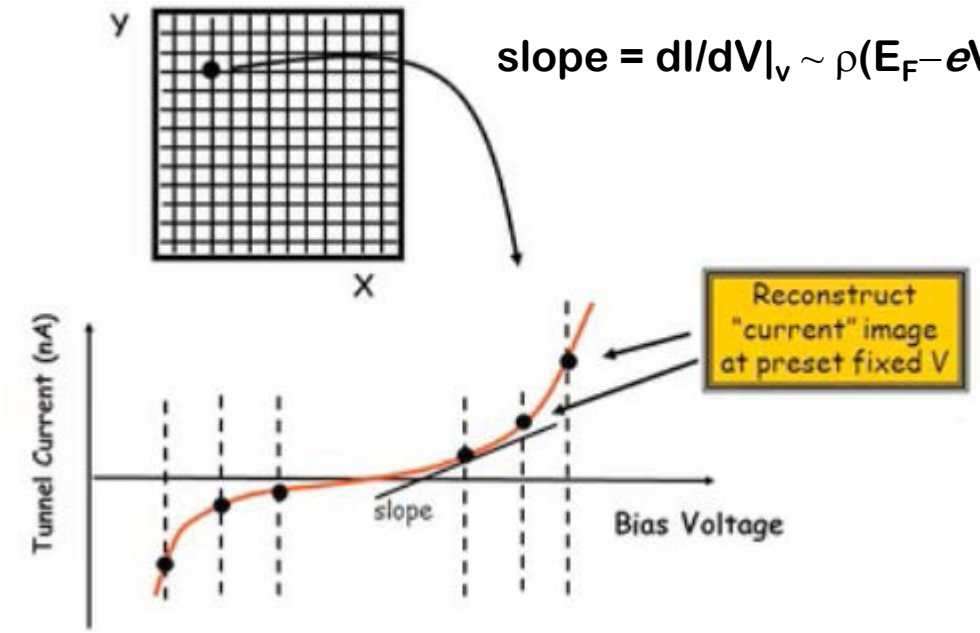


**slope = $dI/dV|_V \sim \rho(E_F - eV)$ → LDOS at each point of substrate**

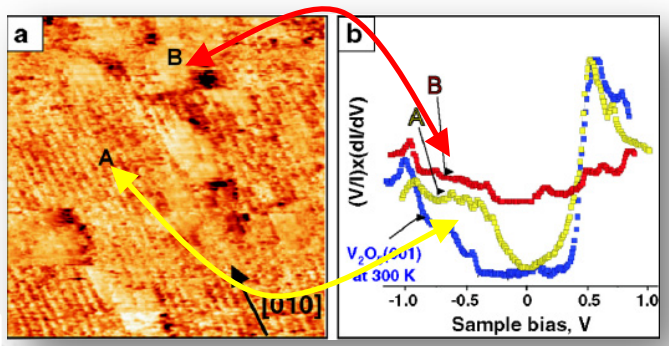


Blum, Niehus, Hucho, Fortrie, Ganduglia Pirovano, Sauer, Shaikhutdinov, Freund, PRL99, 226103 (2007)

# The « beauty » of imperfection at surfaces

Defects at surfaces such as steps, kinks, and edges, as well as point defects usually have much higher reactivity toward adsorbates relative to flat terraces.

## NO dissociation at Ru steps

**STM 0.5 hour after exposure to 0.3 L of NO**

T.Zambelli, J. Wintterlin, J. Trost, G. Ertl,
Science 273273, 1688 (1996)

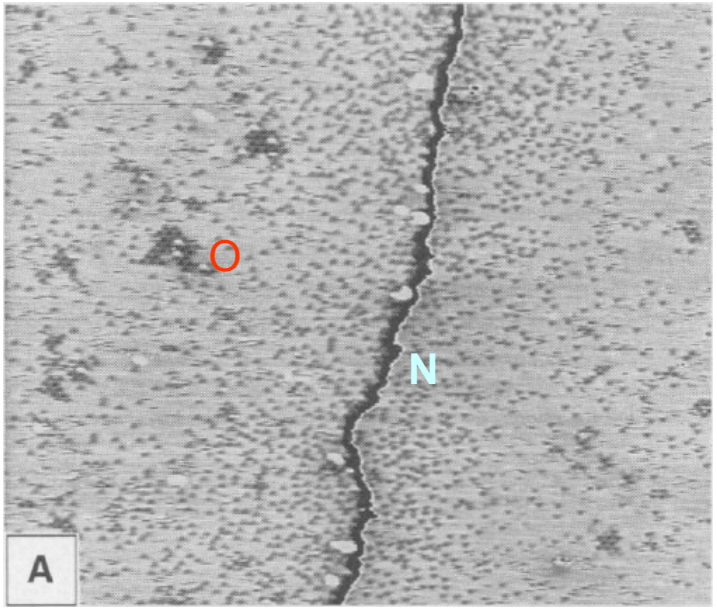


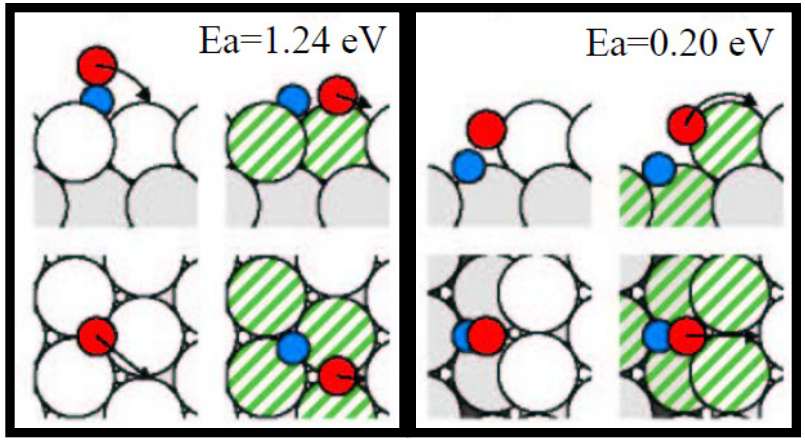


## N–O bond activation at Ru steps

B. Hammer, Phys. Rev. Lett. 83, 3681 (1999)

# Reducible oxides in catalysis: Titania

## $TiO_2$ supported Au clusters: Defects as anchors

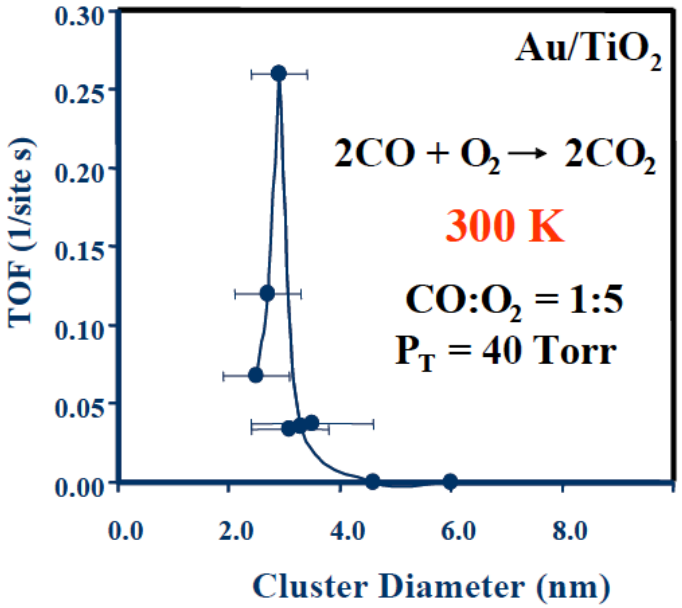


M. Haruta, Catal. Today. 36, 153 (1997)

Important factors in promoting the activation of adsorbed species:

- cluster perimeter
- cluster size
- charge of the Au cluster
- special site (defect) on the oxide support

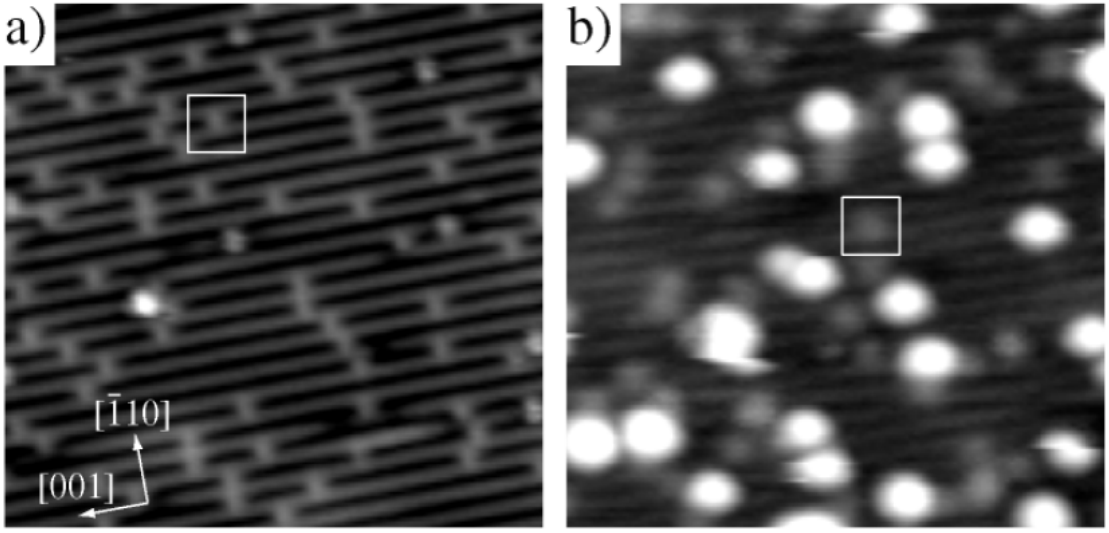


E. Wahlström et al., Phys. Rev. Lett.. 90, 026101 (2003)

$TiO_2(110)$

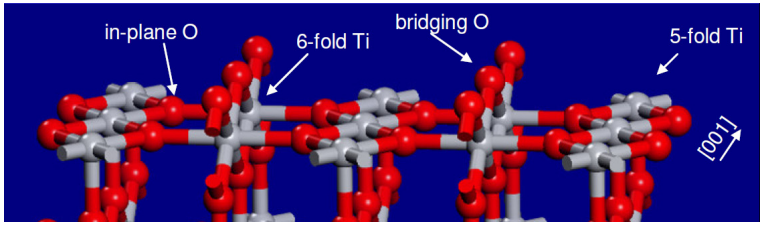

# Reducible oxides in catalysis: Ceria

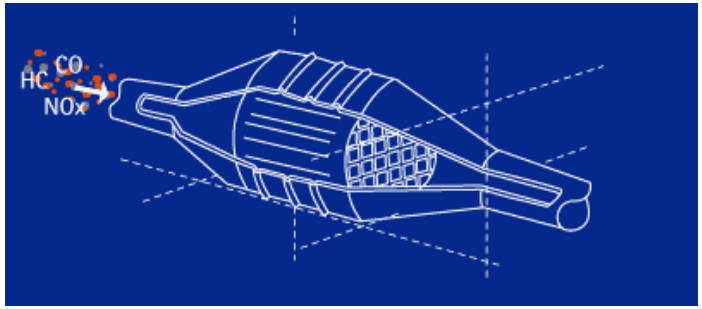


http://www.rhodia-ec.com/site_ec_us/catalysis/index_automotive.htm

## Catalyst formulation

- precious metals Pt, Rh, Pd → active phase
- alumina → support
- Zr-doped ceria → oxygen storage capacity (OSC)
- $ZrO_2$ → enhances OSC, thermal stability

## Catalytic converter

transforms the primary pollutants in the exhaust gas into non-toxic less harmful compounds

$$2NO_x \rightarrow xO_2 + N_2$$
$$2CO + O_2 \rightarrow 2CO_2$$
$$2C_xH_y + (2x+y/2)O_2 \rightarrow 2xCO_2 + yH_2O$$

$CO_2$ is a pollutant as a greenhouse gas

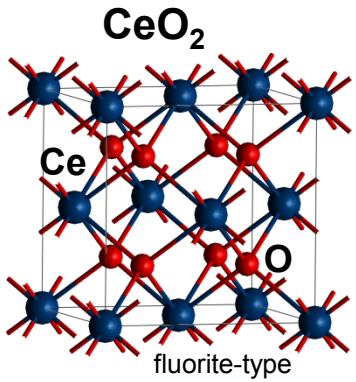


fluorite-type

### Oxygen Storage Capacity

an 'oxygen-sponge'

releasing and absorbing oxygen according to the catalytic reaction required (oxidation or reduction)

$$Ce^{4+} \leftrightarrow Ce^{3+}$$

**$CeO_2$ supported metal and oxide catalysts are singled out as very promising for various reactions; ceria can supply its lattice oxygen**

# Reducible oxides in catalysis: Vanadia

- large variety of oxidation states:

  $V_2O_5$ (5+), $VO_2$ (4+), $V_2O_3$ (3+), $VO$ (2+)

$V^{2+}$ $V^{3+}$ $V^{4+}$ $V^{5+}$

- active and selective in oxidation reactions:

  -$SO_2$ to $SO_3$ in the production of sulfuric acid
  -benzene to maleic anhydride (polyester resins)
  -Selective oxidative dehydrogenation alkanes to alkenes

**Mars-van Krevelen redox mechanism**

e.g., $C_3H_8 + [V^{5+}O] \longrightarrow C_3H_7 + [V^{4+}OH] \xrightarrow[-C_3H_6]{} [V^{3+}]\cdots H_2O \xrightarrow[-H_2O]{} [V^{3+}]$

**lattice oxygen participation**

**The surface reducibility is key to their function**

# Oxygen defects on transition metal and rare earth oxide surfaces: Questions

- Defect structure?

  Structure relaxation?

Atomic Force Microscopy (AFM)

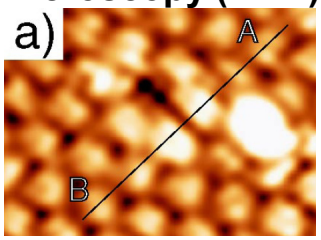


Torbrügge et al., PRL (2007)

Scanning Tunneling Microscopy (STM)

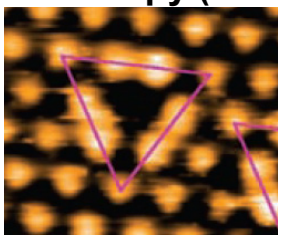

Esch, Fabris, et al., Science (2005)

Oxygen

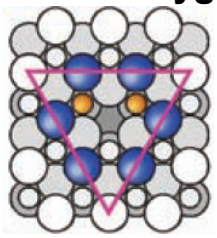


**$CeO_2$(111): surface O defect**

- Electronic stucture?

  Which states do the „left" electrons populate?

  Interplay between defects, localization, and structure relaxation

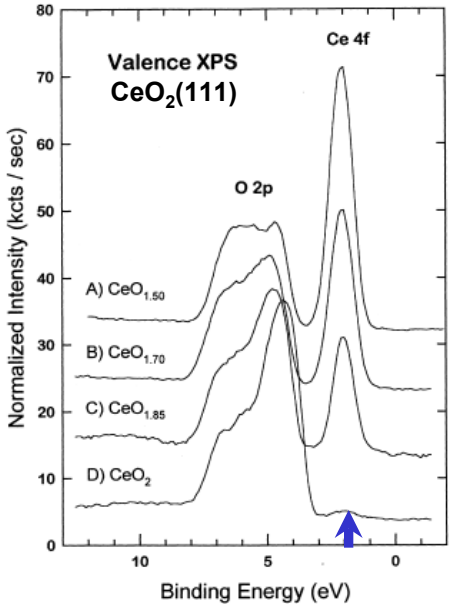


D. R. Mullins et al., Surf. Sci. (1999)

- Energy cost?

$$\frac{N_s}{N} = \exp\left(\frac{-W}{kT}\right)$$

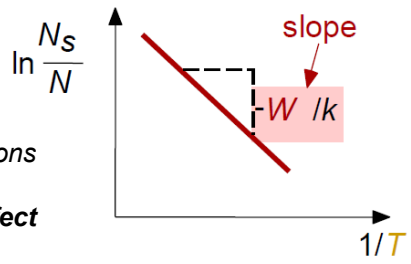


$N_s$: defect number under *equilibrium conditions*
$N$: number of lattice positions
***W*: energy difference of defect vs. no defect**
*k: Boltzmann constant; T: temperature*

# Oxygen defects on transition metal and rare earth oxide surfaces: Questions

Notwithstanding the experimental progress, a full picture which includes

- the effect on the electronic structure,
- the fate of the left electrons,
- the defect induced structure relaxation
- the defect formation energy

would still remain, in most cases, an elusive goal without the support from theory

⇩

Computer modelling

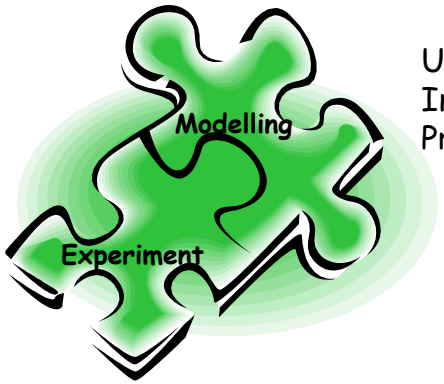


Understanding
Insight
Prediction

# Theoretical Modelling

## Surface models

**Periodic approach:** supercell or slab geometry

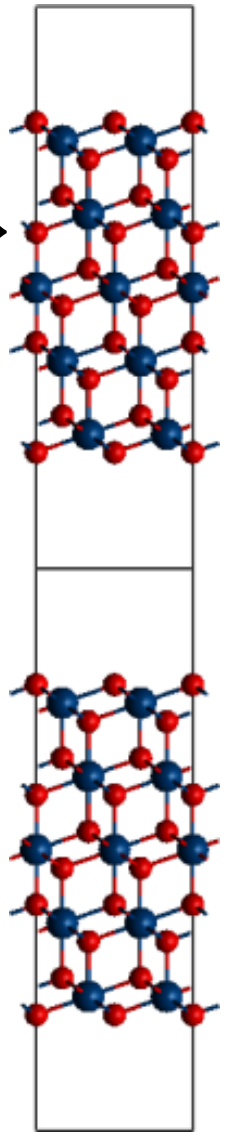

(2×2) $CeO_2$(111)

## Methods

**Density Functional Theory** DFT

W. Kohn

Chemistry Nobel Prize 1998

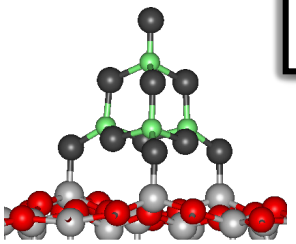

# The 3 minutes Density Functional Theory gist

$$H = \sum_{i=1}^{N_e}\left[-\frac{\hbar}{2m_e}\nabla_i^2 + V_N(\mathbf{r}_i)\right] + \frac{1}{2}\sum_{\substack{i,j=1 \\ i\neq j}}^{N_e}\frac{e^2}{|\mathbf{r}_i-\mathbf{r}_j|}$$

$$V_N \leftrightarrow n_0$$

$$E_0[n_0] = \min_{\Psi\to n_0}\langle\Psi|H|\Psi\rangle$$

**Hohenberg-Kohn '64**

**Kohn-Sham DFT '65**

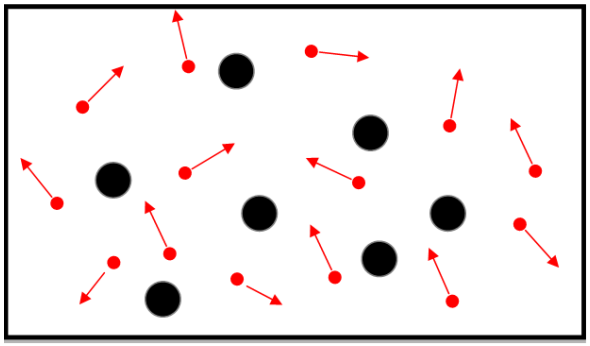

Interacting particles in real potential

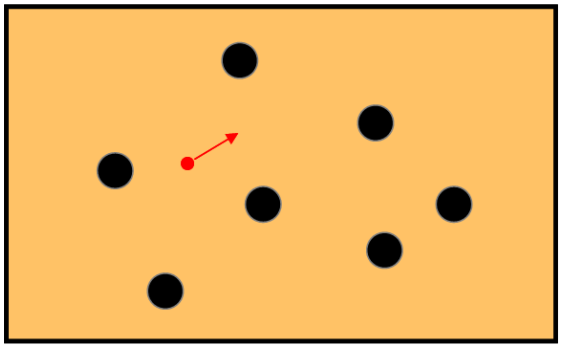

Non-interacting fictitious particles in effective potential

$$\Psi(\mathbf{r}_1,\ldots,\mathbf{r}_N) \rightarrow |\varphi_1(\mathbf{r}_1)\varphi_2(\mathbf{r}_2)\ldots\varphi_N(\mathbf{r}_N)|$$

**Variational Principle**

$$n(\mathbf{r}) \equiv n_s(\mathbf{r}) = \sum_{i=1}^{N_e}|\varphi_i(\mathbf{r})|^2$$

$$V_H(\mathbf{r}) = \int d^3\mathbf{r}'\frac{e^2\, n(\mathbf{r}')}{|\mathbf{r}-\mathbf{r}'|}$$

**Hartree**

$$\left[-\frac{\hbar}{2m_e}\nabla_i^2 + V_N(\mathbf{r}) + V_H(\mathbf{r}) + V_{XC}(\mathbf{r})\right]\varphi_i(\mathbf{r}) = \varepsilon_i\,\varphi_i(\mathbf{r})$$

**KS equations**

**DFT-KS is exact!!**

# DFT: The approximated $E_{xc}[n]$ functional

**The Local Density Approximation (LDA):** The „mother“ of all approximations

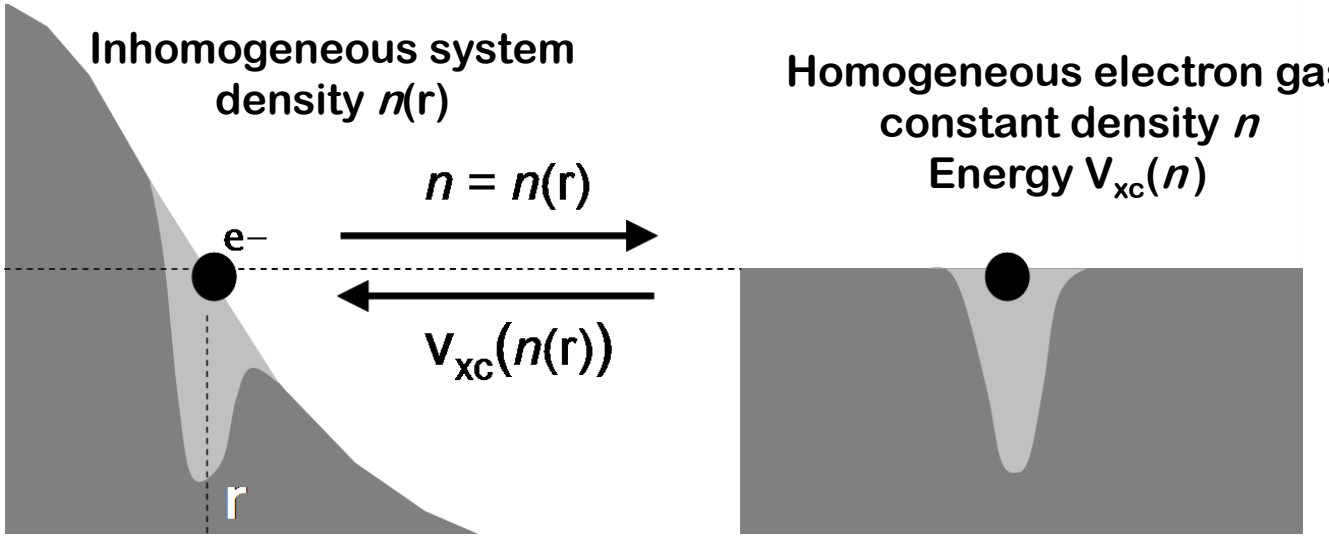


**Generalized Gradient Approximation (GGA):** $V_{xc}( n(r), \nabla n(r) )$

- Many many flavours: PW91, PBE, revPBE, BP86, BLYP, …
- Include (at least partially) correlation effects where overlap is appreciable
- Dispersion interactions (vdW) NOT included
- Self-interaction NOT fully canceled

**Defficiencies**
- Overestimation: Electron delocalization, metallic character, atomization energies
- Underestimation: Band gaps, energy barriers

# vdW interactions: London forces

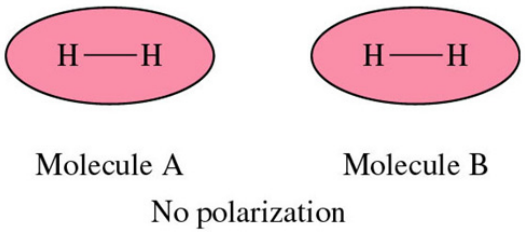


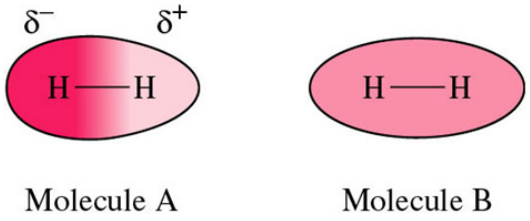


**electrons are constantly moving!**

**instantaneous dipole**

**Depends on the electronic *response* of the system; stronger between easily polarizable molecules**

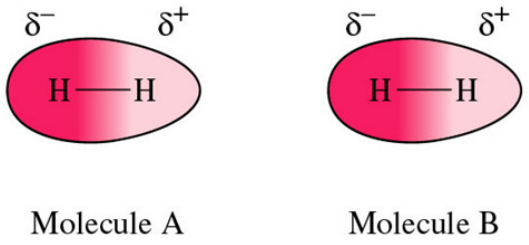


**instantaneous dipole on A induces dipole on B**

**Correlated**
**spontaneous & induced charge-density fluctuations give net attractive Coulomb interaction**

**A true quantum-mechanical effect !!**

# DFT: The Jacob's ladder

J. P. Perdew, A. Ruzsinszky, J. Tao, V. N. Staroverov,
G. Scuseria, G. I. Csonka, JCP 123, 062201 (2005)

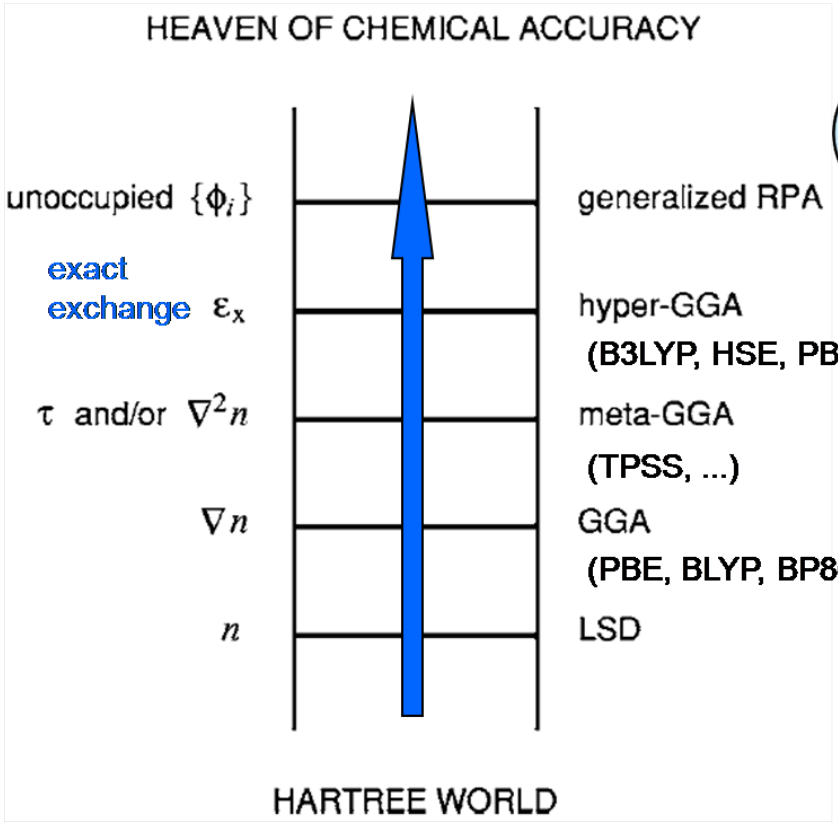


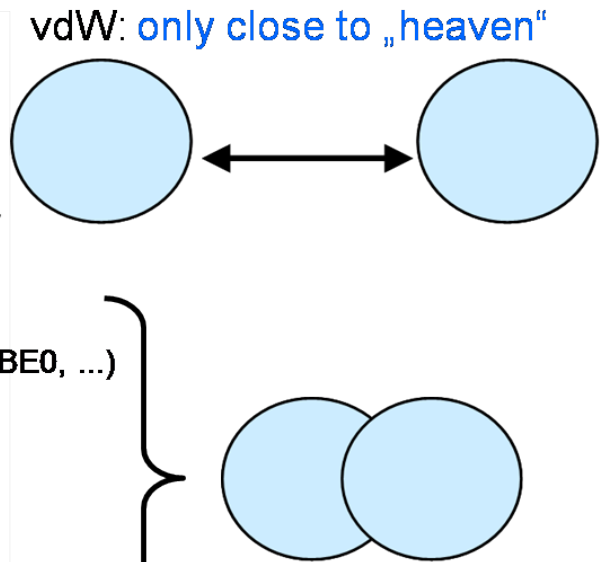


Bath Abbey

# DFT: Basis sets and pseudopotentials

Relativistic
**Non-relativistic**

LDA
GGA
Hybrid

$$\left(-\frac{\hbar^2}{2m}\nabla^2 + v_{\text{ext}}(\mathbf{r}) + v^e_{\text{coul}}(\mathbf{r}) + v_{\text{xc}}(\mathbf{r})\right)\psi_{n\mathbf{k}}(\mathbf{r}) = \epsilon_{n\mathbf{k}}\psi_{n\mathbf{k}}(\mathbf{r})$$

Full-potential
pseudopotential

Planewave : VASP, ABINIT
LAPW : FLAPW, WIEN2K
Numerical : SIESTA

→ **no preconceptions regarding the form of the solution, the absence of basis set superposition error, and the ability to efficiently calculate the forces on atoms**

## Pseudopotential

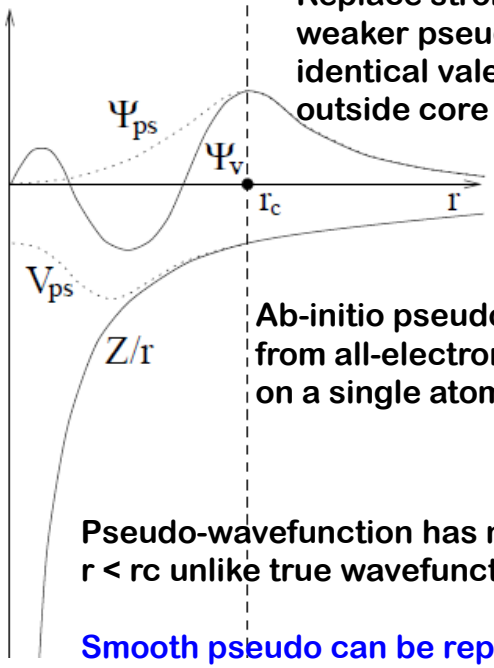


**Replace strong ionic potential with weaker pseudopotential which gives identical valence electron wavefunctions outside core region, r > rc.**

**Ab-initio pseudopotentials are calculated from all-electron DFT calculations on a single atom.**

**Pseudo-wavefunction has no nodes for r < rc unlike true wavefunction.**

**Smooth pseudo can be represented with few plane waves.**

## Planewaves

$$|\psi_{n\mathbf{k}}\rangle = \sum_{\mathbf{G}} C_{n\mathbf{k}}(\mathbf{G})|\phi_{\mathbf{k}}(\mathbf{G})\rangle$$

**Planewave**

$$\langle \mathbf{r}|\phi_{\mathbf{k}}(\mathbf{G})\rangle = \frac{1}{\sqrt{\Omega}}e^{i(\mathbf{k}+\mathbf{G})\cdot\mathbf{r}}$$

**Maximum kinetic energy of a plane wave**

$$\langle\phi_{\mathbf{k}}(\mathbf{G})|-\frac{\hbar^2}{2m}\nabla^2|\phi_{\mathbf{k}}(\mathbf{G})\rangle = \frac{\hbar^2(\mathbf{k}+\mathbf{G})^2}{2m} \leq E_{\text{cut}}$$

# Periodic Table

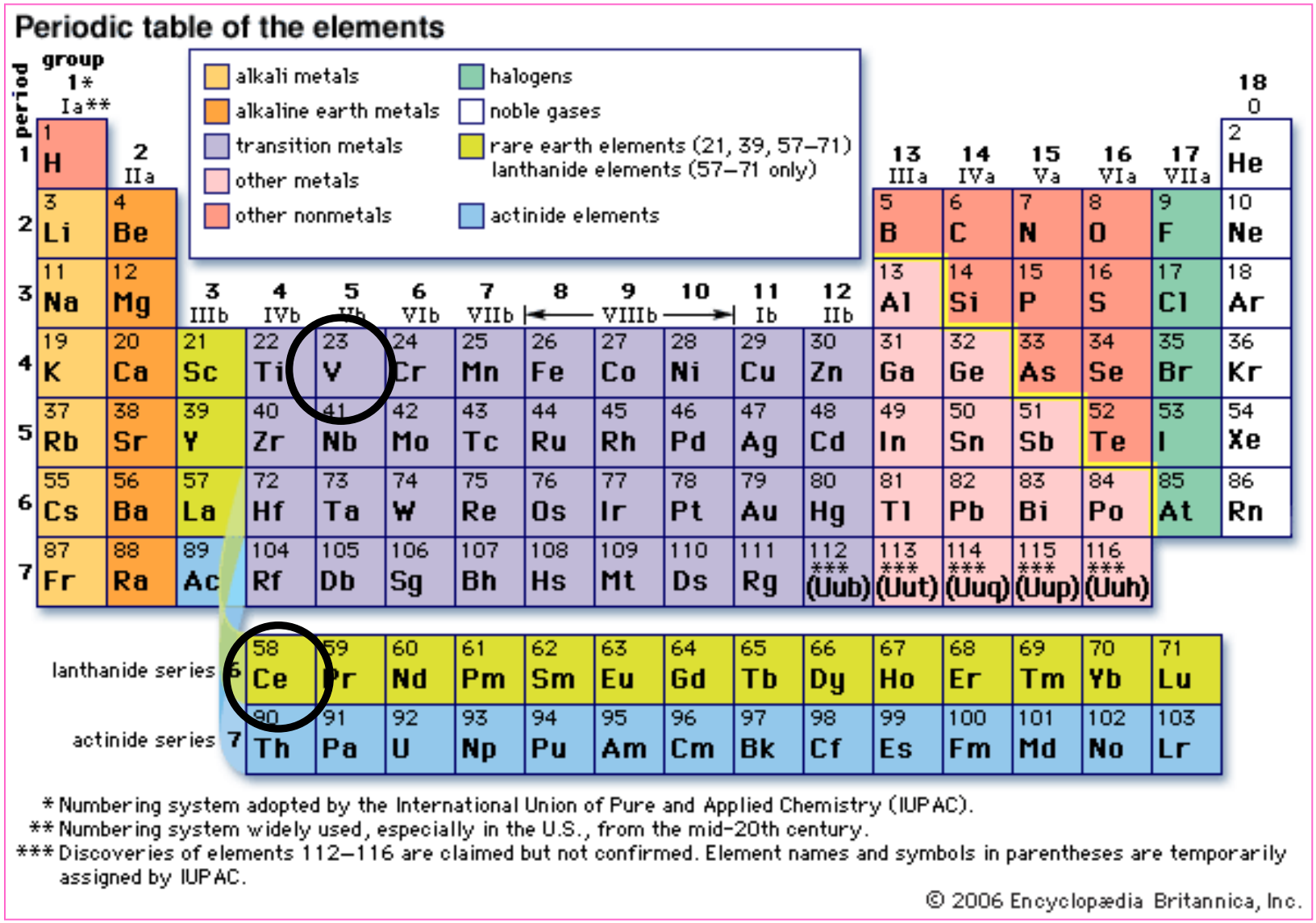

# The $V_2O_5$ (001) surface

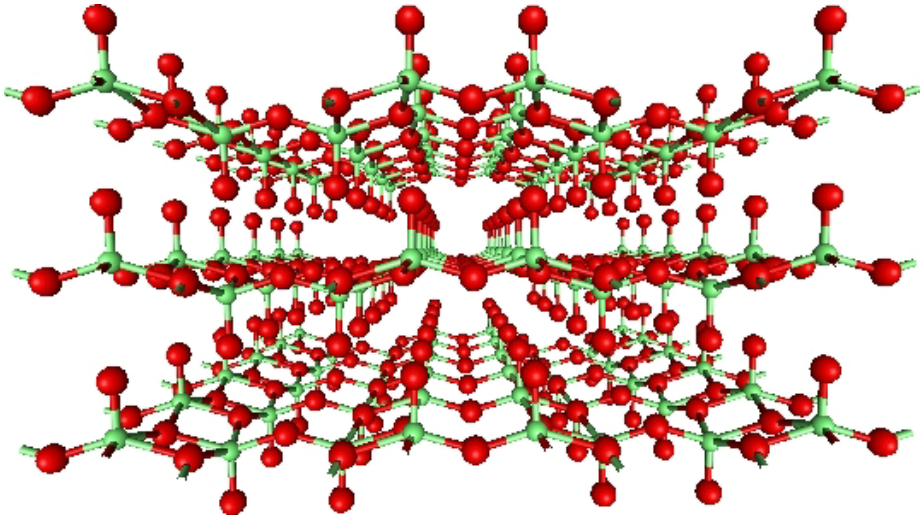

Weak interaction

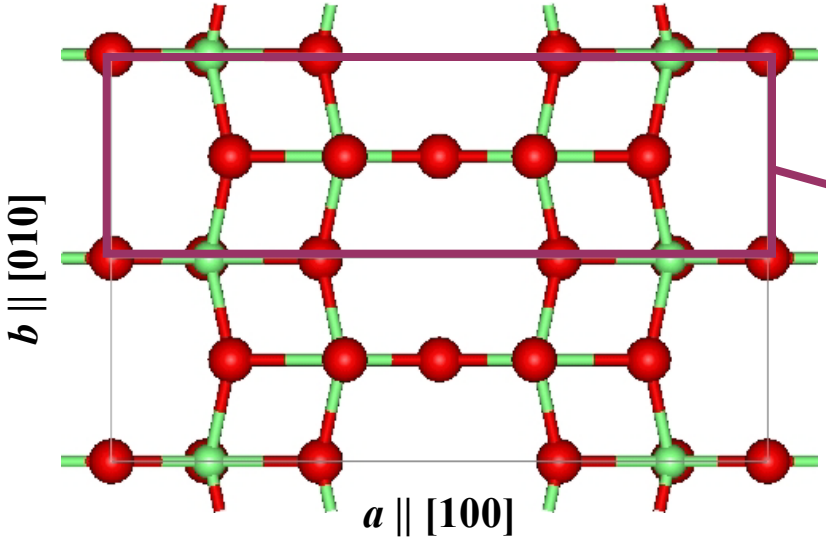


STM @ 300 K (occup. states)

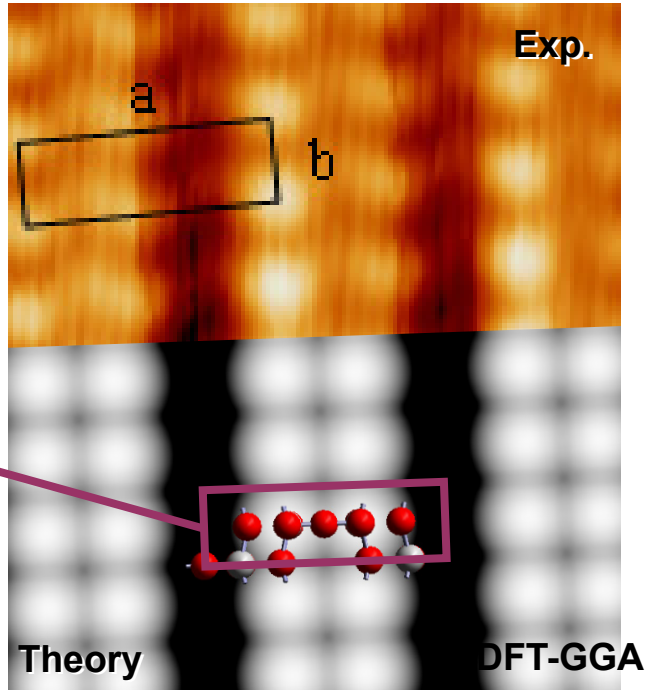


4×2 nm², -1.1 V, 0.45 nA

Blum, Niehus, Hucho, Fortrie, Ganduglia Pirovano, Sauer, Shaikhutdinov, Freund, Phys. Rev. Lett. 99, 226103 (2007)

# Vanadium oxide bulk phases

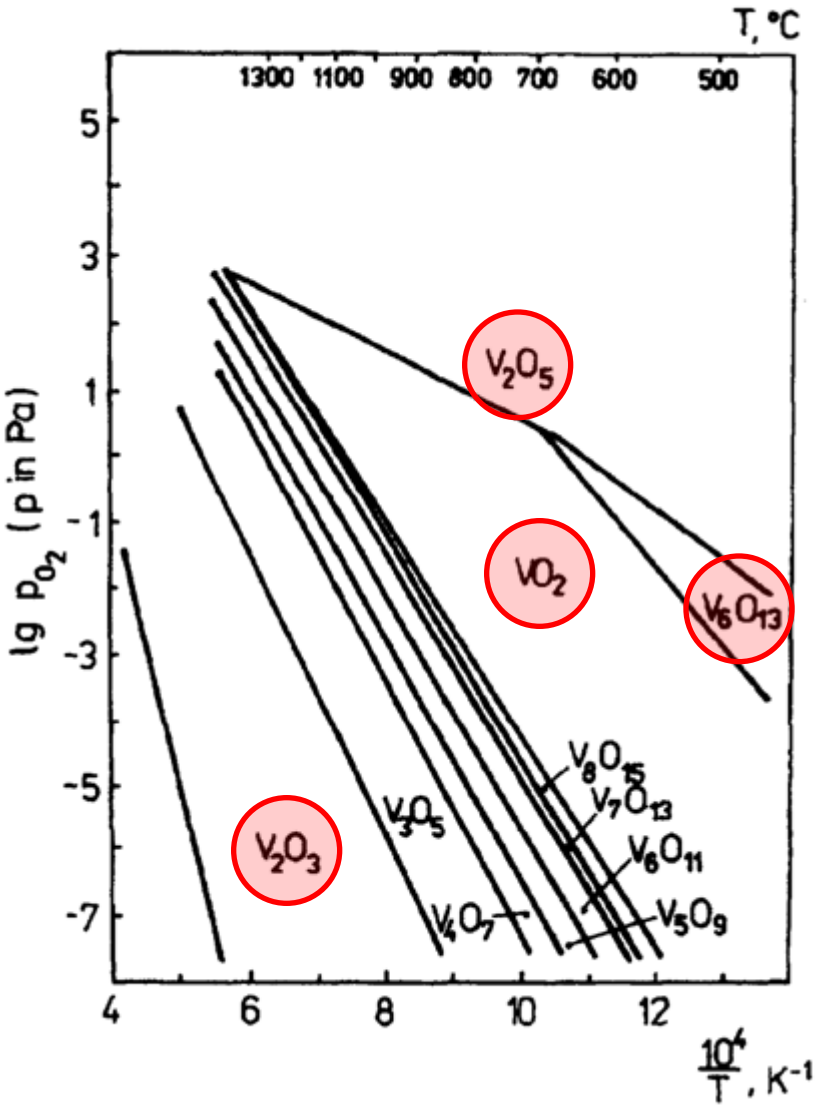


Most vanadium oxide bulk phases exhibit a metal-insulator transition

- $V_6O_{13}$: $V^{4+}$, $V^{5+}$ **MIT @ 150 K**
- $V_2O_3$: $V^{3+}$ **MIT @168 K**
- $VO_2$: $V^{4+}$ **MIT @ 340 K**
- $V_2O_5$: $V^{5+}$ **no MIT**

# $V_2O_5$(001): Formation of neutral oxygen defects

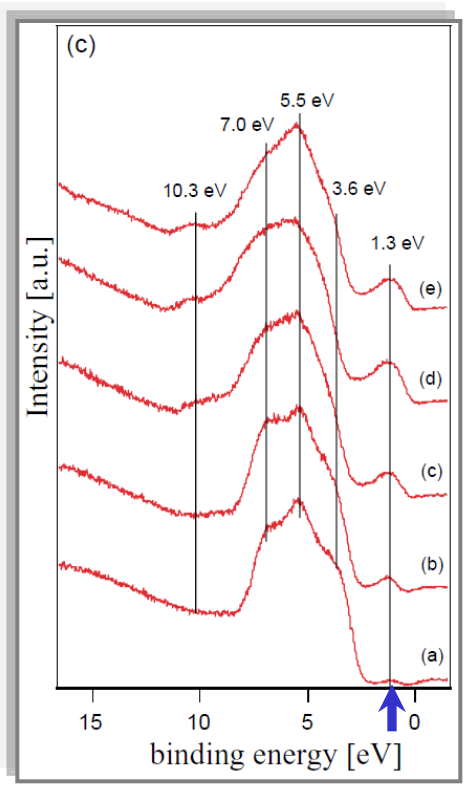


ultraviolet photoelectron spectroscopy

Reduction by thermal annealing

Q.-H. Wu et al., Applied Surface Science 236, 473 (2004)

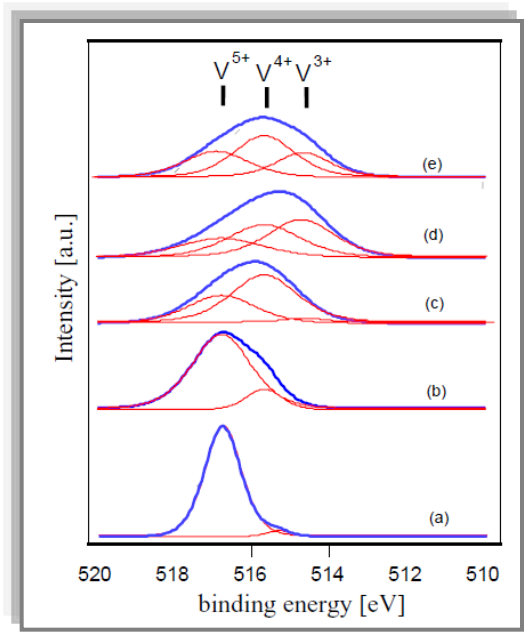


Fig. 4. Fitted data of V $2p_{3/2}$ lines after removal of background for different treatments in UHV chamber: (a) RT, (b) 200 °C, (c) 300 °C, (d) 400 °C, (e) 400 °C in $10^{-6}$ mbar oxygen.

- **UPS: Defect state in the $O_{2p}$–$V_{3d}$ gap (2.3 eV), ~1 eV below $E_F$; $V_{3d}$ nature**
- **XPS: $V^{5+} \rightarrow V^{4+} \rightarrow V^{3+}$**
- **STM: surface oxygen defects with non-random structure**

Blum et al, Phys. Rev. Lett. 99, 226103 (2007)

# $V_2O_5$ bulk and the $V_2O_5$ (001) surface

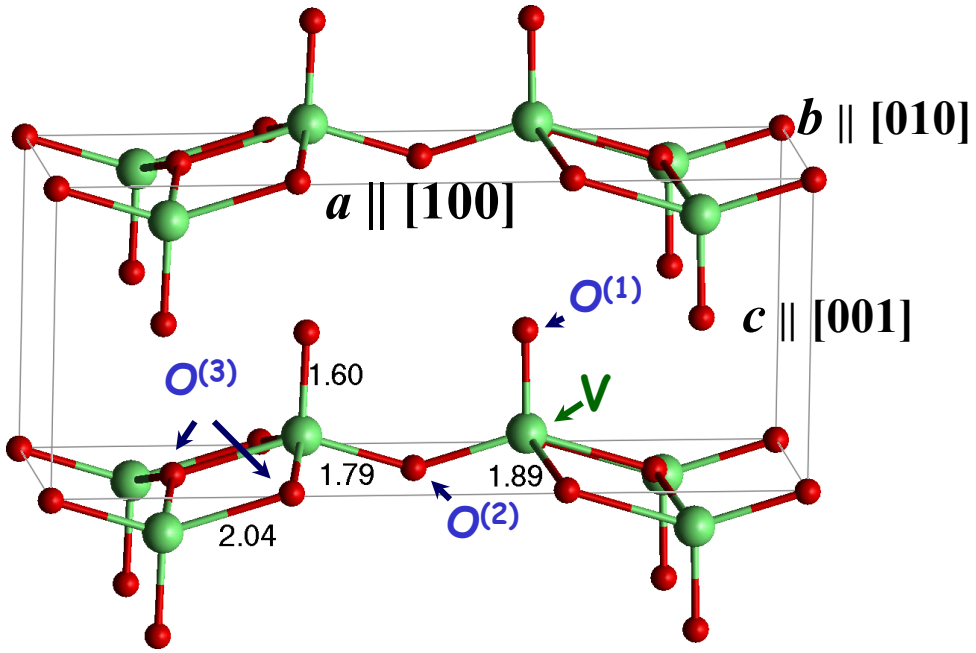


| Å | PW91 | Exp. | |
|---|---|---|---|
| *a* | 11.55 | 11.51 | Δa/a = 2% |
| *b* | 3.58 | 3.56 | Δb/b = 1% |
| *c* | 4.84 | 4.37 | Δc/c = 11% |

weak interacting layers

$$E_{xc}^{vdW-DF}[n] = E_x^{GGA}[n] + E_c^{LDA}[n] + E_c^{nl}$$

exchange — shorter range LDA — non-local long range

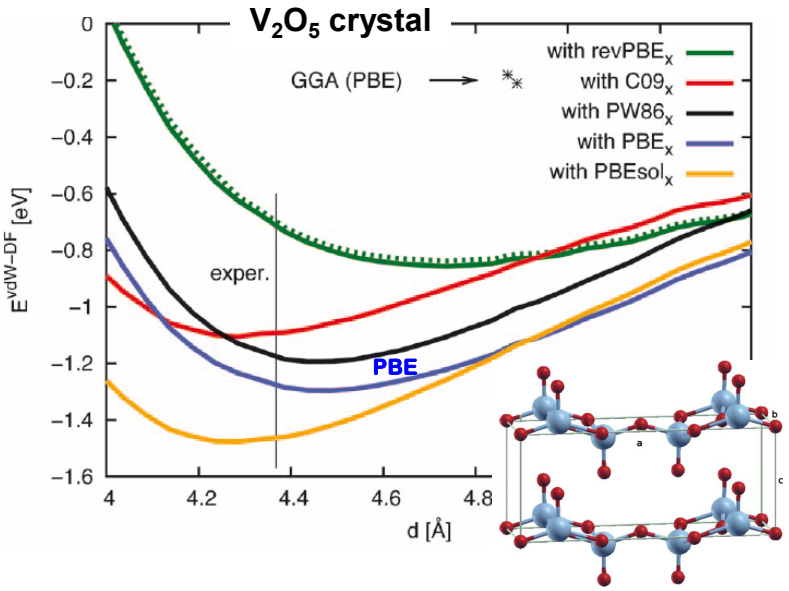


Ganduglia-Pirovano, Sauer, Phys. Rev. B 70, 45422 (2004)

Vienna Ab initio Simulation Package VASP

Londero, Schröder, PRB 82, 054116 (2010)

# $V_2O_5$ bulk and the $V_2O_5$ (001) surface

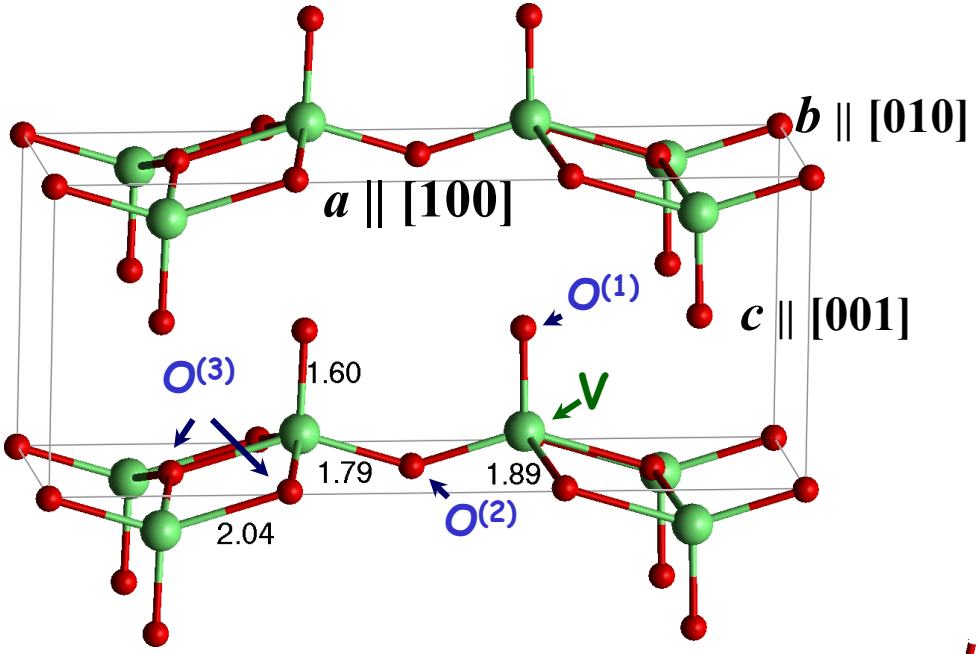


| Å | PW91 | Exp. | |
|---|---|---|---|
| *a* | 11.55 | 11.51 | Δa/a = 2% |
| *b* | 3.58 | 3.56 | Δb/b = 1% |
| *c* | 4.84 | 4.37 | Δc/c = 11% |

weak interacting layers

$V_2O_5$ (001)

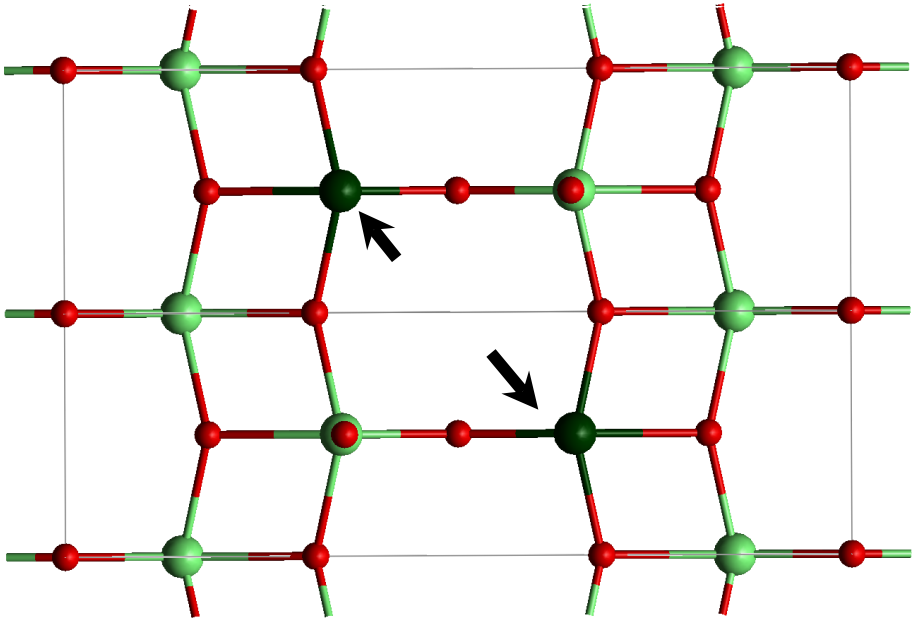

*b* || [010]

Vienna Ab initio Simulation Package VASP

# Simulation of reduced $V_2O_5$ (001)

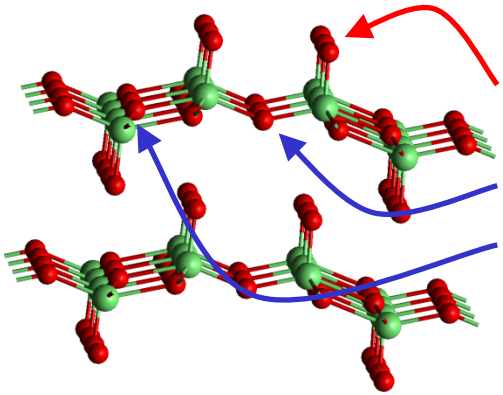

1.95 eV
3.65 eV
3.97 eV

$E_f^{\frac{1}{2}O_2} = E^{reduced} - E^{clean} + \frac{1}{2} E_{O_2}$

**O-defect formation energy**

**Θ = 1/6**

**Θ = 1/4**

**Θ = 1/3**

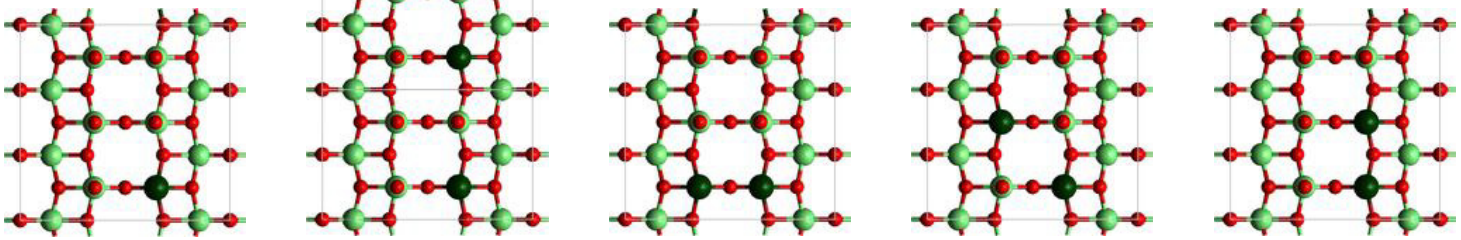

**Θ = 1/2**

**Θ = 3/4**

**Θ = 1**

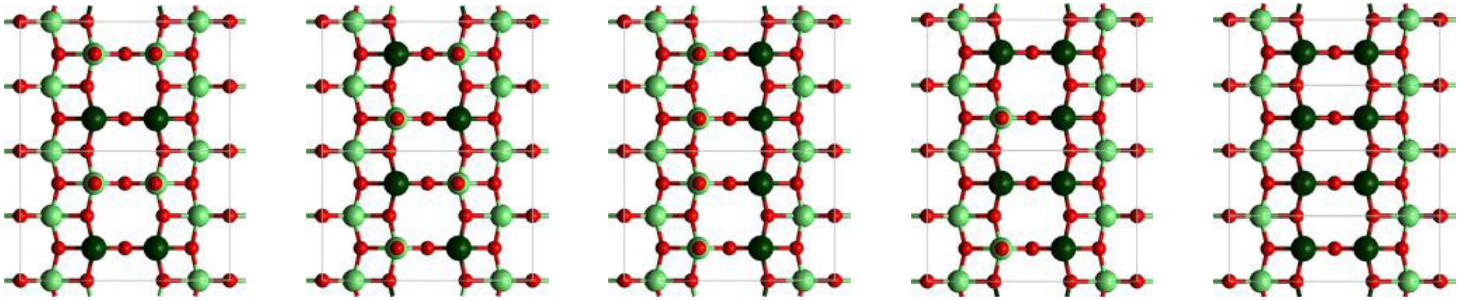

**Θ = Vanadyl defect concentration**

# Stability of reduced $V_2O_5$(001)

$$V_2O_5^{\text{clean}} \rightleftarrows V_2O_5^{\text{reduced}} + N_{def}\ ½\ O_2$$

$$\Delta\gamma_{surf}(T,p) = [\, G_{slab}^{\text{reduced}}(T,p,N_{def}) - G_{slab}^{\text{clean}}(T,p) + N_{def}\ ½\ \mu_{O_2}(T,p)] \,/A$$

$$G = E - TS + pV$$

$$G(p,T) = E(0\ K) + E^{vib}(T) - T\,[S^{vib}(T) + S^{config}] + pV$$

$$G(p,T) = E(0\ K) + F^{vib}(T) - T\,S^{config} + pV$$

Total Energy — Helmholtz Energy — Entropy

$$\Delta\gamma_{surf}(T,p) \approx [\, E_{slab}^{\text{reduced}}(N_{def}) - E_{slab}^{\text{clean}} + N_{def}\ ½\ \mu_{O_2}(T,p)] \,/A$$

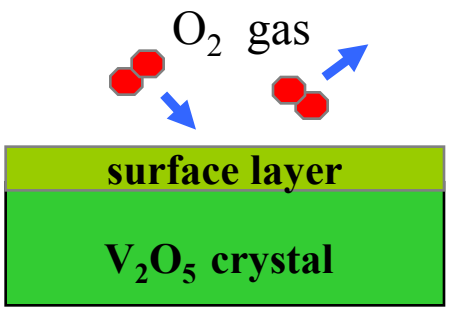

# Stability of reduced $V_2O_5(001)$

$$V_2O_5^{\text{clean}} \rightleftarrows V_2O_5^{\text{reduced}} + N_{def}\ ½\ O_2$$

$$\Delta\gamma_{surf}(T,p) = [\ G_{slab}^{\text{reduced}}(T,p,N_{def}) - G_{slab}^{\text{clean}}(T,p) + N_{def}\ ½\ \mu_{O_2}(T,p)]\ /A$$

$$\Delta\gamma_{surf}(T,p) \approx [\ E_{slab}^{\text{reduced}}(N_{def}) - E_{slab}^{\text{clean}} + N_{def}\ ½\ \mu_{O_2}(T,p)]\ /A$$

$$\Delta\gamma_{surf}(T,p) \approx N_{def}\ [\ E_f^{½O_2}(\Theta) + ½\ \Delta\mu_{O_2}(T,p)]\ /A$$

$$\tfrac{1}{2}\Delta\mu_{O_2} = \tfrac{1}{2}\mu_{O_2} - \tfrac{1}{2}E_{O_2}$$

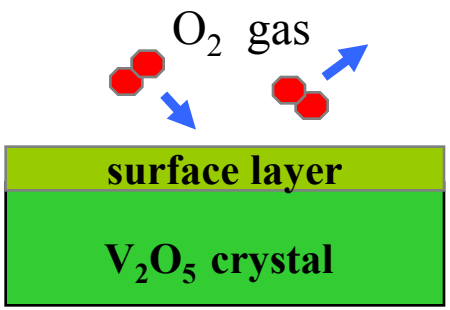


**Oxygen chemical potential**

$$\mu_{O_2}(T,p) = \mu_{O_2}(T,p^o) + RT\ln(p/p^o)$$

# Stability of reduced $V_2O_5$(001)

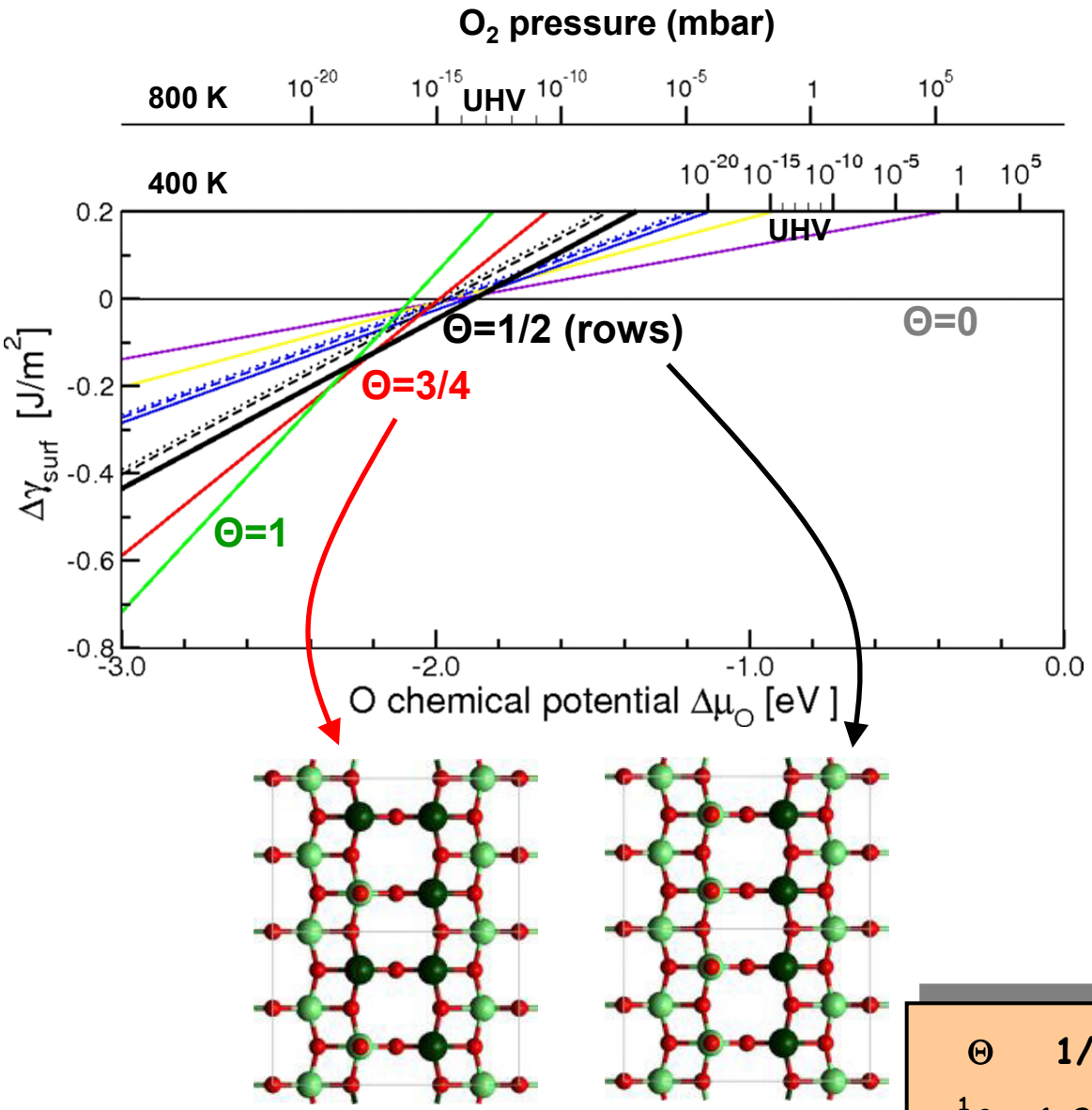


| | |
|---|---|
| Θ | 1/6 → 1/3 → 1/2 |
| $E_f^{\frac{1}{2}O_2}$ | 1.93 → 1.87 → 1.83 eV |

Ganduglia-Pirovano, Sauer, Phys. Rev. B 70, 45422 (2004)

# Defect induced relaxations  Θ= 1/6 → 1/3

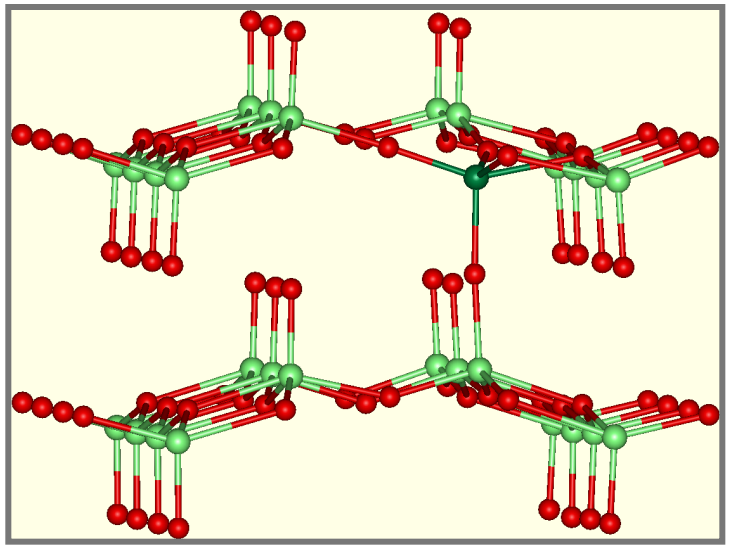

Isolated defect

Induced relaxations take place in a concerted way

Pairs || [010]

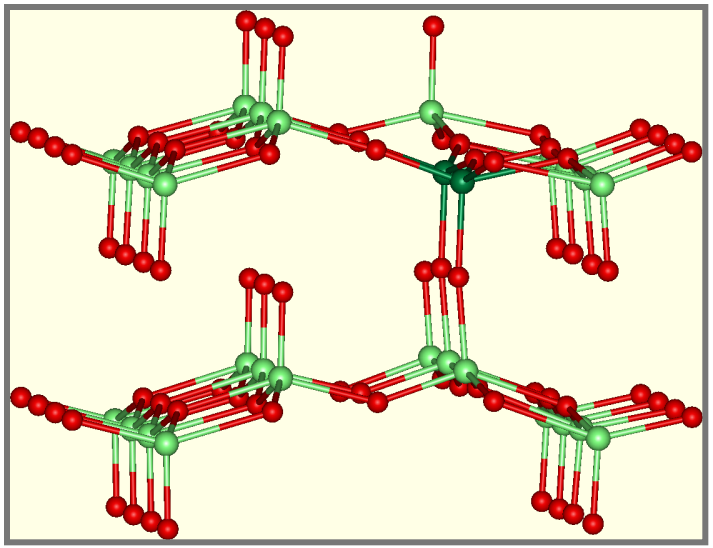

Induced relaxations do not take place cooperatively

Pairs || [100]

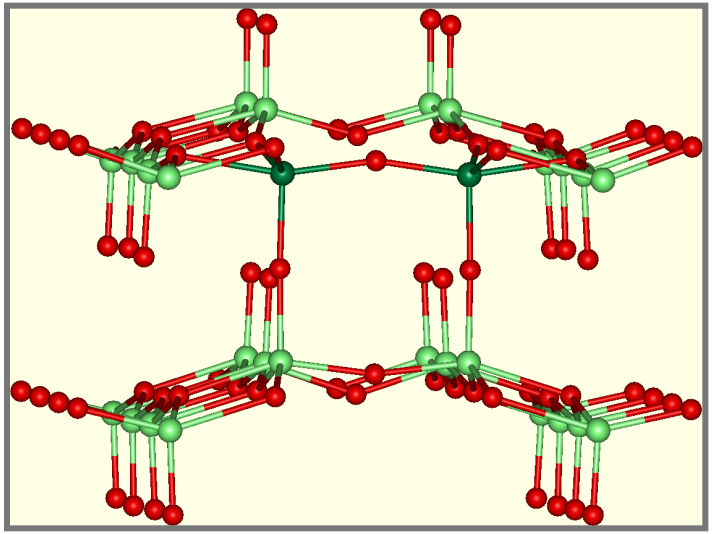

# $V_2O_5$(001) reduction

STM @350K

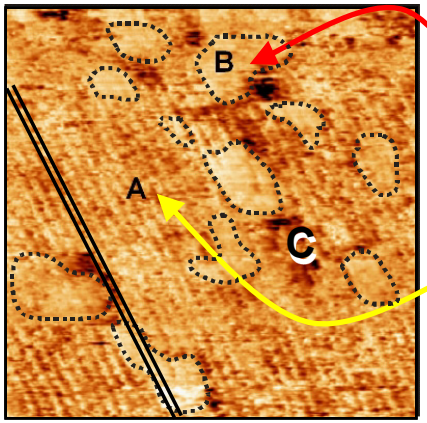


50x50 nm$^2$ -1.3 V 0.24 nA

STS @350K

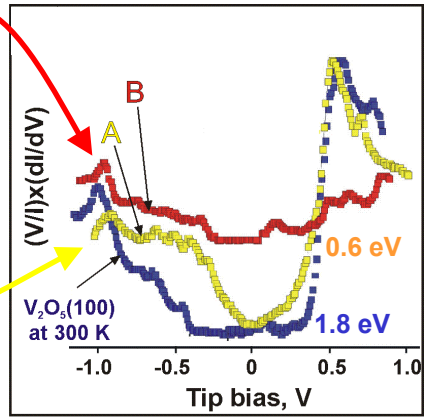


@350K

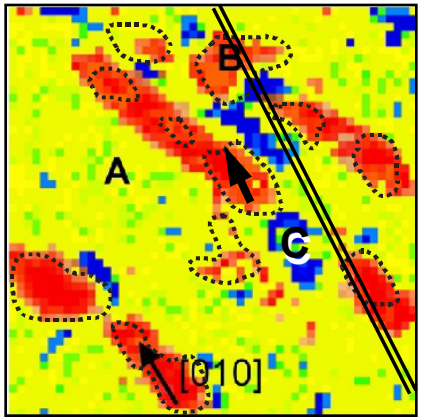


@400K

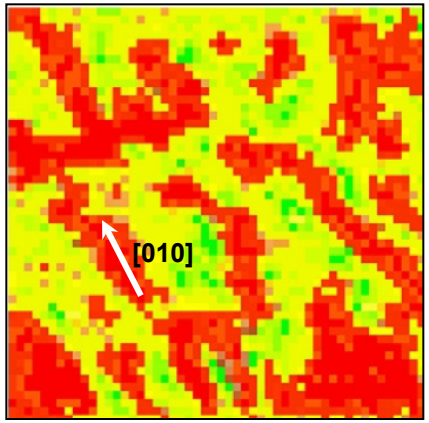


surface insulator-metal transition

350-400 K

Bandgap map

Blum, Niehus, Hucho, Fortrie, Ganduglia Pirovano, Sauer, Shaikhutdinov, Freund, PRL99, 226103 (2007)

# O-defect induced structural and electronic effects

Isolated defect Θ=1/6

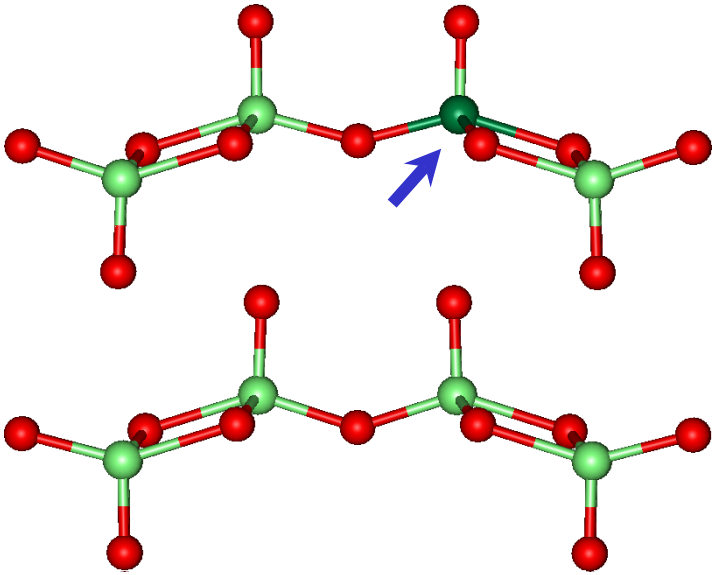

Spin density

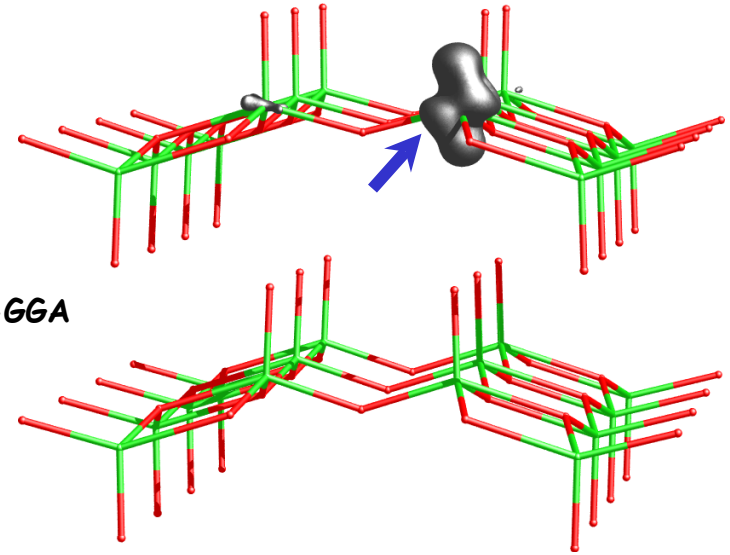

DFT-GGA

Ganduglia-Pirovano, Hofmann, Sauer,
Surf. Sci. Rep. 62, 219 (2007)

# O-defect induced structural and electronic effects

Isolated defect Θ=1/6

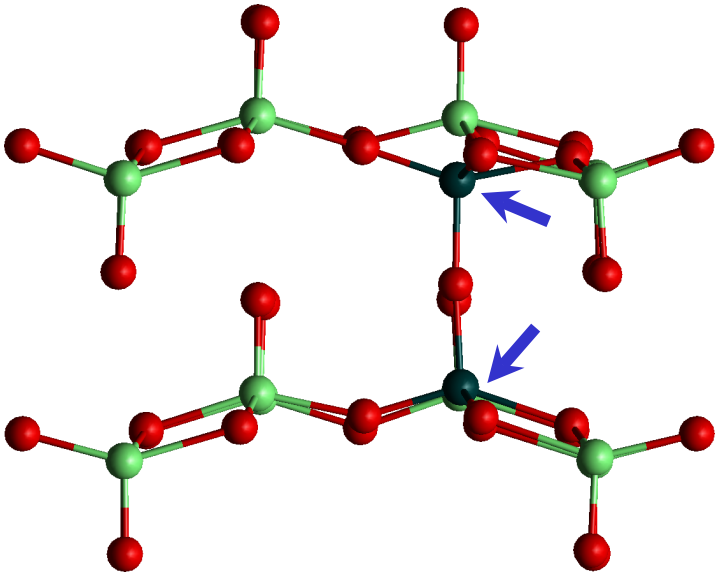

Spin density

DFT-*GGA*

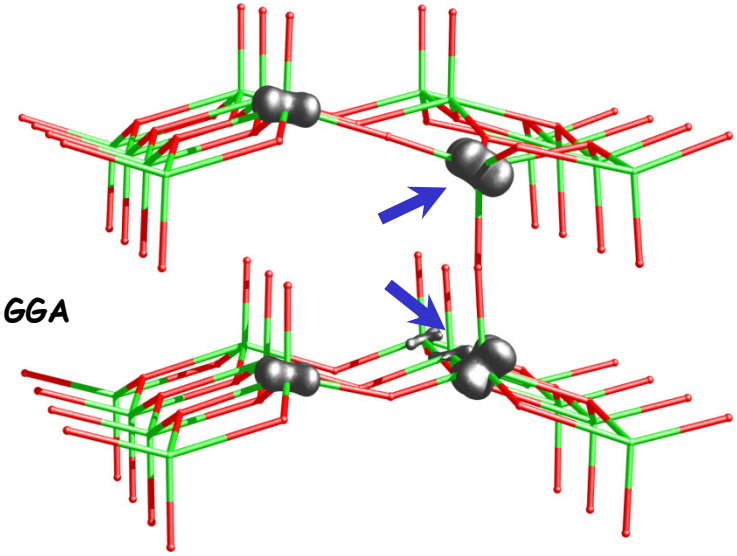

DFT-*GGA*

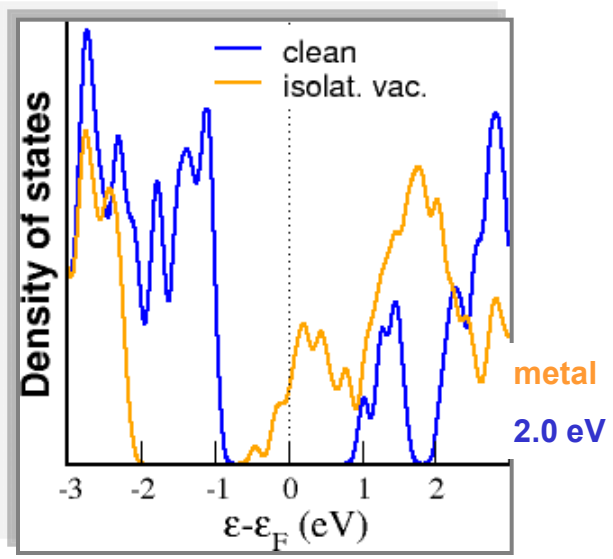


Ganduglia-Pirovano, Hofmann, Sauer,
Surf. Sci. Rep. 62, 219 (2007)

# The choice of the computational method

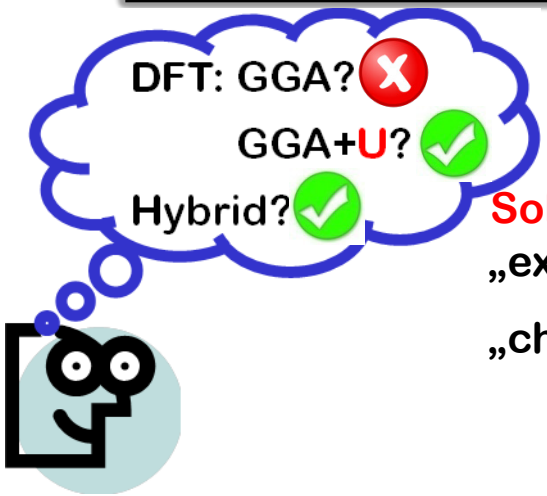


**Problems**: electron delocalization
metallic character

Da Silva, Ganduglia-Pirovano, Sauer, Bayer, Kresse, PRB 75 (2007)

Ganduglia-Pirovano, Hofmann, Sauer, Surf. Sci. Rep. 62 (2007)

**Solutions**:

„expensive“ solution: Hybrid-DFT — exact-exchange

„cheap“ solution: DFT (LDA/GGA)+U — on-site Coulomb repulsion

Dudarev st al., PRB 57 (1998)

# O-defect induced structural and electronic effects

Isolated defect Θ=1/6

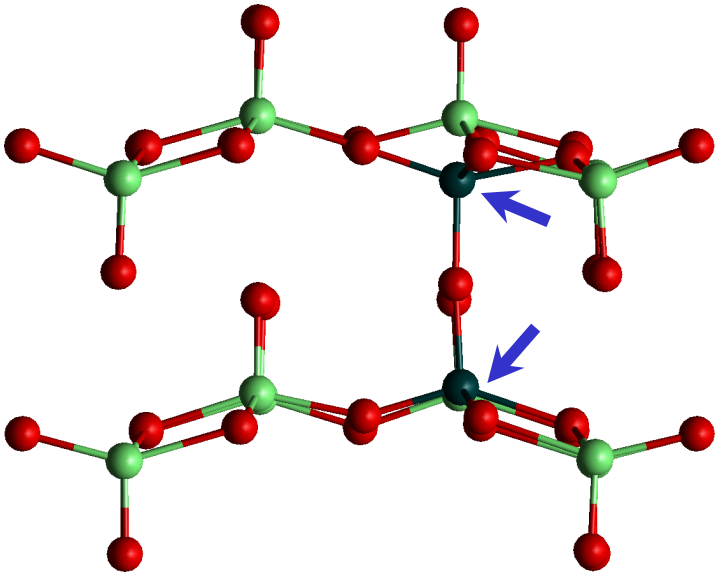

Spin density

DFT+U

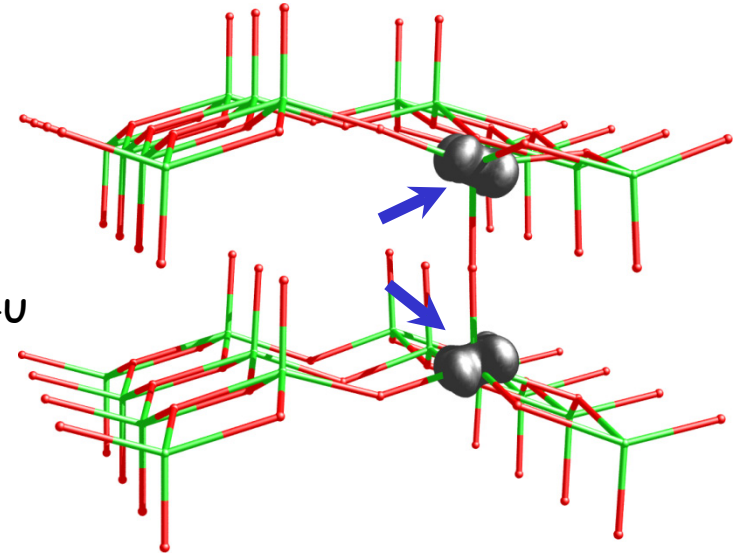

DFT+U U'=3 eV

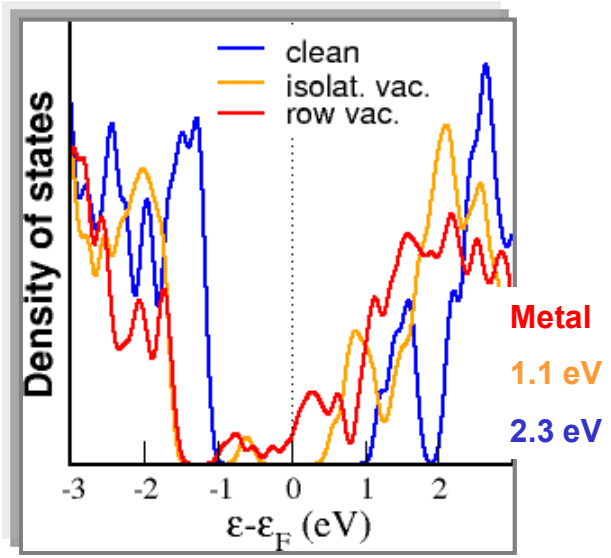


DFT-*GGA*

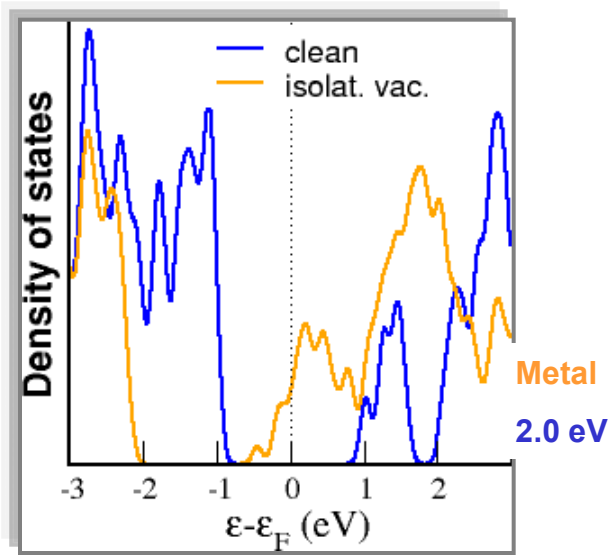

# O-defect induced structural and electronic effects

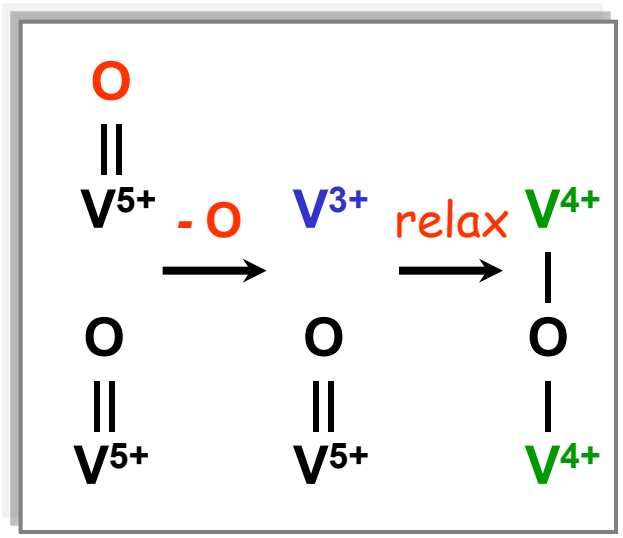


The existence of $V^{4+}$ is explained !

$$E_f^{\frac{1}{2}O_2}[eV] = E^{reduced} - E^{clean} + \frac{1}{2} E_{O_2}$$

3.76

↓ relax

1.93

| Defect formation energy $E_f^{\frac{1}{2}O_2}$ [eV] | | | $O_2$ dissociation energy [eV per atom] | |
|---|---|---|---|---|
| PW91: | 1.93 | slab | PW91: 3.10 | |
| PW91+U: | 1.41 | slab | ⇒ ~ **0.5 eV** | |
| B3LYP: | 1.17 | cluster | B3LYP: 2.60 | |
| exp: | 1.3 | bulk (molten) | exp: 2.62 | |


Ganduglia-Pirovano, Sauer, PRB (2004); Sauer, Döbler, Dalton Trans. (2004)

Ganduglia-Pirovano, Hofmann, Sauer, Surf. Sci. Rep. (2007)

# $V_2O_5$(001) reduction

STM @350K

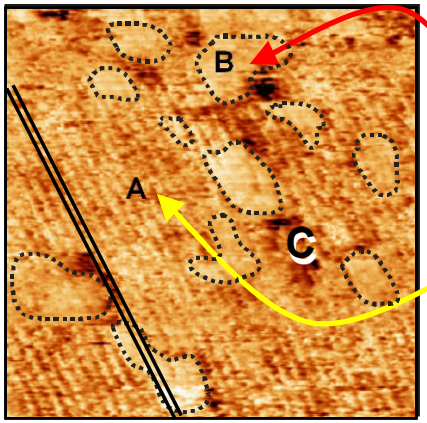


50x50 nm$^2$ -1.3 V 0.24 nA

STS @350K

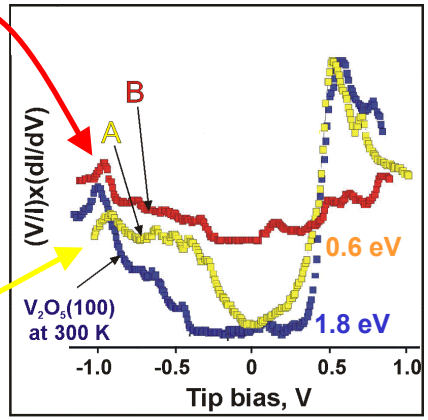


@350K

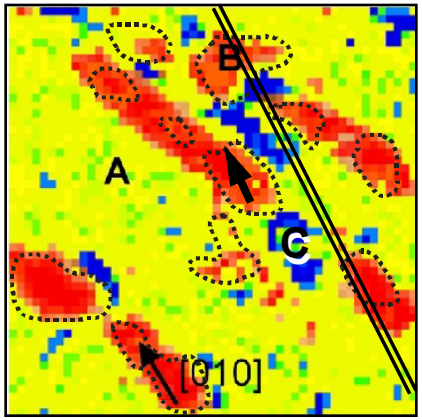


@400K

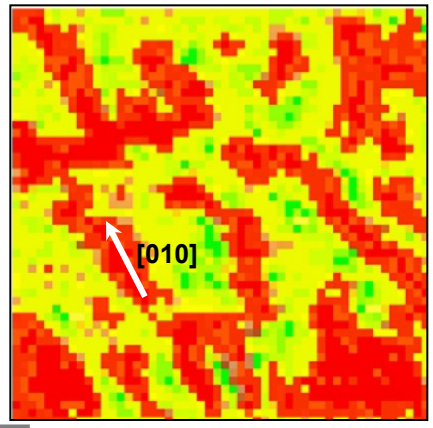


surface insulator-metal transition

350-400 K

Bandgap map

Blum, Niehus, Hucho, Fortrie, Ganduglia Pirovano, Sauer, Shaikhutdinov, Freund, PRL99, 226103 (2007)

# Space and time in materials

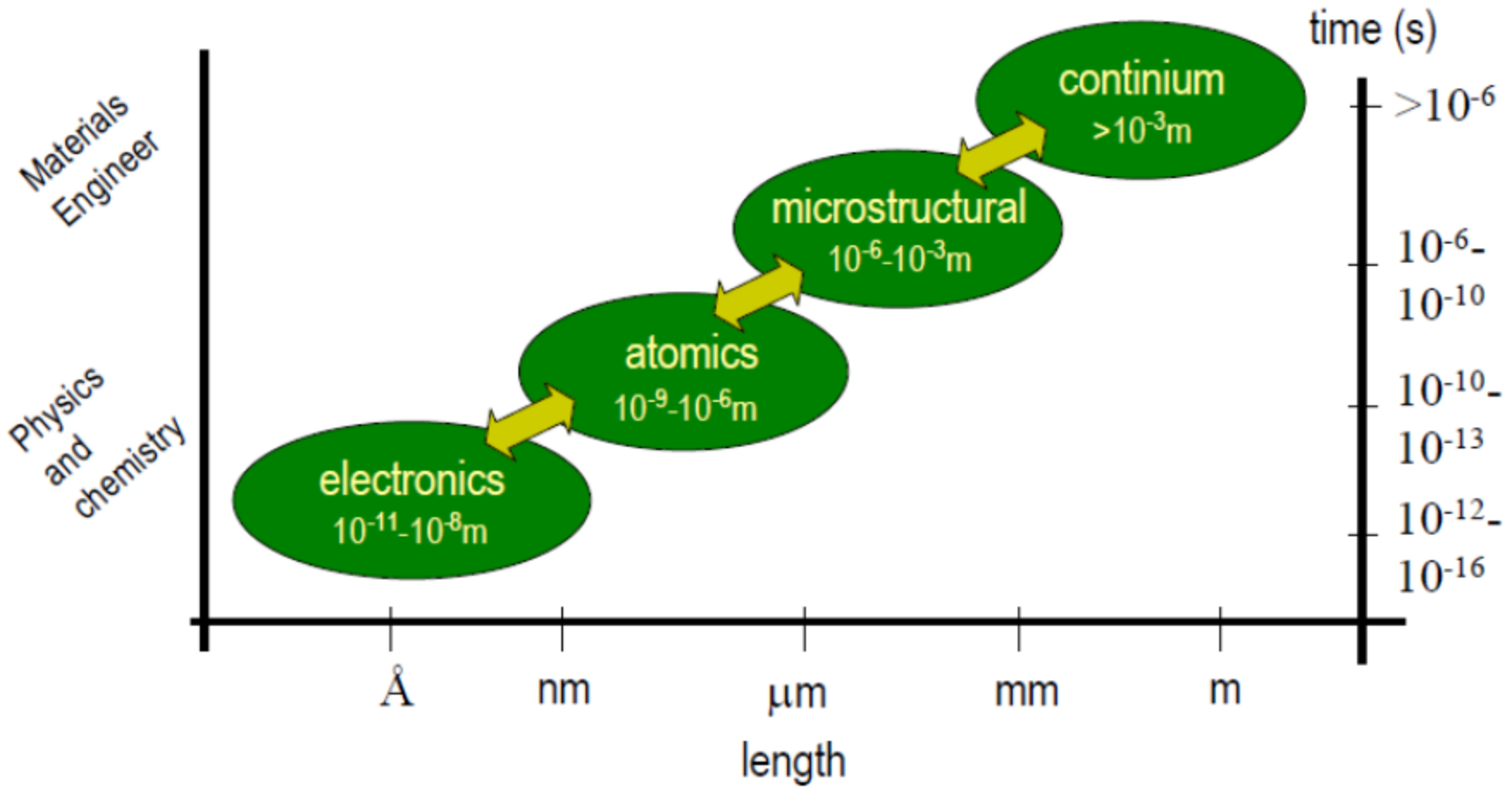

# Monte Carlo Simulations

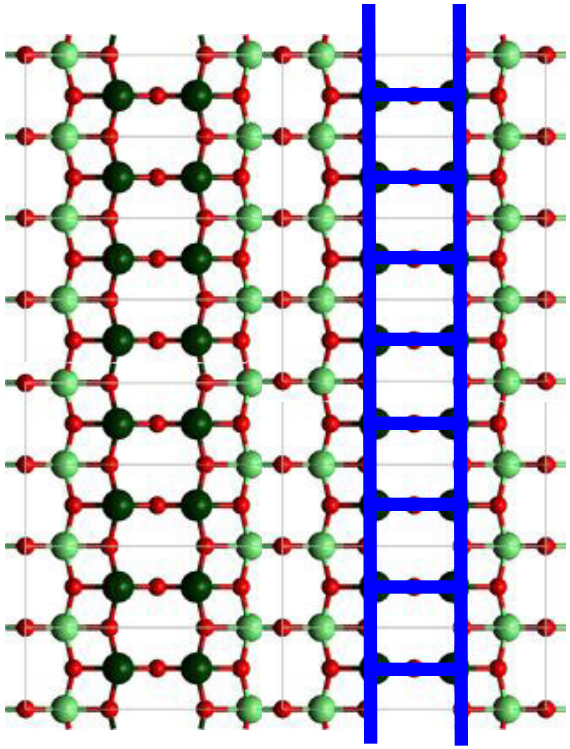

50 double rows
150 sites / row
15,000 sites

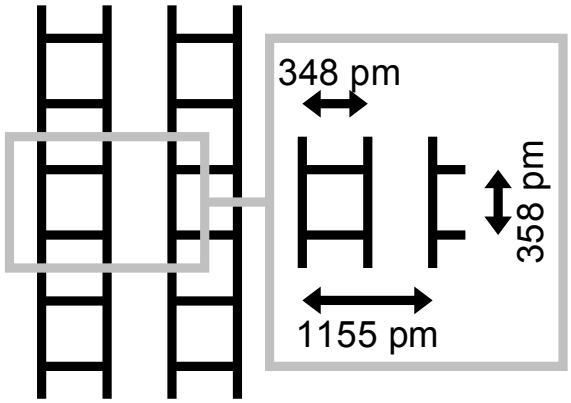


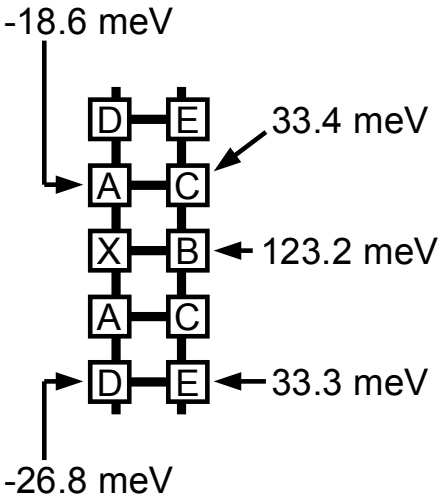

# Principles of Monte Carlo simulations

## Phase-space sampling

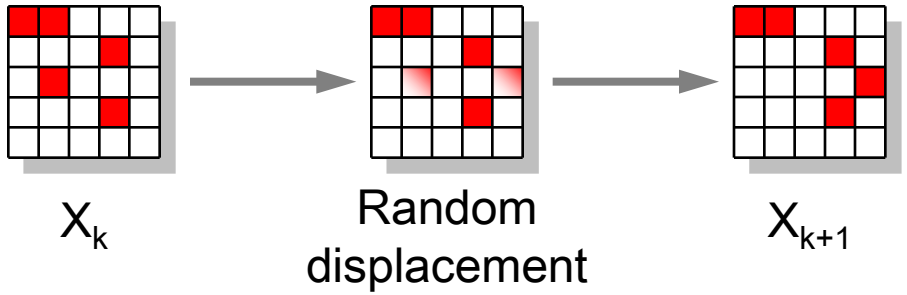


$$\langle X \rangle = \lim_{N \to +\infty} \frac{1}{N} \sum_{k=1}^{N} X_k$$

## For a Boltzmann distribution

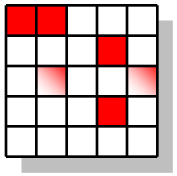

Random displacement

IF $E_{k+1} \leq E_k$ THEN Displacement accepted

**Metropolis Algorithm**

IF $E_{k+1} \geq E_k$ **AND**

$$\exp\left(-\frac{E_{k+1} - E_k}{k_B T}\right) \gtrless R(0,1)$$

Random number between 0 and 1

THEN Displacement accepted

THEN Displacement rejected

# Simulated band gap maps

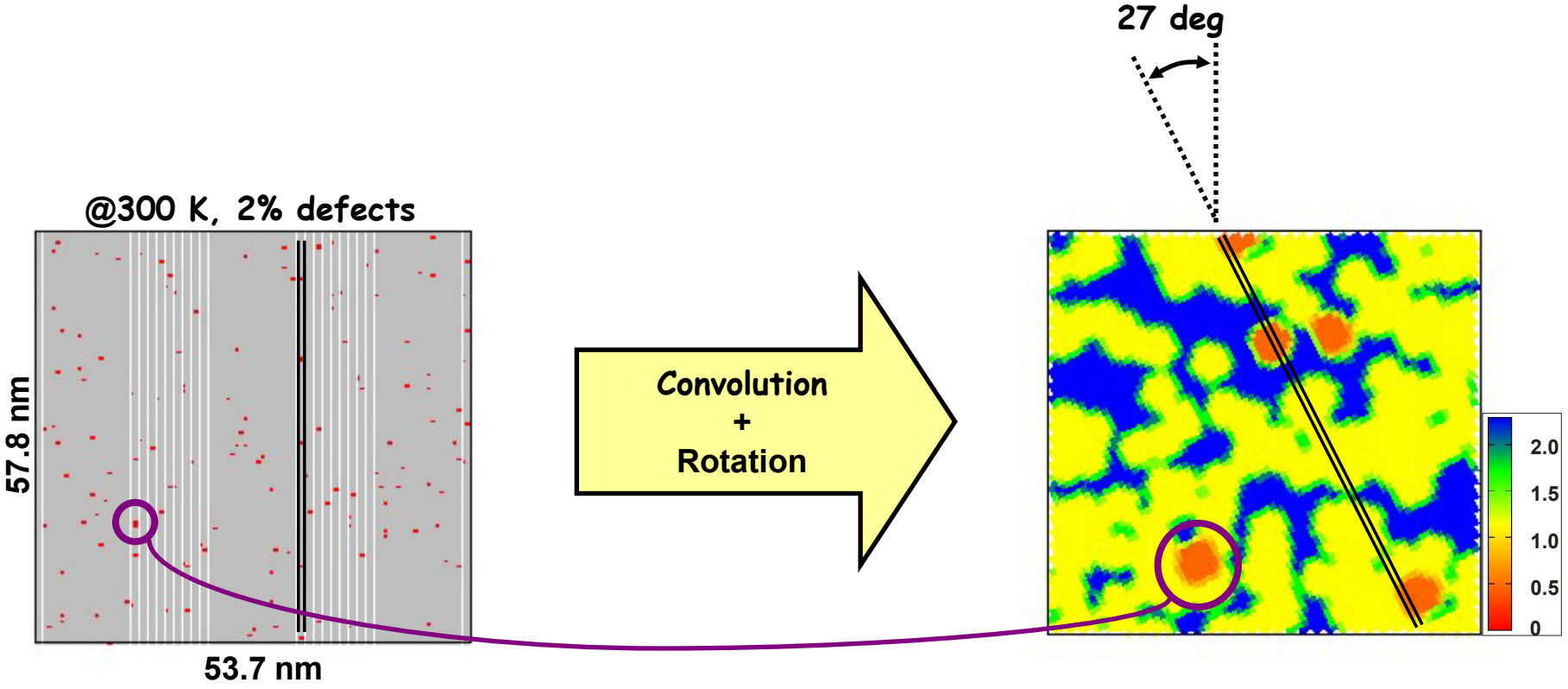


50 double rows
150 sites / row
15,000 sites

Tip sensitivity radius = 2 nm
Effective gap = Smallest gap felt

| | | Gap |
|---|---|---|
| DFT+U | No defect | 2.28 eV |
| | Isolated defects | 1.12 eV |
| | Pair defects | 0.46 eV |
| | Others | 0.00 eV |

# $V_2O_5$(001) reduction

STM @350K

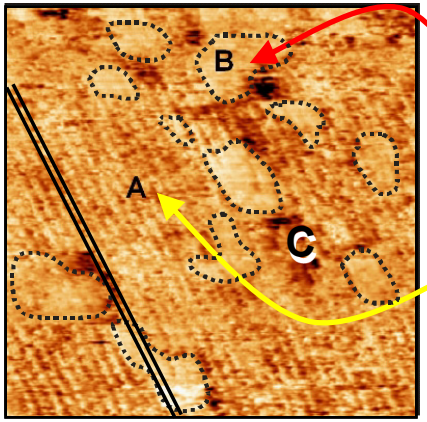


50x50 nm$^2$ -1.3 V 0.24 nA

STS @350K

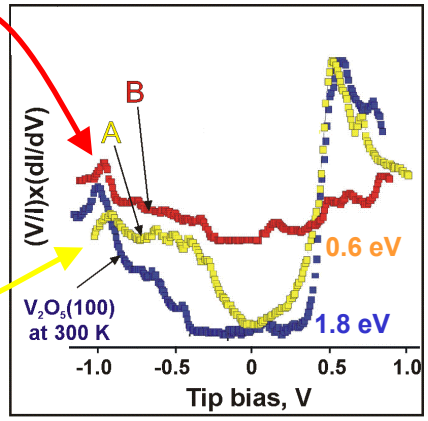


DFT+U U=3 eV

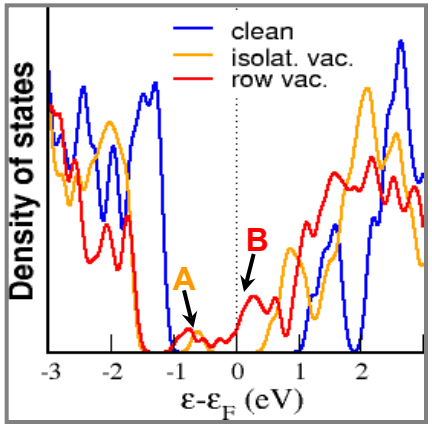


Monte Carlo network

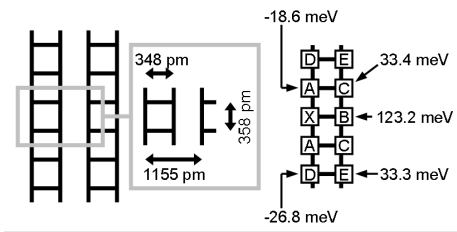


50 double rows
150 sites/row
15,000 sites

@350K

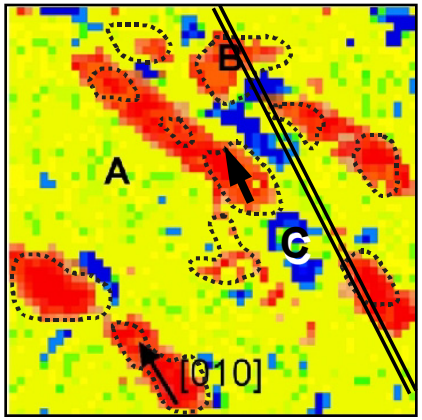


@400K

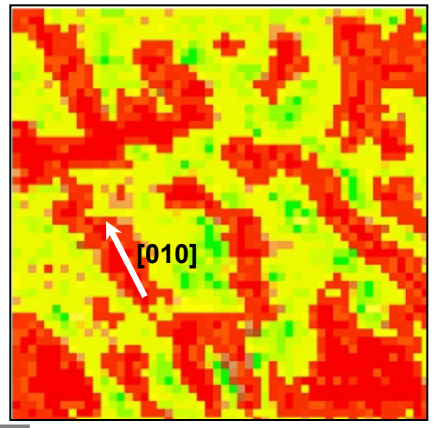


7% reduced sites @300 K

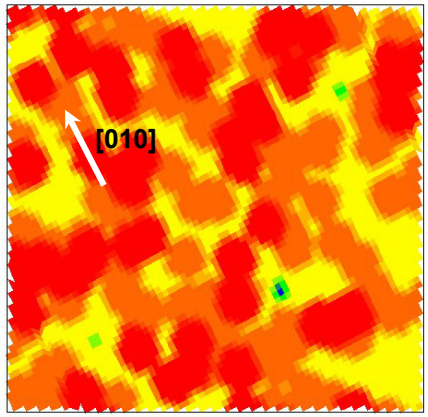


58x54 nm$^2$

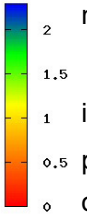


no defect
isolated defect
pairs
other

surface insulator-metal transition
350-400 K

Bandgap map

Monte Carlo simulated Bandgap map

The facile reduction along [010] constitutes a prediction!!

Blum, Niehus, Hucho, Fortrie, Ganduglia Pirovano, Sauer, Shaikhutdinov, Freund, PRL99, 226103 (2007)

# $V_2O_5(001)$ defects: Summary

- **Relaxation:** V–O–V bond formation (GGA & GGA+U & Hybrid)

  - substantial (~1 Å ); reduction of $E_f^{\frac{1}{2}O_2}$ (~2 eV)

  - essential role in the resulting electronic structure ($2\times V^{4+}$ );too delocalized (GGA)

- **Defect formation energy:**

| Method | PW91 | PW91+U | B3LYP |
|---|---|---|---|
| $E_f^{\frac{1}{2}O_2}$ | 1.93 | 1.41 | 1.17 |

quantitative differences exist

We recognize the merit of PW91 in predicting
the alignment of vanadyl defects along the [010] direction


Ganduglia-Pirovano, Sauer, Phys. Rev. B 70, 45422 (2004)
Blum, Niehus, Hucho, Fortrie, Ganduglia Pirovano, Sauer, Shaikhutdinov, Freund, Phys. Rev. Lett. 99, 226103 (2007)
Ganduglia-Pirovano, Hofmann, Sauer, Surf. Sci. Rep. 62 (2007)
*Oxygen Defects at Reducible Oxide Surfaces*: *The Example of Ceria and Vanadia*, M. V. Ganduglia-Pirovano in *Defects on Oxide Surfaces,* edited by G. Thorton and J. Jupille (Springer, 2015), pp. 149-190.

# Monte Carlo Simulations

Effect of the defect concentration @300K

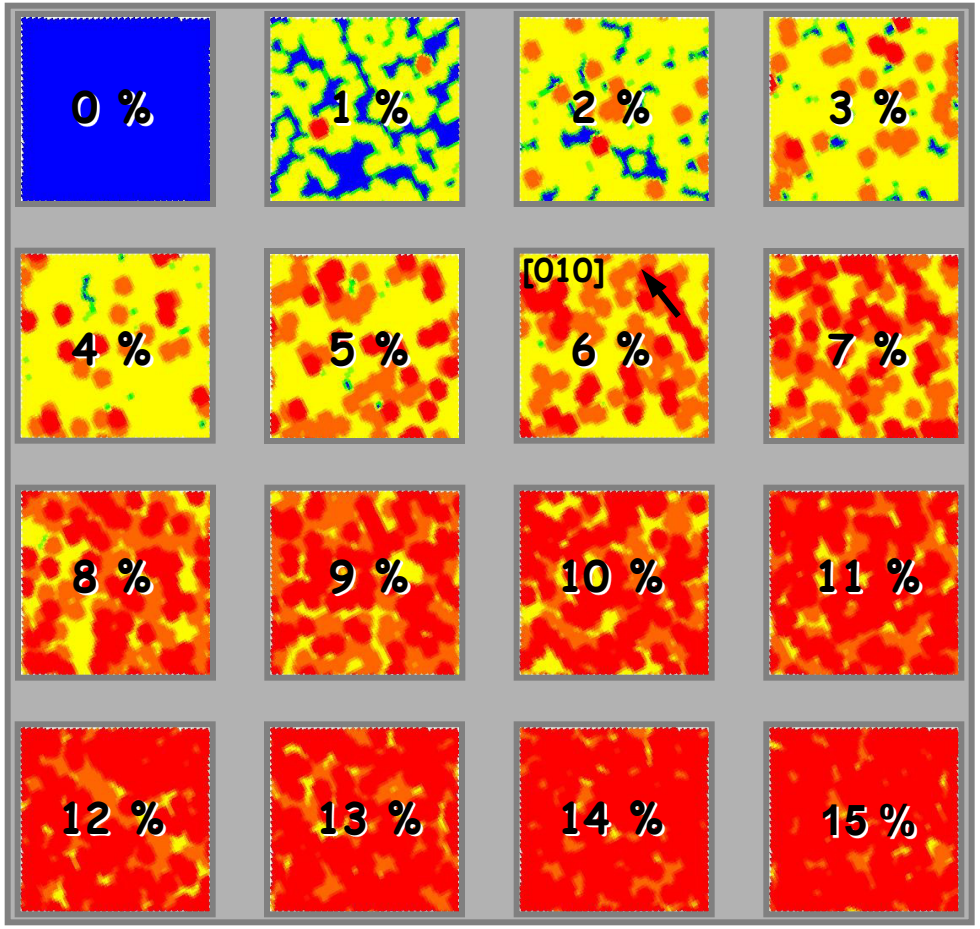


~10% fully metallic surface

Experiment

@350 K @400 K

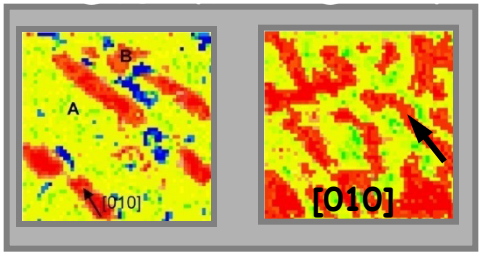


$V_2O_5(010) \rightarrow V_6O_{13}(001) \rightarrow V_2O_3(0001)$ @800 K

# Heating the $V_2O_5$ (001) surface up to 800 K

$$V_2O_5(010) \rightarrow V_6O_{13}(001) \rightarrow V_2O_3(0001)$$

$V_6O_{13}$(001) metal

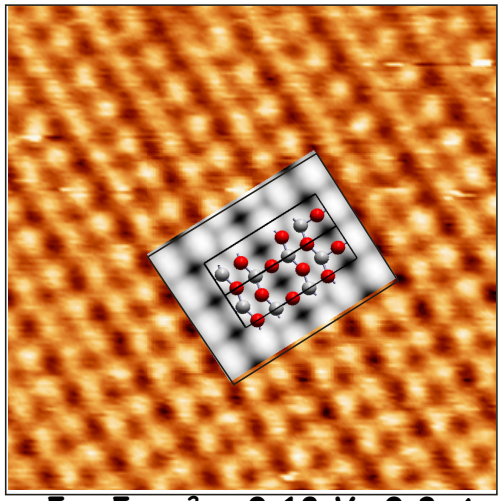

5 × 5 nm², +0.18 V, 0.3nA
Unoccupied states

$V_2O_3$(0001) metal

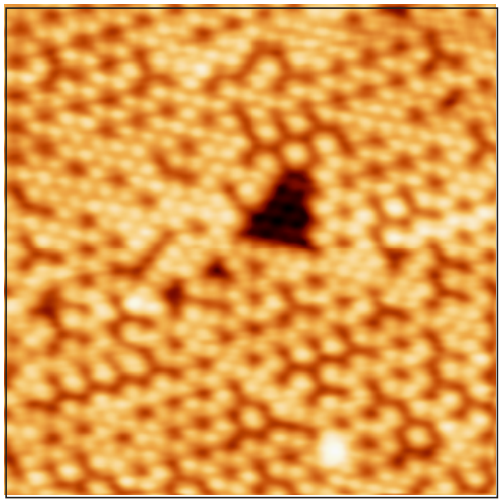

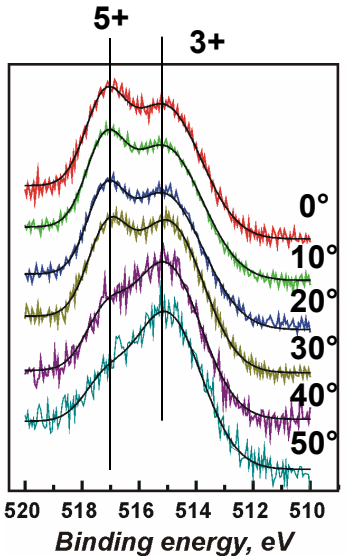


reconstruction involves only the outermost layers

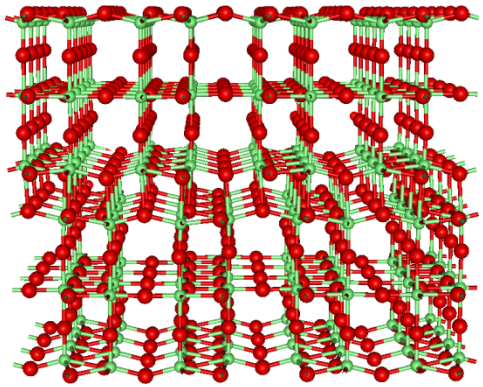

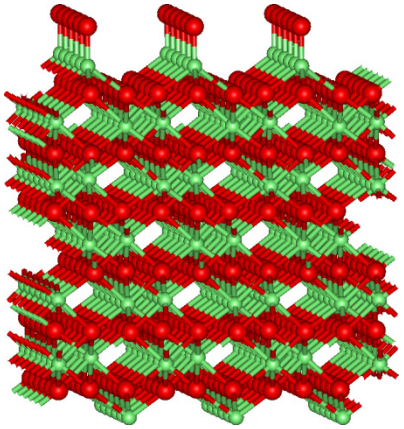

vanadyl terminated
up to 1000 K


Dupuis, Abu Haija, Richter, Kuhlenbeck, Freund, Surf. Sci. 233, 75 (2003)

Schoiswohl, Sock, Surnev, Ramsey, Netzer, Kresse, Andersen, Surf. Sci. 555, 101 (2004)

# Revised stability of reduced $V_2O_5$(001)

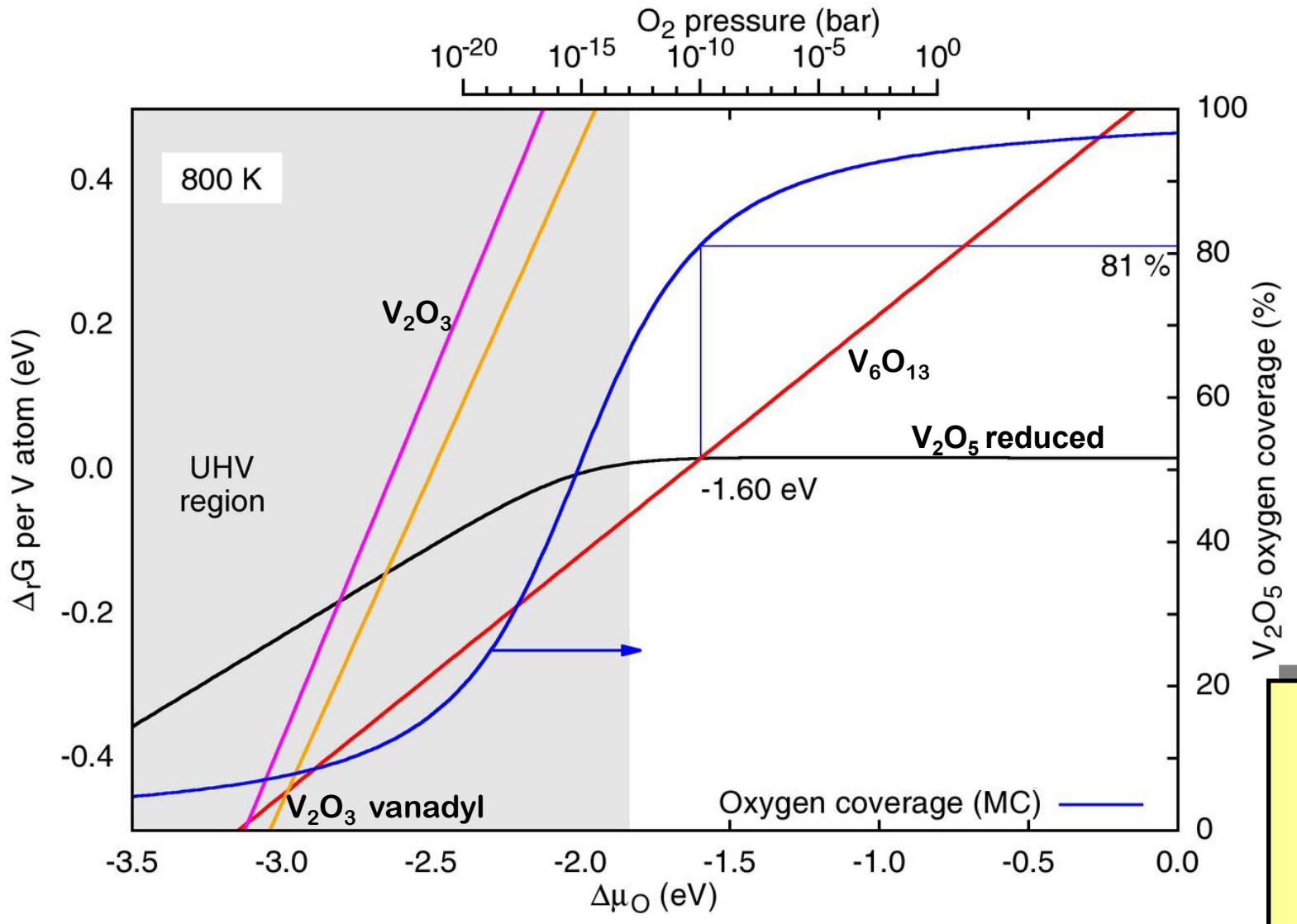


350 K: 2.6%

400 K: 3.4%

800 K: $V_6O_{13}$

# Final remarks

**Theoretical results concur with recent experimental findings**

@300-400 K

$V_2O_5(001)$ surface MIT due to oxygen loss

- Vanadyl defects grow along the [010] direction forming trenches (up to 10 sites)

@800 K

$V_2O_5(001) \rightarrow V_6O_{13}(001) \rightarrow V_2O_3(0001)$

- Transition to metallic $V_6O_{13}(001)$ occurs for ~20 % of defects

**DFT, DFT+U, and Monte Carlo simulations helped us rationalize experiments**

# Reducible oxides in catalysis: Ceria

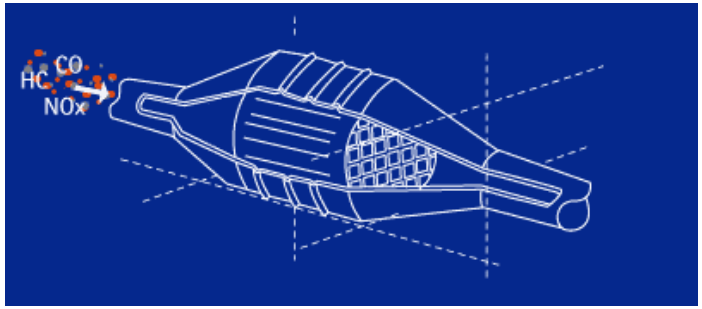


http://www.rhodia-ec.com/site_ec_us/catalysis/index_automotive.htm

## Catalyst formulation

- precious metals Pt, Rh, Pd → active phase
- alumina → support
- Zr-doped ceria → oxygen storage capacity (OSC)
- $ZrO_2$ → enhances OSC, thermal stability

## Catalytic converter

transforms the primary pollutants in the exhaust gas into non-toxic less harmful compounds

$$2NO_x \rightarrow xO_2 + N_2$$
$$2CO + O_2 \rightarrow 2CO_2$$
$$2C_xH_y + (2x+y/2)O_2 \rightarrow 2xCO_2 + yH_2O$$

$CO_2$ is a pollutant as a greenhouse gas

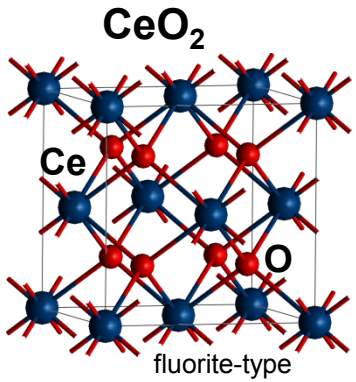


fluorite-type

### Oxygen Storage Capacity

an 'oxygen-sponge'

releasing and absorbing oxygen according to the catalytic reaction required (oxidation or reduction)

$$Ce^{4+} \leftrightarrow Ce^{3+}$$

**$CeO_2$ supported metal and oxide catalysts are singled out as very promising for various reactions; ceria can supply its lattice oxygen**

# $CeO_2(111)$: Formation of neutral oxygen defects

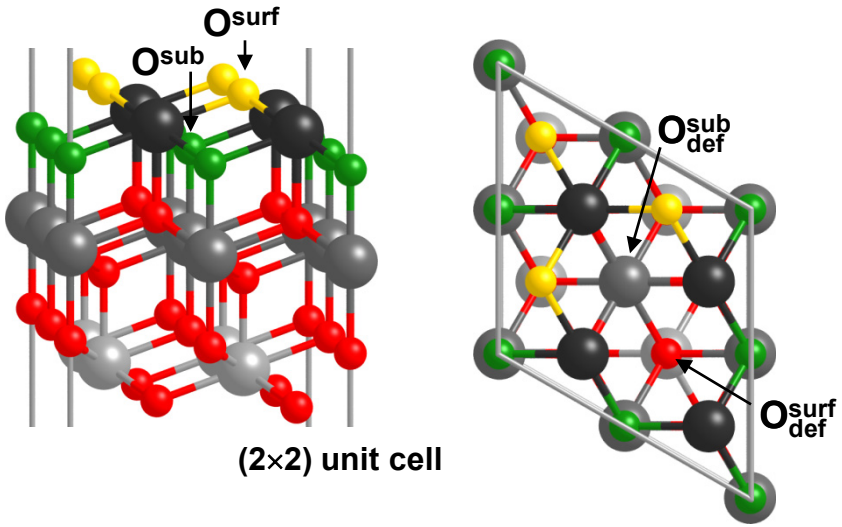


(2×2) unit cell

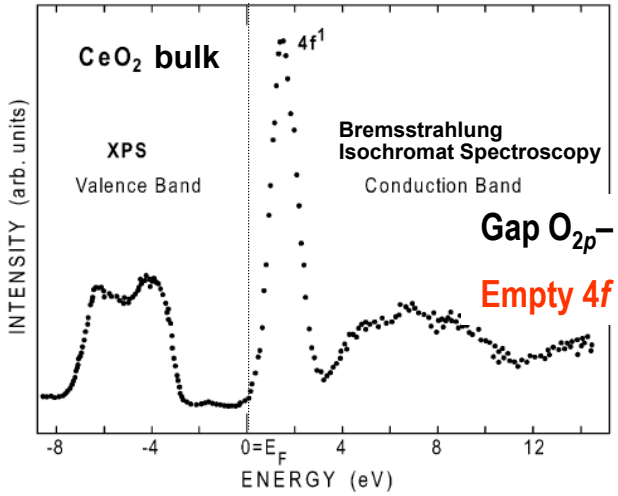


Fig. 3. XPS and BIS spectra of $CeO_2$.

Ce $4f^0$

Gap $O_{2p}$– $Ce_{5d}$: 6.0 eV

Empty *4f* states in the gap

P. Wachter, Physica A (2001)

- **UPS/XPS:** Defect state in the $O_{2p}$–$Ce_{4f}$ gap, ~1.2 eV above top valence band; $Ce_{4f}$ nature
- **XPS/EPR:** $Ce^{4+} \rightarrow Ce^{3+}$

Generally accepted view:

$Ce^{3+}$ in nearest neighbor positions

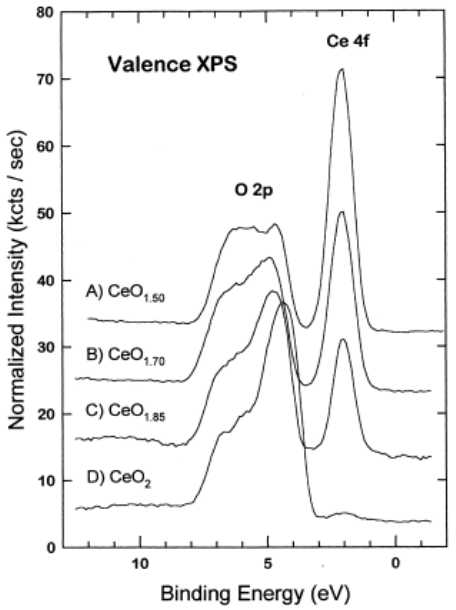


D. R. Mullins et al., Surf. Sci. (1999)

# The choice of the computational method

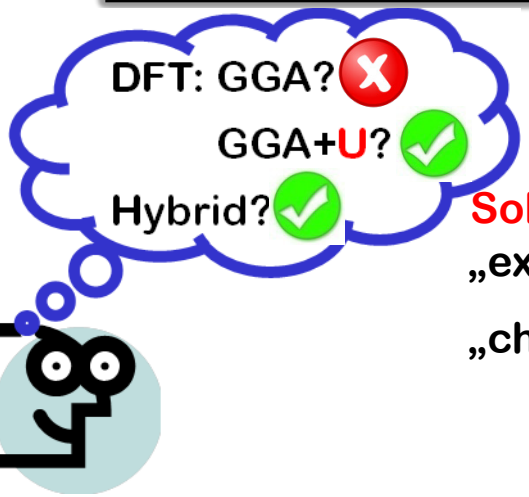


**Problems**: electron delocalization
metallic character

Da Silva, Ganduglia-Pirovano, Sauer, Bayer, Kresse, PRB 75 (2007)

Ganduglia-Pirovano, Hofmann, Sauer, Surf. Sci. Rep. 62 (2007)

**Solutions**:

„expensive“ solution: Hybrid-DFT — exact-exchange

„cheap“ solution: DFT (LDA/GGA)+U — on-site Coulomb repulsion

Dudarev st al., PRB 57 (1998)

$U_{GGA}$ = 4.5 eV Cococcioni, de Gironcoli, PRB 71 (2005)

❑ Creation of a neutral O vacancy $2 \times Ce^{4+} \rightarrow 2 \times Ce^{3+}$

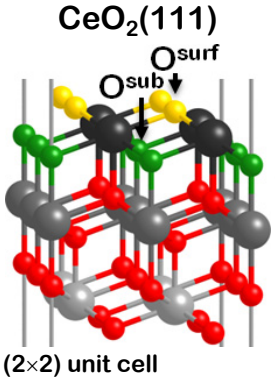


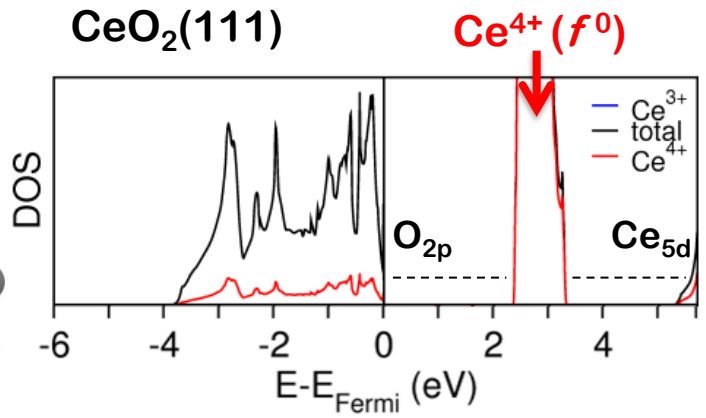


insulator $Ce^{4+}$ ($f^0$)

$CeO_{2-x}(111)$

Θ=1/4

all Ce ions partially reduced !

$Ce^{(4-\delta)+}$

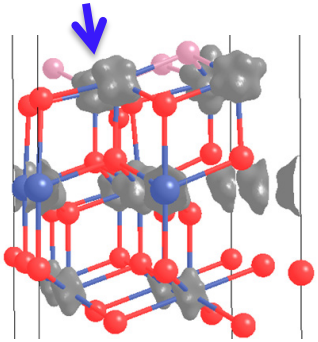

metal $Ce^{(4-\delta)+}$

PBE

# The choice of the computational method

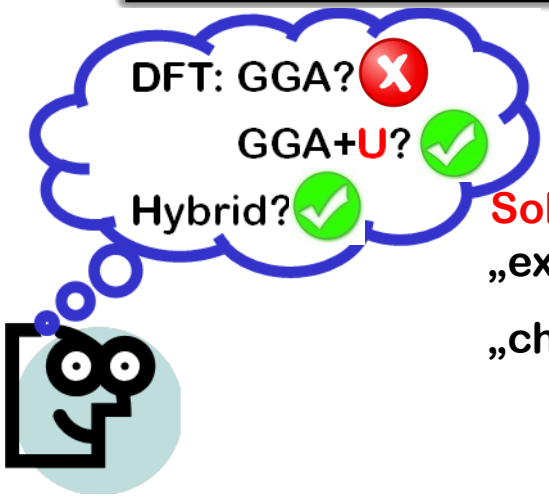


**Problems**: electron delocalization
metallic character

Da Silva, Ganduglia-Pirovano, Sauer, Bayer, Kresse, PRB 75 (2007)

Ganduglia-Pirovano, Hofmann, Sauer, Surf. Sci. Rep. 62 (2007)

**Solutions**:

„expensive“ solution: Hybrid-DFT — exact-exchange

„cheap“ solution: DFT (LDA/GGA)+U — on-site Coulomb repulsion

Dudarev st al., PRB 57 (1998)

$U_{GGA}$ = 4.5 eV Cococcioni, de Gironcoli, PRB 71 (2005)

❑ Creation of a neutral O vacancy $2 \times Ce^{4+} \rightarrow 2 \times Ce^{3+}$

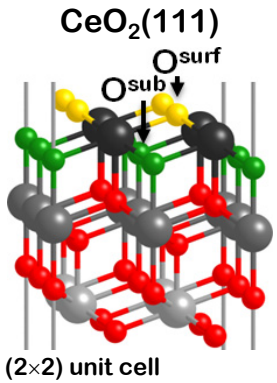


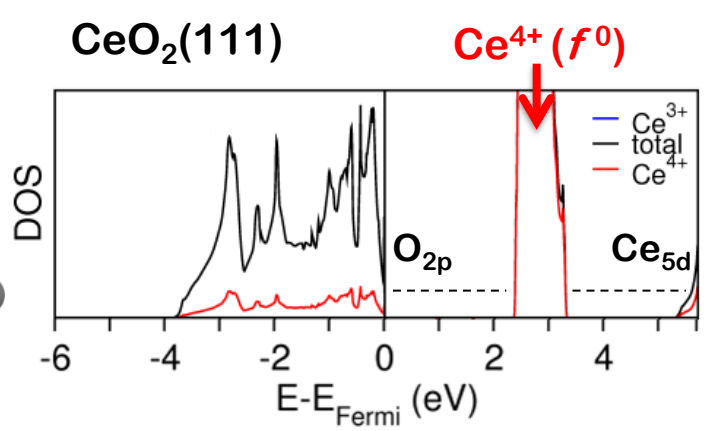


insulator $Ce^{4+}$ ($f^0$)

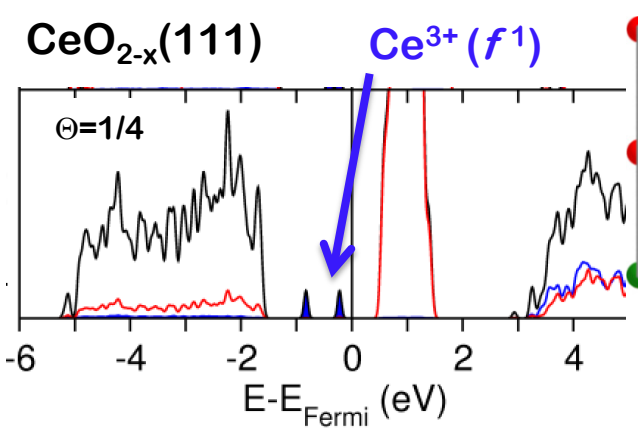


insulator $Ce^{3+}$ ($f^1$)

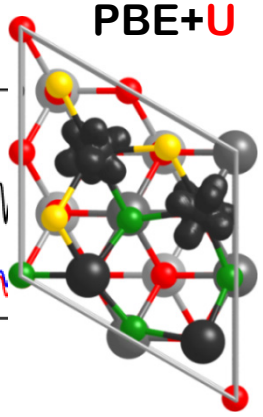

# Ceria bulk: Structure and electronic properties

Da Silva, Ganduglia-Pirovano, Sauer, Bayer, Kresse, PRB 75, 045121 (2007)

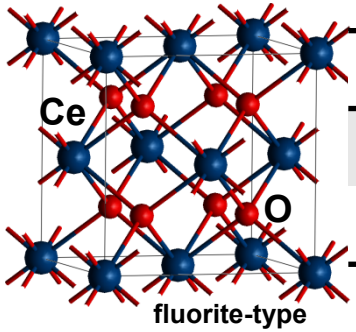

fluorite-type

| $CeO_2$ | HSE* | exp. |
|---|---|---|
| $a_0$ (Å) | 5.40 | 5.41 |
| $O_{2p}$-$Ce_{5d}$ gap (eV) | 7.0 | 6.0 |

| $Ce_2O_3$ –AF | HSE* | exp. |
|---|---|---|
| $a_0$ (Å) | 3.87 | 3.89 |
| $c_0$ (Å) | 6.08 | 6.06 |
| $Ce_{4f}$-$Ce_{5d+4f}$ gap (eV) | 2.5 | 2.4 |

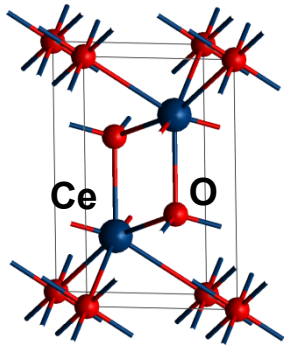

hexagonal-type

## Equilibrium volume

- **Hybrid:** –1% underestimation

## Band gap

- **Hybrid:** ~1 eV larger than exp $CeO_2$

* In agreement with P.J. Hay, R.L. Martin, J. Uddin, G. Scuseria, J. Chem. Phys. 125, 034712 (2006)

# Ceria bulk: Structure and electronic properties

Da Silva, Ganduglia-Pirovano, Sauer, Bayer, Kresse, PRB 75, 045121 (2007)

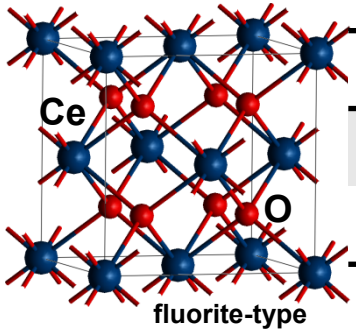

fluorite-type

| $CeO_2$ | HSE* | LDA+U | PBE+U | exp. |
|---|---|---|---|---|
| $a_0$ (Å) | 5.40 | 5.40 | 5.49 | 5.41 |
| $O_{2p}$-$Ce_{5d}$ gap (eV) | 7.0 | 5.3 | 5.3 | 6.0 |

$U_{LDA}$= 5.3 eV

$U_{GGA}$= 4.5 eV

| $Ce_2O_3$ –AF | HSE* | LDA+U | PBE+U | exp. |
|---|---|---|---|---|
| $a_0$ (Å) | 3.87 | 3.86 | 3.92 | 3.89 |
| $c_0$ (Å) | 6.08 | 5.96 | 6.18 | 6.06 |
| $Ce_{4f}$-$Ce_{5d+4f}$ gap (eV) | 2.5 | 2.4 | 2.6 | 2.4 |

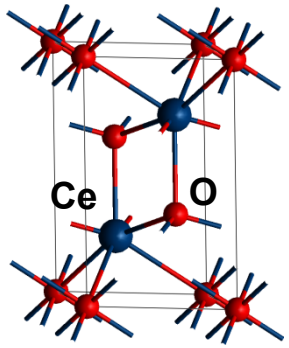

hexagonal-type

## Equilibrium volume

- **Hybrid:** –1% underestimation
- **LDA+U:** –0.6% ($CeO_2$); –3.2% ($Ce_2O_3$)
- **PBE+U:** +4.5% ($CeO_2$); +3.6% ($Ce_2O_3$)

## Band gap

- **Hybrid:** ~1 eV larger than exp. gap $CeO_2$
- **DFT+U:** ~1 eV smaller than exp. gap ($CeO_2$)
  U shifts *f*-states in the gap

# The dependence on the U parameter: Structure

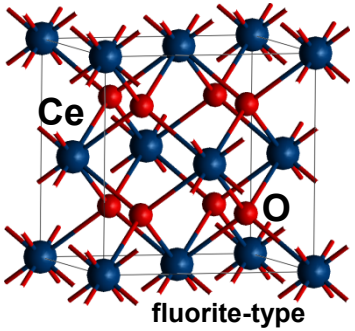


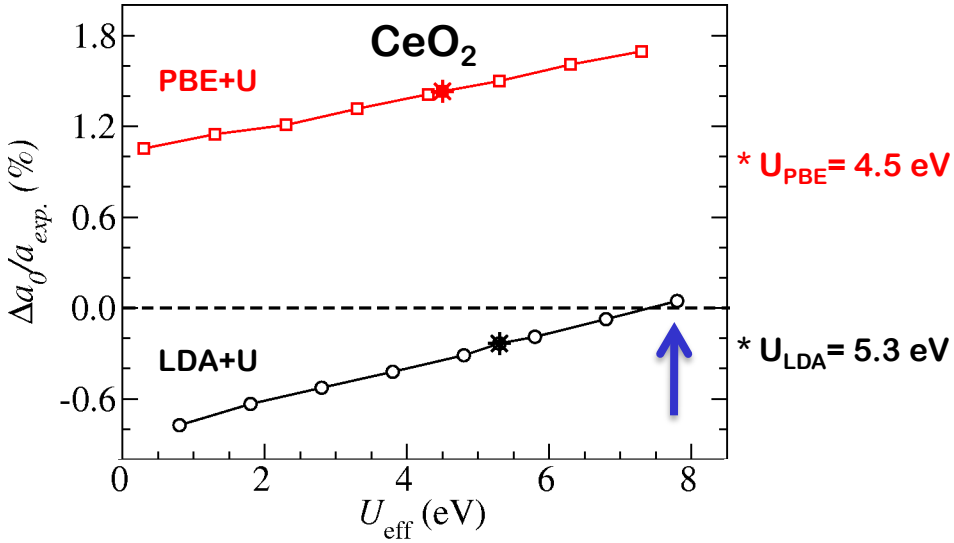


* $U_{PBE}$= 4.5 eV

* $U_{LDA}$= 5.3 eV

❑ linear increase with U

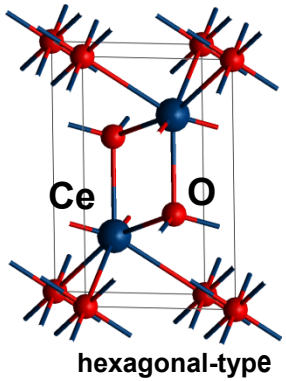


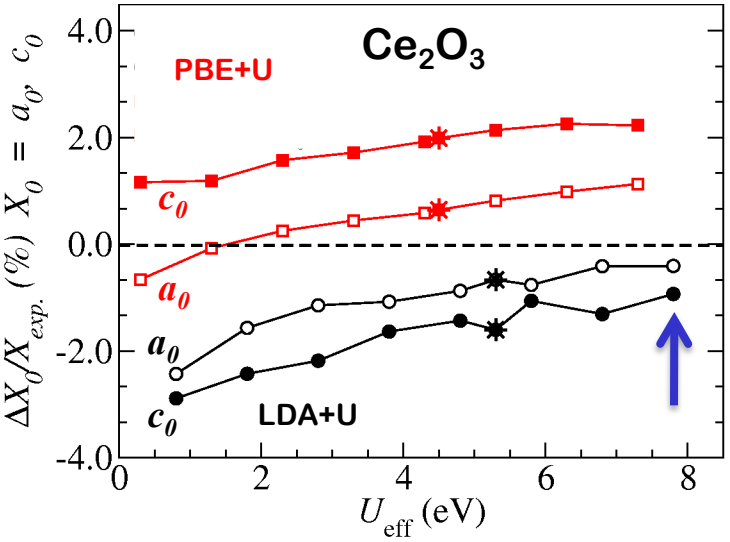


❑ LDA+U(~8 eV) close to exp.

# The dependence on the U parameter: Band gap

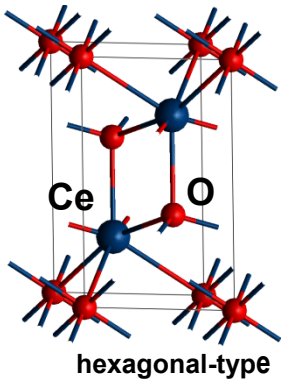


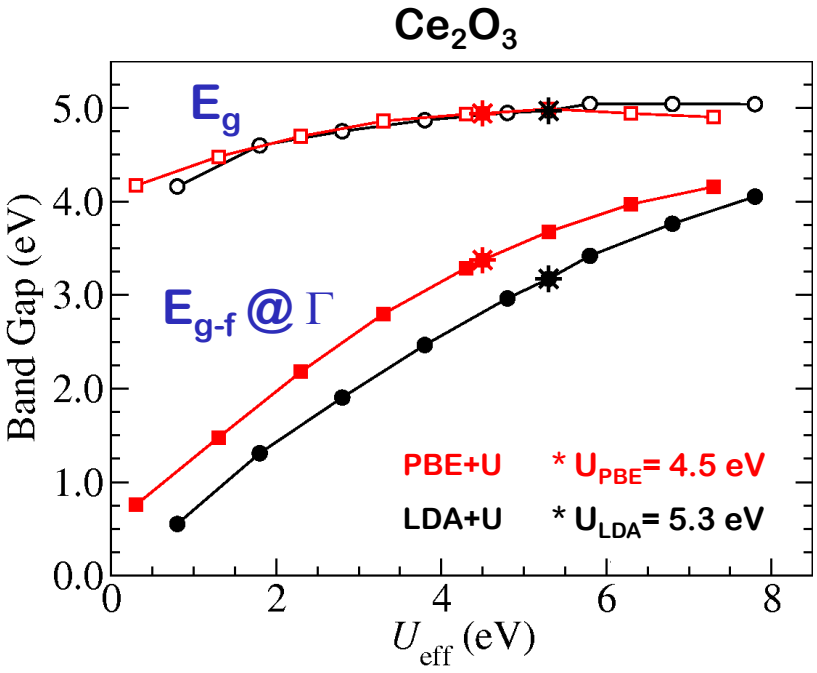


- $E_g$ roughly constant
- U shifs f-states

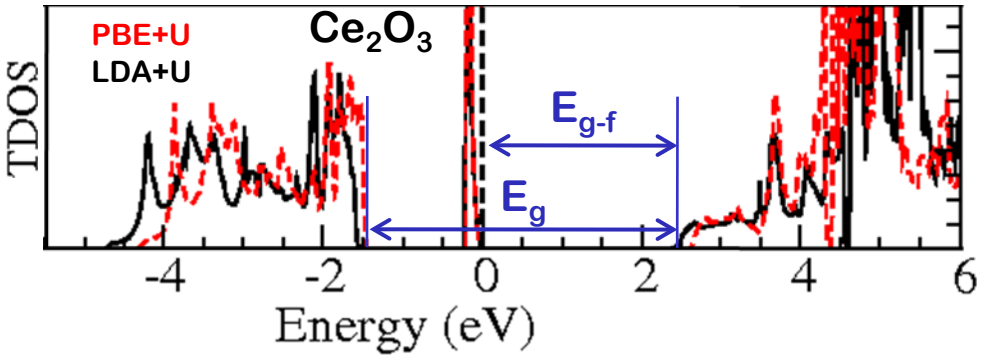


smaller U:

- occupied f-states toward CB ($Ce_2O_3$); smaller $E_{g-f}$ gap
- empty f-states away CB ($CeO_2$)

# Ceria bulk: Thermodynamic properties

Da Silva, Ganduglia-Pirovano, Sauer, Bayer, Kresse, PRB 75, 045121 (2007)

$$2CeO_2 \rightarrow Ce_2O_3 + \frac{1}{2} O_2$$

| | HSE | LDA+U | PBE+U | exp. |
|---|---|---|---|---|
| $\Delta H$(eV) | 3.16 | 3.04 | 2.29 | 3.57/4.03 |

## Reduction energy

- Hybrid: 0.4 – 0.9 eV underestimation
- LDA+U: 0.5 – 1.0 eV
- PBE+U: 1.3 – 1.7 eV

Not fully satisfactory ☹

# The dependence on the U: Thermodynamic properties

$$2CeO_2 \rightarrow Ce_2O_3 + \tfrac{1}{2} O_2$$

| | PBE0 | HSE | LDA+U | PBE+U | exp. |
|---|---|---|---|---|---|
| $\Delta H$(eV) | 3.14 | 3.16 | 3.04 | 2.29 | 3.57/4.03 |

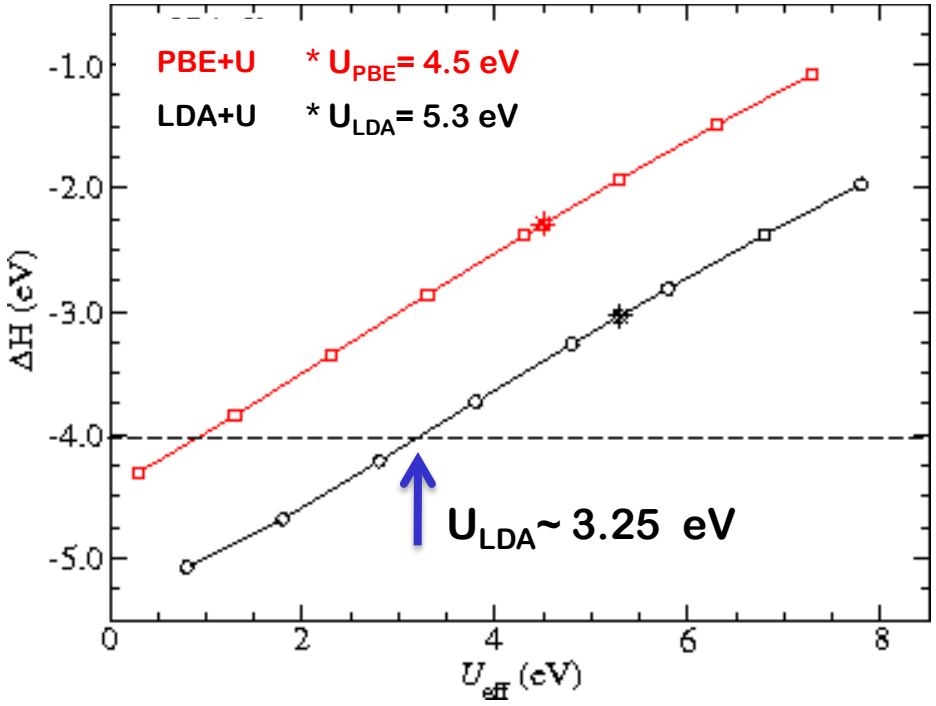


- linear dependence with U

smaller U:

- corrects reduction energy ☺
- yields a smaller $E_{g\text{-}f}$ $Ce_2O_3$ gap ☹
- yields a smaller $Ce_2O_3$ volume ☹

**No unique U for best description of all properties**

# $CeO_2(111)$: Structure of near-surface oxygen defects

STM
occupied states–O lattice

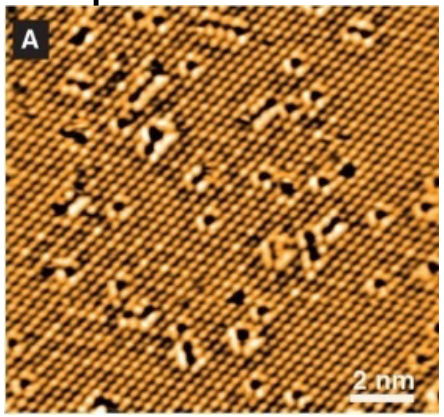


1 min 900ºC + cooling 300ºC

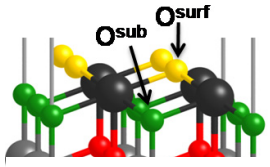


surface defect

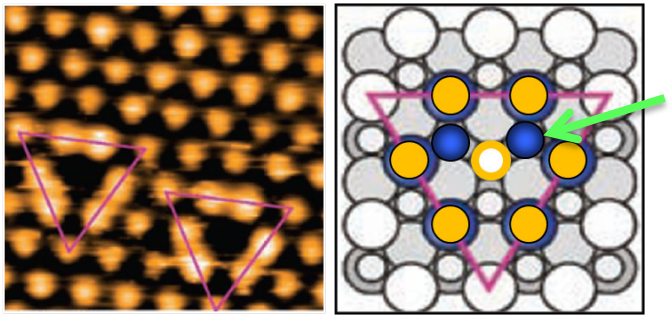


subsurface defect

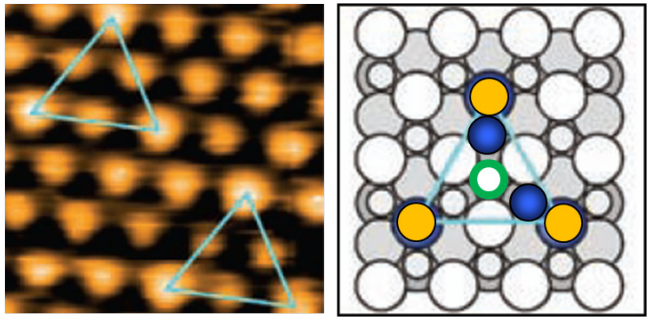

Esch, Fabris, et al., Science 309, 752 (2005)

LDA+U

**Theory: Excess charge on N.N.**

Defect formation energy [eV]

$\Delta E_{def}^{surf\text{-}sub}$

| $Ce^{3+}$ | LDA+U |
|---|---|
| NN–NN | –0.03 |

$U_{LDA}$= 5.3 eV

$\Delta E$ { + sub, - surf

**50%-50% surf-sub**

Defect formation energy [eV]

| $Ce^{+3}$ | surface | | subsurface | | $\Delta E_{def}^{surf\text{-}sub}$ | |
|---|---|---|---|---|---|---|
| | PBE+U | LDA+U | PBE+U | LDA+U | PBE+U | LDA+U |
| NN–NN[1] | 2.15 | 2.92 | 1.89 | 2.95 | +0.26 | –0.03 |

[1] Fabris et al., J. Phys. Chem. B 109, 22860 (2005)

# $CeO_2(111)$: Structure of near-surface oxygen defects

AFM-Topography

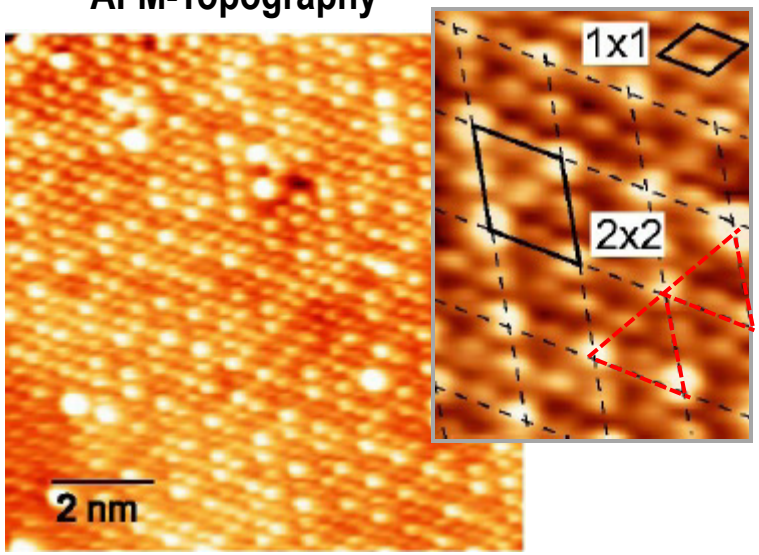


2 min 900ºC + cooling 80 K

Torbrügge et al., PRL 99, 056101 (2007)

STM

Ceria film grown on Pt(111)

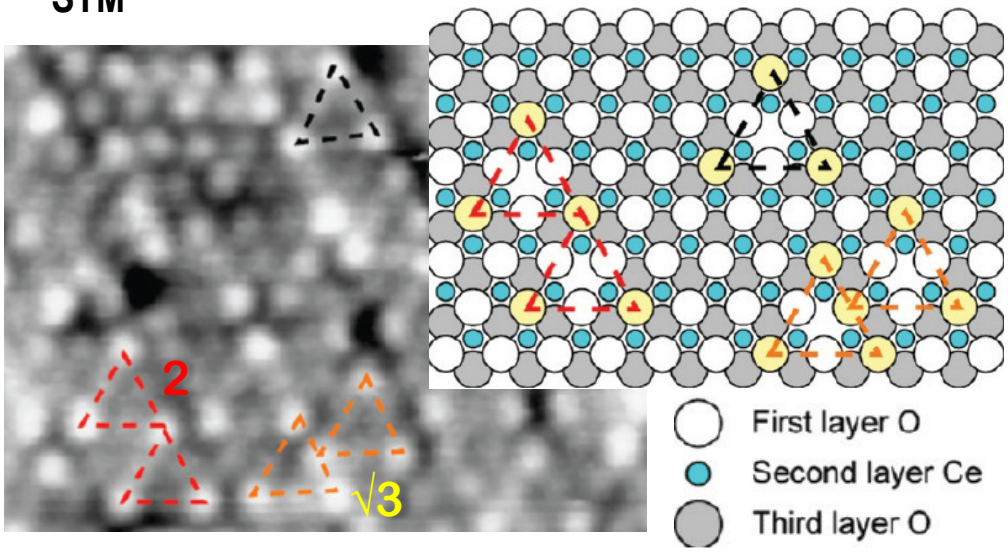


Grinter et al., J. Phys. Chem. C 114, 17036 (2010)

**subsurface** defects

2 lattice spacings separation

**subsurface** defects pairs

√3 and 2 lattice spacings separation

❑ Nature of the repulsive interaction underlying the vacancy ordering?

# $CeO_2(111)$ and its oxygen defect structure

- **isolated** defects and electron localization

Surface or subsurface?

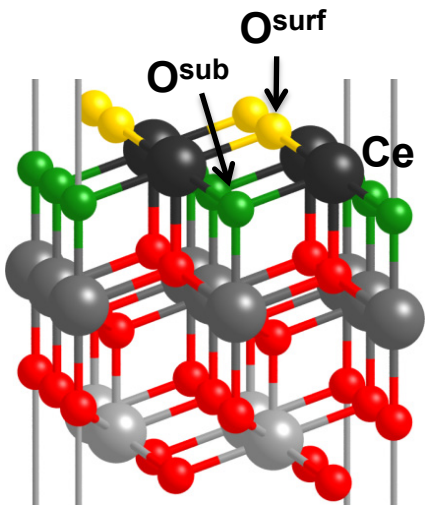


(2×2) unit cell

Where are the $Ce^{3+}$ ?

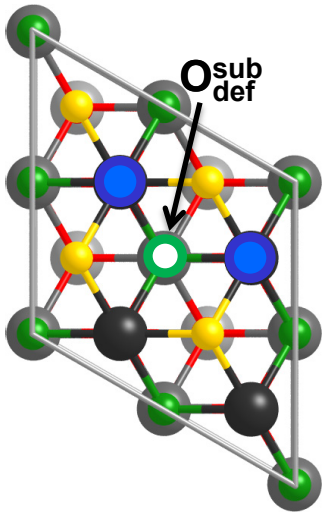


Accepted view:
$Ce^{3+} \rightarrow$ nearest neighbor

- **higher** defect concentration
  - –Thermodynamically stable phase for reducing conditions?
  - –Surface , subsurface, mixed?
  - –Repulsive or attractive interaction? Origin of interaction?

# $CeO_2$(111) subsurface and surface defects: Unrelaxed structures

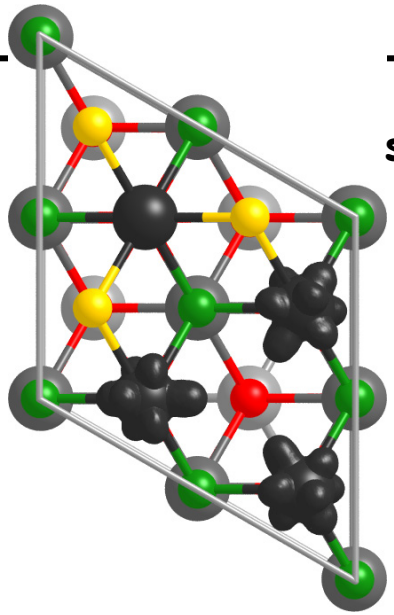

PBE+U spin density

**surface** **subsurface**

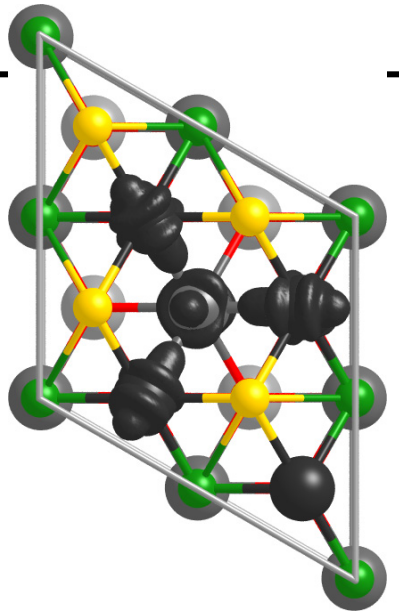

**Defect Formation Energy** $E_{def}$ [eV]

$\Delta E_{def}^{surf\text{-}sub}$

**–0.18 (PBE+U)** **–0.27 (LDA+U)**

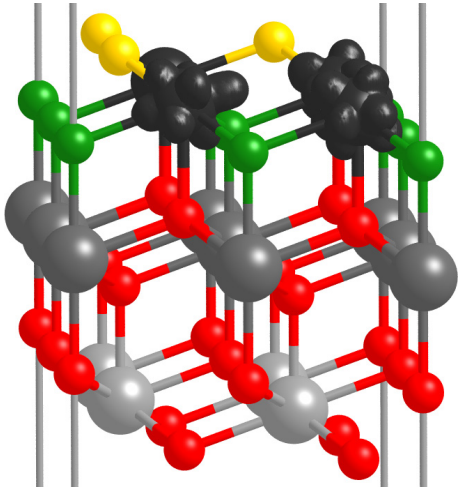

unrelaxed strutures:

preference for surface defects

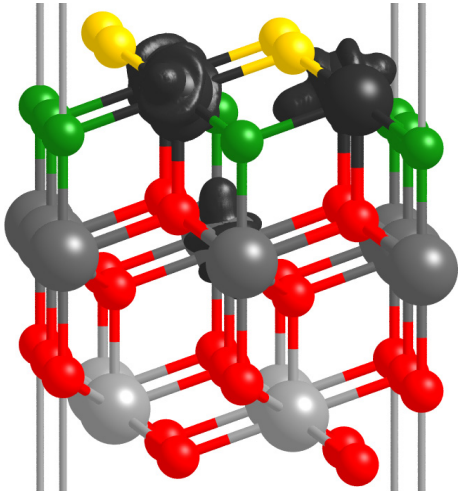

localization on the 3 nearest neighbors

localization on the 4 nearest neighbors

M. V. Ganduglia-Pirovano, J. L. F. Da Silva, J. Sauer, PRL 102, 026101 (2009)

# $CeO_2$(111) defects: The excess charge localization

Ganduglia-Pirovano, Da Silva, Sauer, PRL 102, 026101 (2009)

**surface**

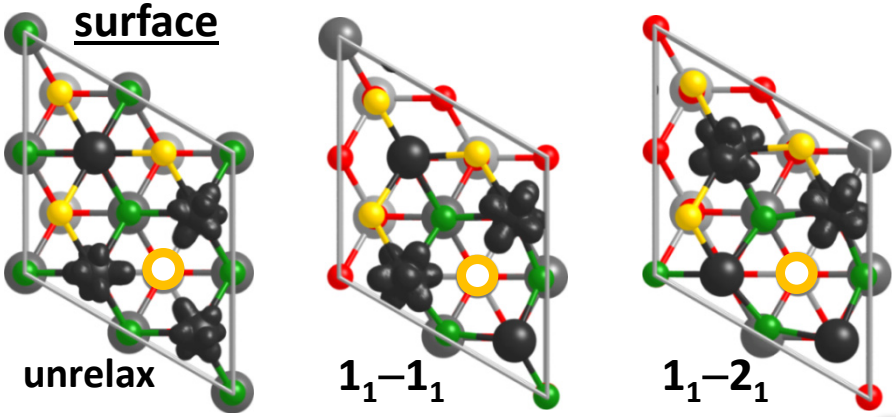


**HSE spin density–FM**

❑ DFT predicts multiple local minima

**subsurface**

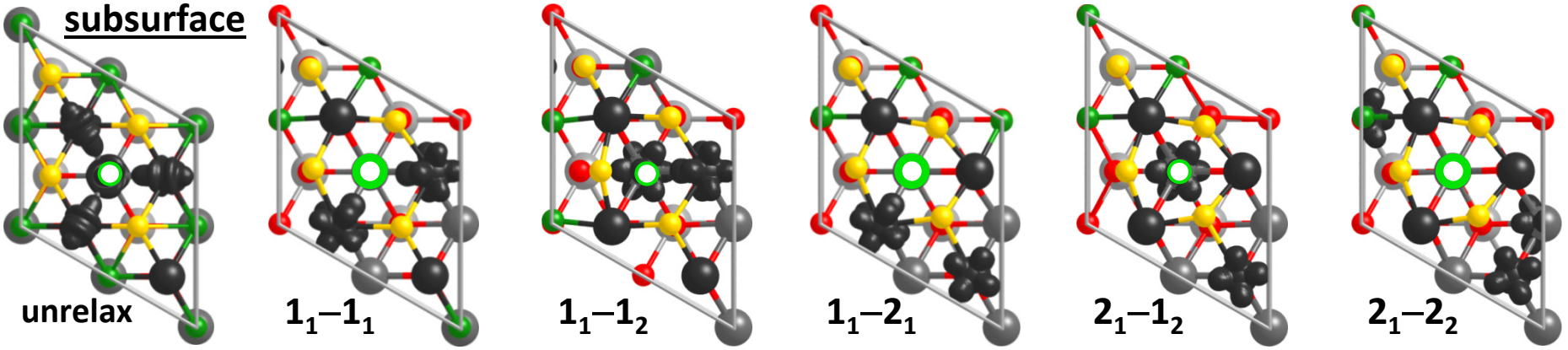

# The defect formation energy wrt. ½ $O_2$ [eV]

Ganduglia-Pirovano, Da Silva, Sauer, PRL 102, 026101 (2009)

**surface**

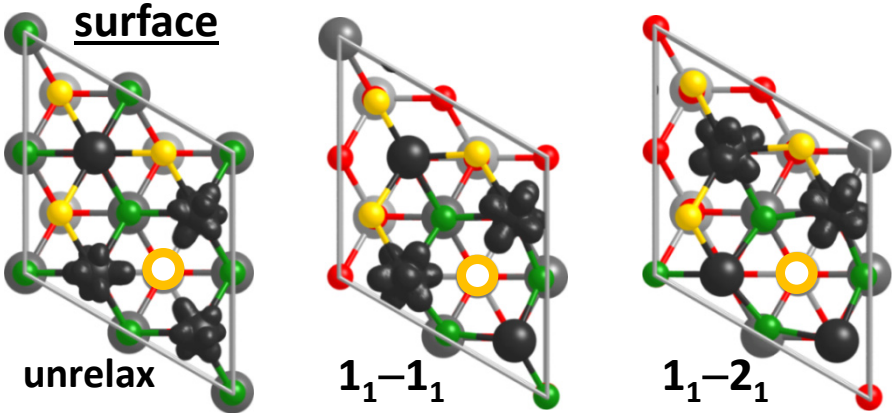


| | $1_1$–$1_1$ | $1_1$–$2_1$ |
|---|---|---|
| HSE | 3.30 | 3.10 |
| LDA+U | 3.31 | 3.21 |
| PBE+U | 2.50 | 2.34 |

**Defects are prone to be bound to $Ce^{4+}$ !!**

**subsurface**

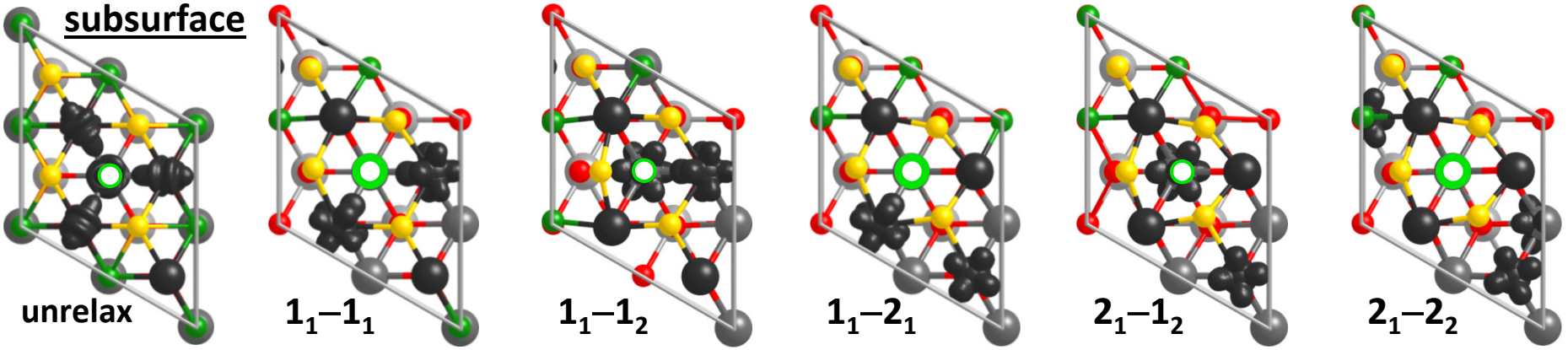


| | $1_1$–$1_1$ | $1_1$–$1_2$ | $1_1$–$2_1$ | $2_1$–$1_2$ | $2_1$–$2_2$ |
|---|---|---|---|---|---|
| HSE | 3.21 | | 2.79 | | 2.65 |
| LDA+U | 3.39 | 3.40 | 3.08 | 3.17 | 2.99 |
| PBE+U | 2.38 | 2.40 | 2.00 | 2.08 | 1.87 |

# $CeO_2(111)$ defects: Surface vs. subsurface

**STM & LDA+U**: Esch et al., Science 309,752 (2005) → **50%–50%**

**AFM**: Torbrügge et al., PRL 99, 056101(2007)→ **subsurface**

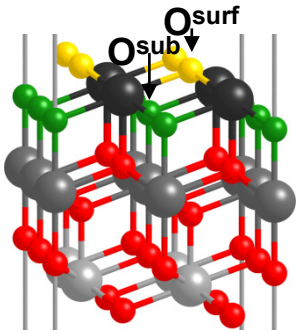


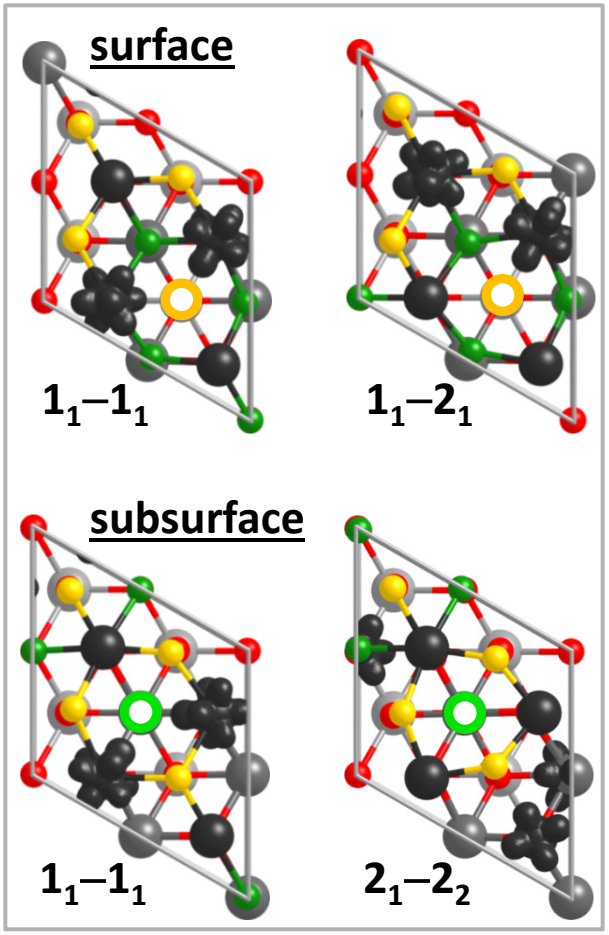


Defect formation energy [eV]

$\Delta E_{def}^{surf\text{-}sub}$

| $Ce^{3+}$ | HSE | LDA+U | PBE+U |
|---|---|---|---|
| NN[1] | | –0.03 | +0.26 |
| NN | +0.09 | –0.08 | +0.12 |
| NNN | +0.45 | +0.22 | +0.47 |

$\Delta E$ { + sub, – surf

[1] Fabris et al., JPCB 109, 22860 (2005)

**The subsurface position is considerable more stable than the surface one**

Ganduglia-Pirovano, Da Silva, Sauer, PRL 102, 026101 (2009)

# The lattice relaxation effects

Ganduglia-Pirovano, Da Silva, Sauer, PRL 102, 026101 (2009)

❑ Ce move away and O towards the vacant site → **tension-compression regions**

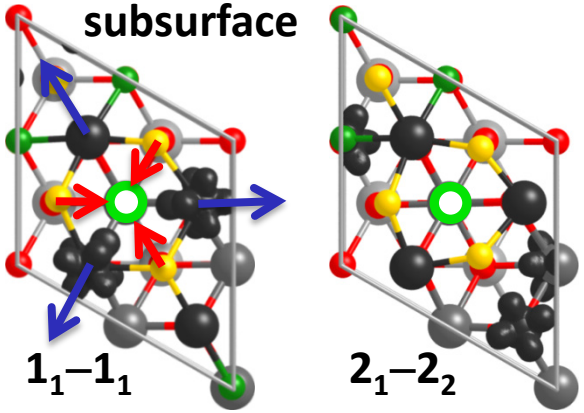


Compressed $Ce^{3+}$ in NN sites

subsurface defect

| $Ce^{3+}$ | $E_{def}$(eV) | $Ce^{3+}$–O (Å) |
|---|---|---|
| NN | 3.10 | 2.39; 2.39 |
| NNN | 2.65 | 2.47; 2.44 |

HSE-structures

$Ce_2O_3$: 2.50 Å

**Lattice relaxation effects are crucial**

- ❑ **localization phenomenon**
- ❑ **proneness of defects to be bound by $Ce^{4+}$**

# Lattice relaxation effects and the subsurface preference

Energy gain due to relaxation [eV]

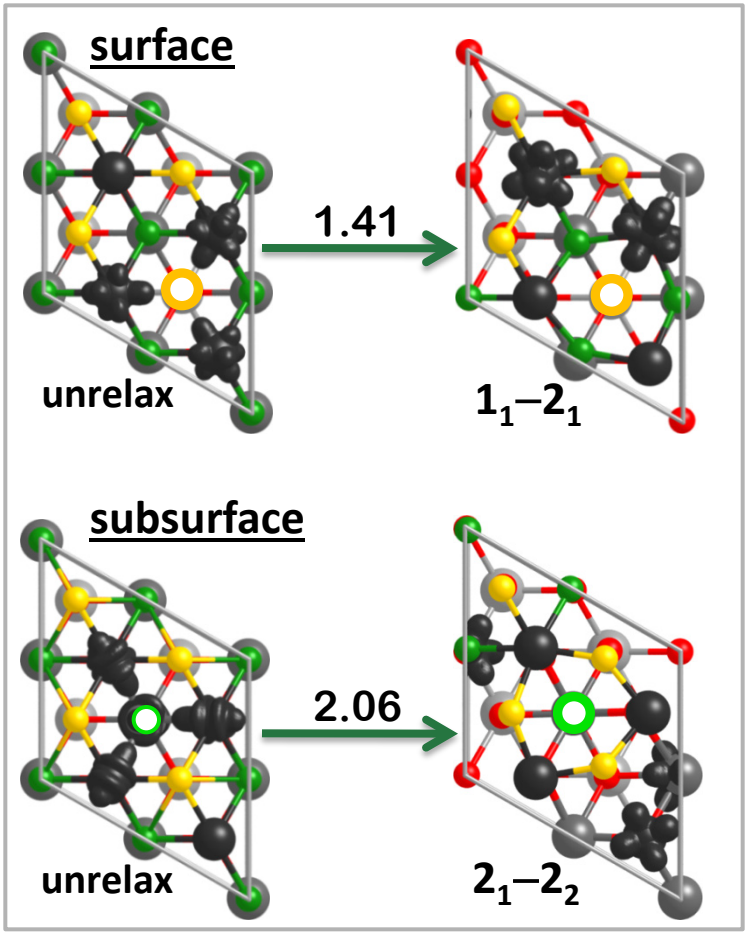


Defect formation energy [eV]

$\Delta E \begin{cases} + \text{ sub} \\ - \text{ surf} \end{cases}$

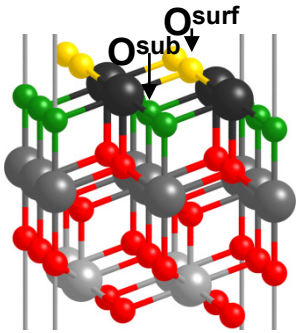


| | $\Delta E_{def}$ PBE+U |
|---|---|
| unrelax | –0.18 |
| NNN | +0.47 |

Lattice relaxation effects are crucial to the subsurface preference

Ganduglia-Pirovano, Da Silva, Sauer, PRL 102, 026101 (2009)

# Electron localization in defective $CeO_2(111)$ films

## Ceria film grown on Ru(0001)

Jerratsch, Shao, Nilius, Freund, Popa, Ganduglia-Pirovano, Sauer, PRL 106, 246801 (2011)

**STM**

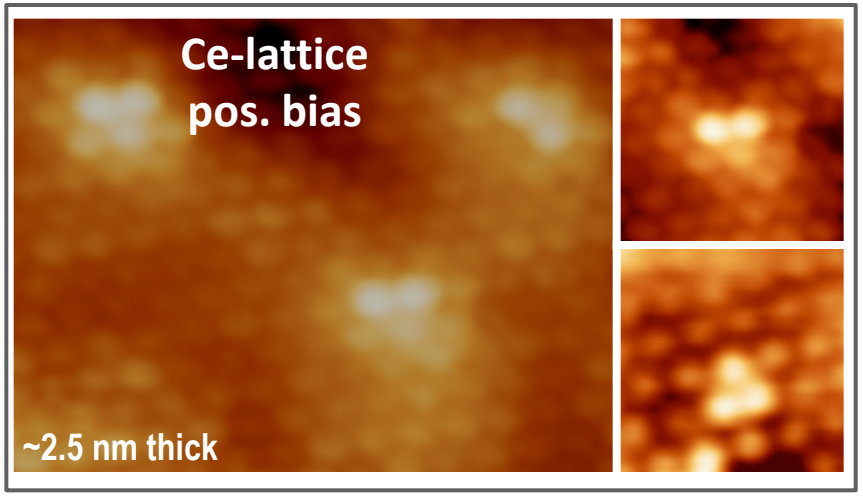


$U_s$ = 1.1 V, 5.5 × 5.5 nm$^2$ 1.8 × 1.8 nm$^2$

- irradiation with 50 eV electrons → surface defects
- double/triple protrusions at positive bias
- O-lattice at negative bias

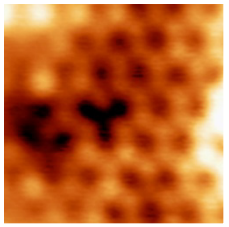

**STS** unreduced ceria

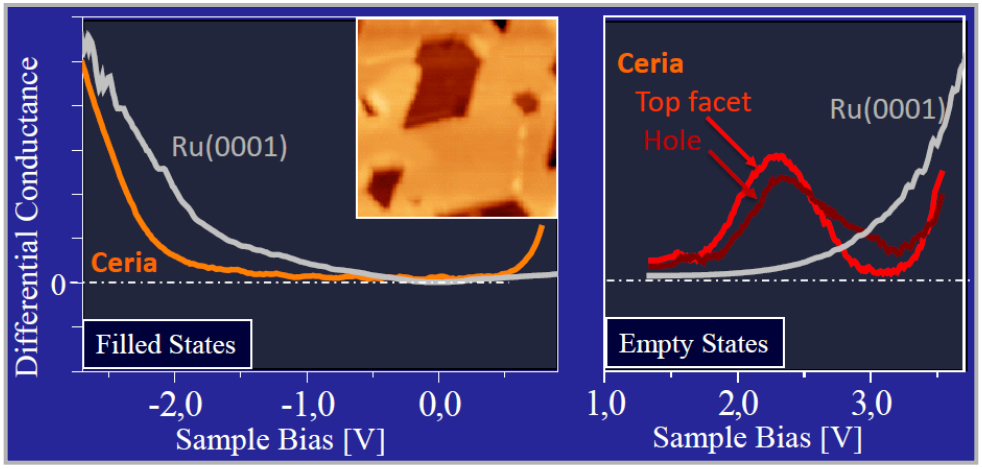


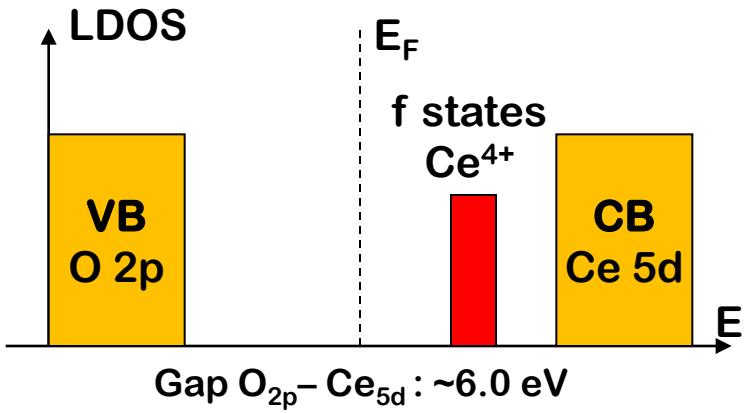


Gap $O_{2p}$– $Ce_{5d}$ : ~6.0 eV

Empty 4f states *in* the gap

# Reduced $CeO_2$(111): STS-Experiment

Jerratsch, Shao, Nilius, Freund, Popa, Ganduglia-Pirovano, Sauer, PRL 106, 246801 (2011)

reduced ceria

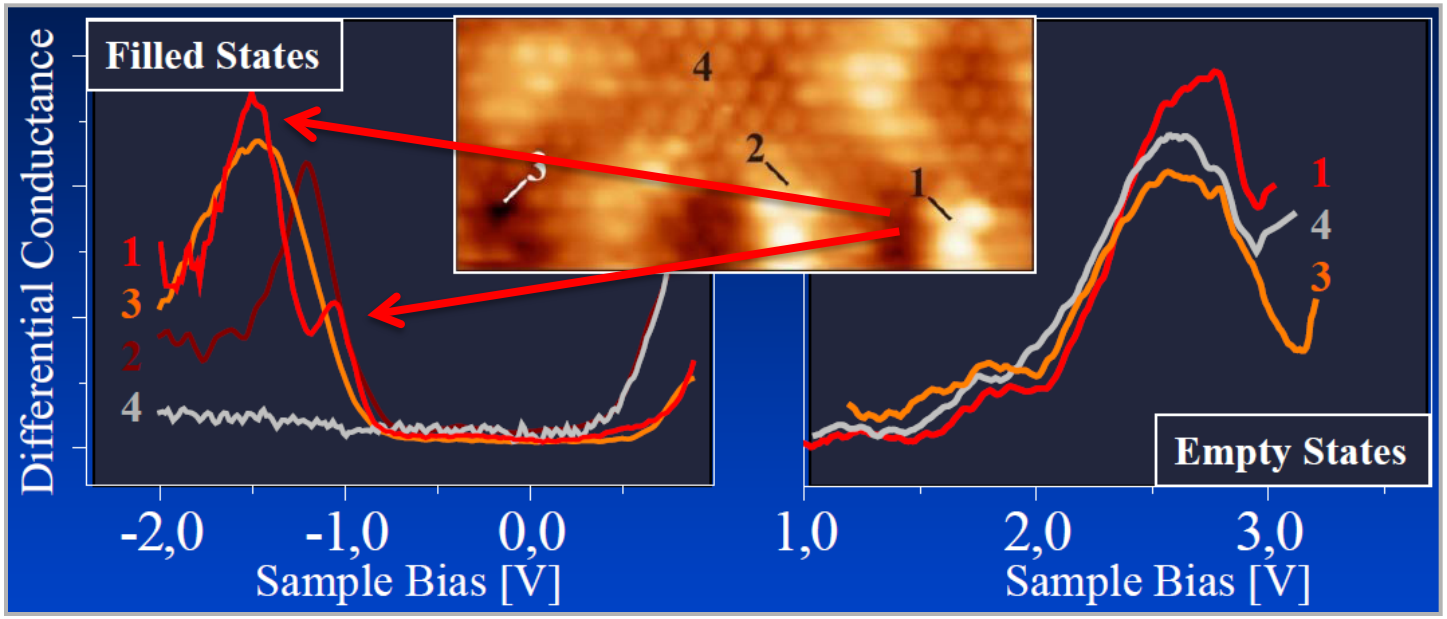


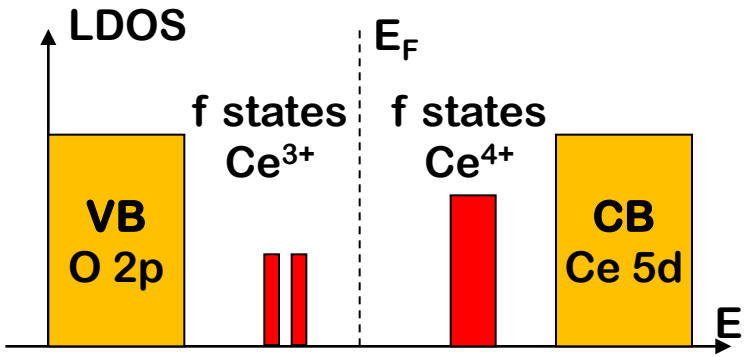


- Filled 4f states in reduced $CeO_2$ films
- Splitting of 4f states for pair protusion

# Reduced $CeO_2$(111): STS-Experiment

Jerratsch, Shao, Nilius, Freund, Popa, Ganduglia-Pirovano, Sauer, PRL 106, 246801 (2011)

reduced ceria

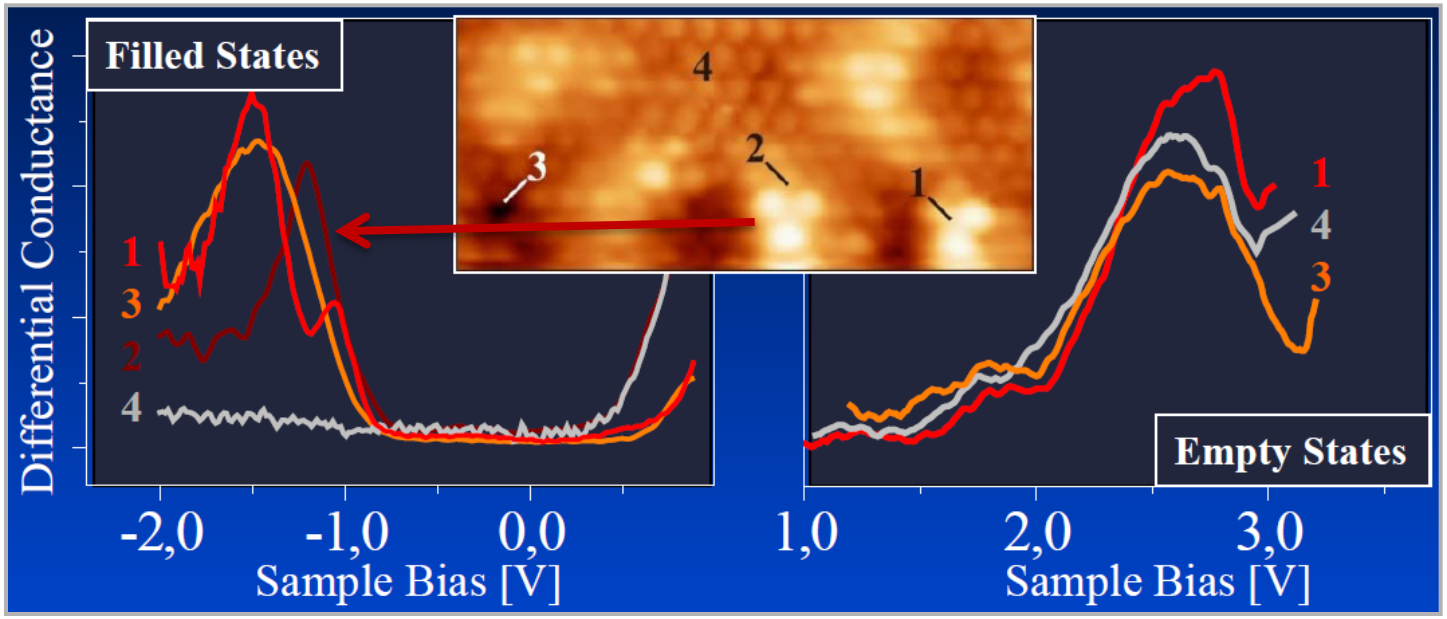


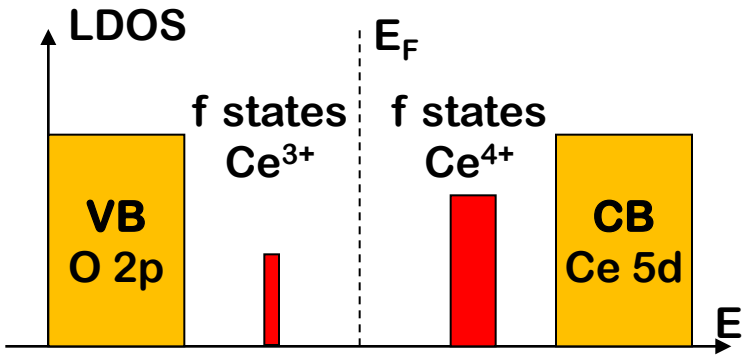


**Where are the $Ce^{3+}$ ions?**

- Filled 4f states in reduced $CeO_2$ films
- No splitting of 4f states for triple protusion

# STM-theory

DFT prediction: defects are prone to be bound to $Ce^{4+}$

Empty state image

$Ce^{3+}$

$Ce^{4+}$

$O^{2-}$

$O_{def}$

| NN–NN | NN–NNN | NNN–NNN |
|---|---|---|
| 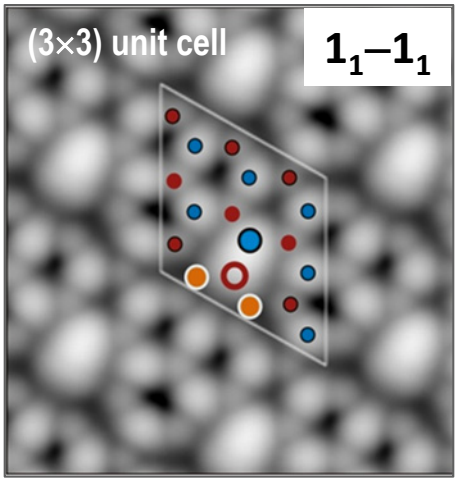  | 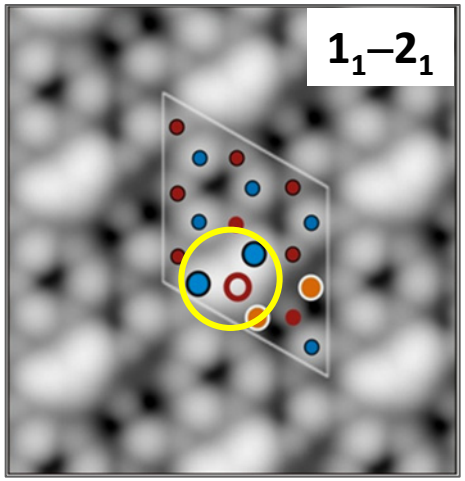  | 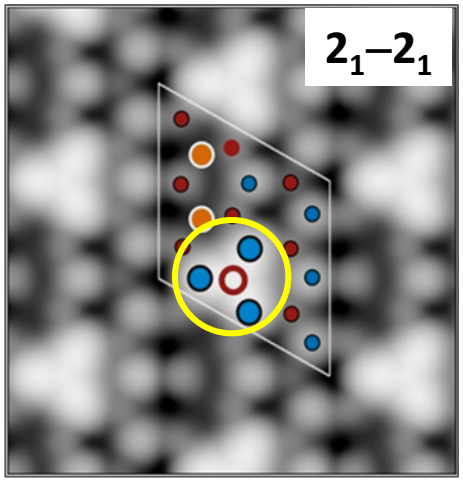  |
| one $Ce^{4+}$ | two $Ce^{4+}$ | three $Ce^{4+}$ |
| Not observed in the Experiment | 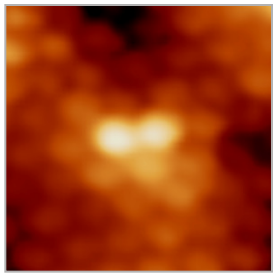 | 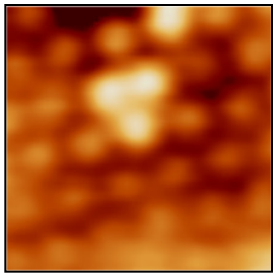 |

- Characteristic defect patterns induced by $Ce^{4+}$ ions next to the defect

  ($2_1$–$2_1$; $3_1$–$2_1$; $4_1$–$2_1$ → triple protusion)

- Tendency of $Ce^{3+}$ ions to be away from the defect; $Ce^{3+}$ are not visible

The DFT prediction is confirmed !

# STM-theory

Jerratsch, Shao, Nilius, Freund, Popa, Ganduglia-Pirovano, Sauer, PRL 106, 246801 (2011)

Empty state image

NNN–NNN

$Ce^{3+}$

$Ce^{4+}$

$O^{2-}$

$O_{def}$

O

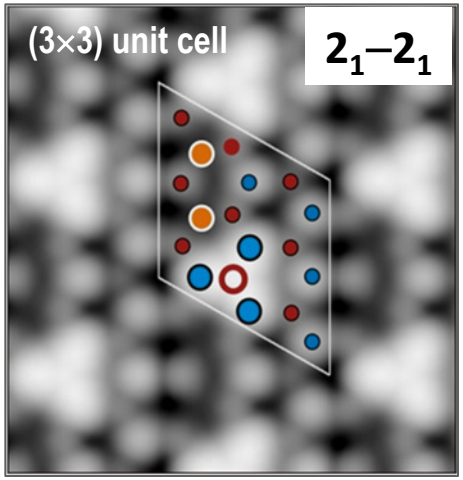


three $Ce^{4+}$

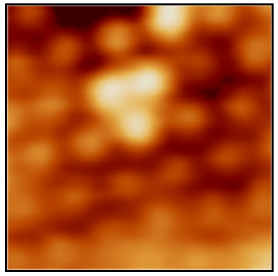

LUMO

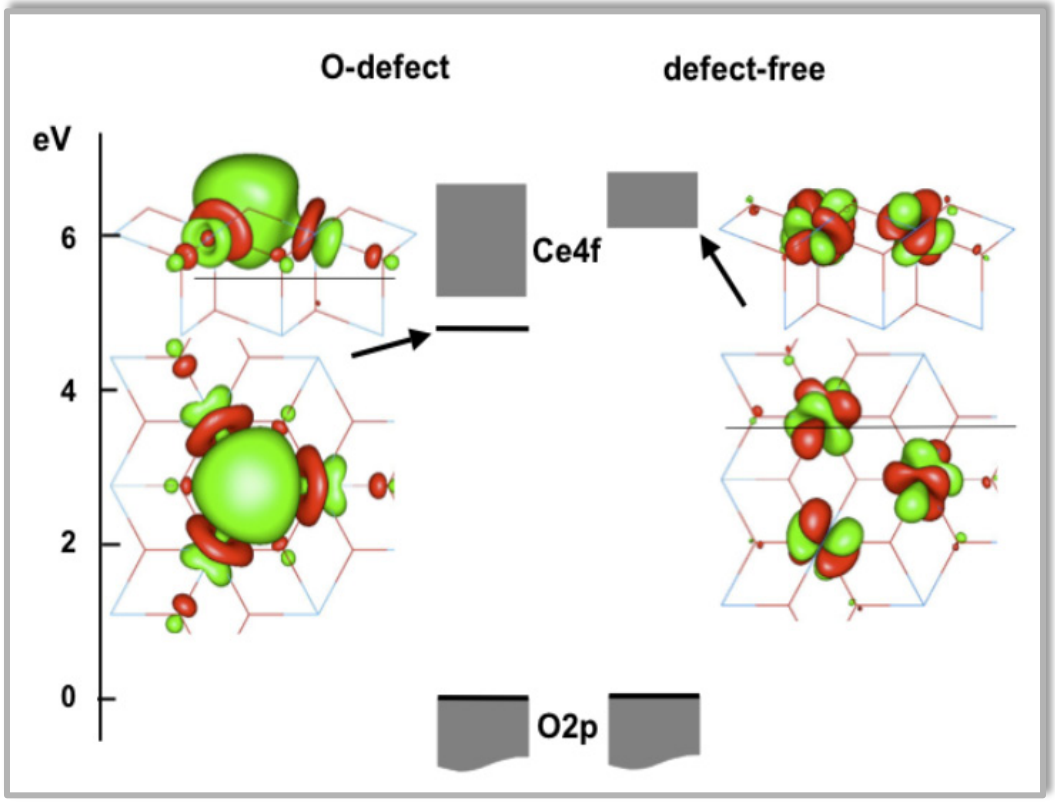


PBE0 embedded cluster

$(CeO_2)_3(O^{2-})_9[Ce^{3.8+}]_{15}[Ce^{4+}]_{15}$

$(CeO_2)_3(O^{2-})_{10}[Ce^{4+}]_{15}$

- Bright appearance due to `delocalized´ 4f orbitals with respect to regular $Ce^{4+}$

# STS-theory

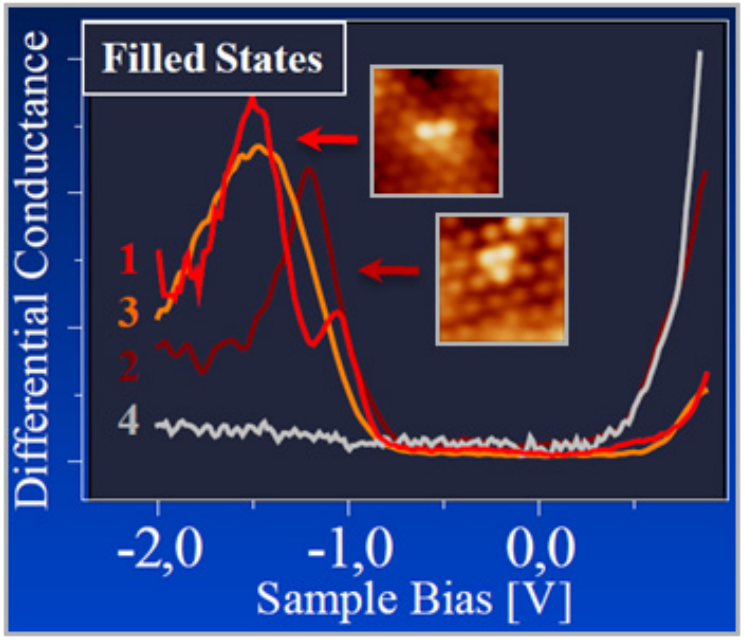


**pair** protusion:
splitting of 4f states

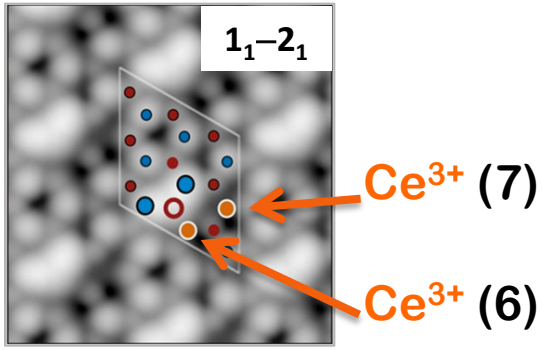


- different coordination number
  ~0.1 eV splitting

**triple** protusion:
no splitting of 4f states

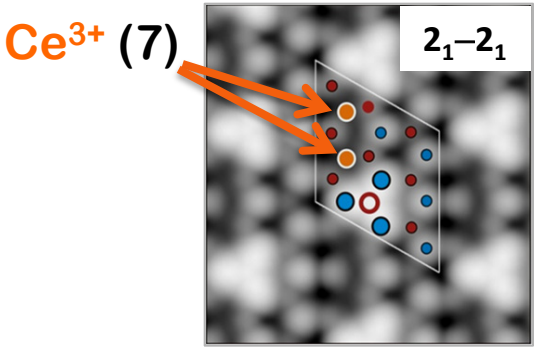


- same coordination number
  0 eV splitting

# O-vacancy structures at varying concentration

G. E. Murgida and M.V. Ganduglia-Pirovano, PRL 110, 246101 (2013)

- $\Theta$ ($1/16 \leq \Theta \leq 1$): 1/16, 1/8, 1/4, 1/2, 3/4, 1
- subsurface: $a_{ss} < b_{ss} < c_{ss} < \ldots$
- surface/subsurface: $a_{s\text{-}ss} < b_{s\text{-}ss} < c_{s\text{-}ss} < \ldots$
- surface: $a_s < b_s < c_s < \ldots$

**33 structures!!**

- $Ce^{3+}$ preference for NNN positions & outermost Ce-layer; max. $Ce^{3+}$–$Ce^{3+}$ distance

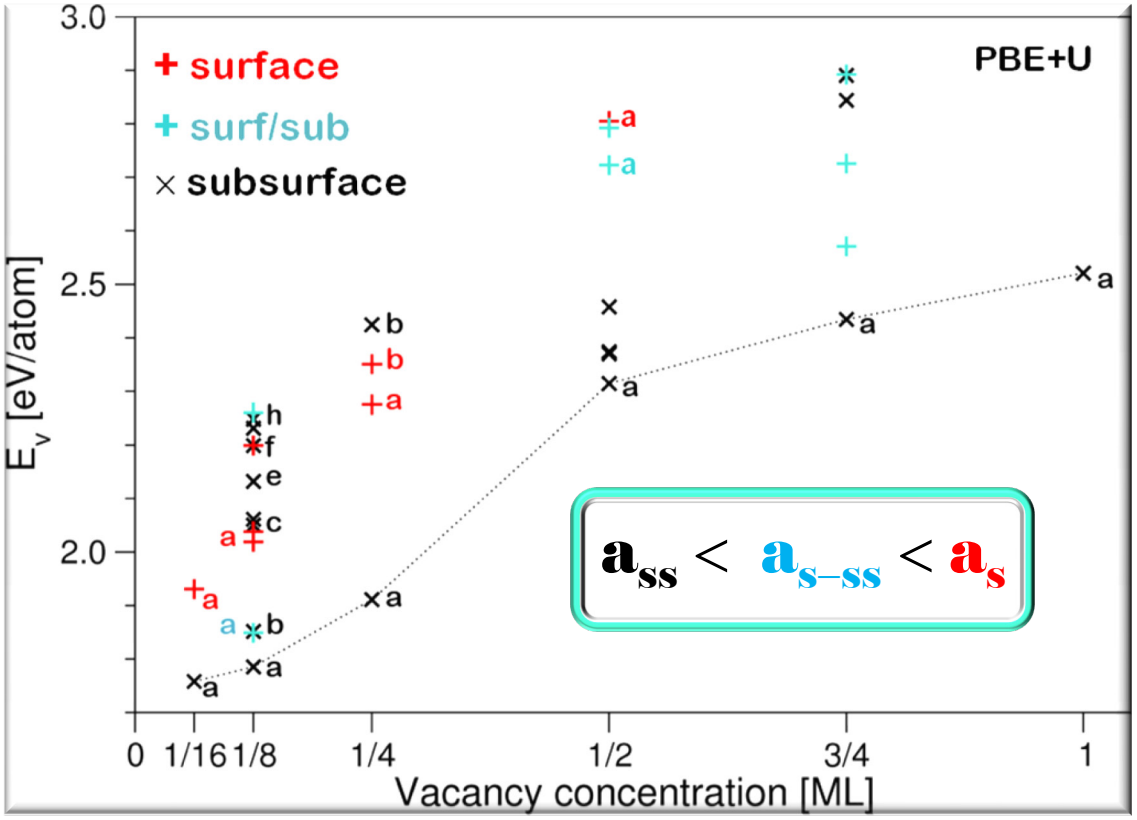


**Most stable structures subsurface vacancies only !**

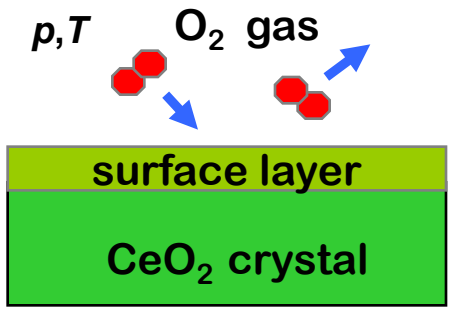

# Stability of reduced $CeO_2(111)$

$$CeO_2^{clean} \rightleftarrows CeO_2^{reduced} + N_{vac}\ ½\ O_2$$

$$\Delta\gamma_{surf}(T,p) = [\ G_{slab}^{reduced}(T,p,N_{def}) - G_{slab}^{clean}(T,p) + N_{vac}\ ½\ \mu_{O_2}(T,p)]\ /A$$

$$\Delta\gamma_{surf}(T,p) \approx [\ E_{slab}^{reduced}(N_{def}) - E_{slab}^{clean} + N_{def}\ ½\ \mu_{O_2}(T,p)]\ /A$$

$$\Delta\gamma_{surf}(T,p) \approx N_{def}\ [\ E_v(\Theta) + ½\ \Delta\mu_{O_2}(T,p)]\ /A$$

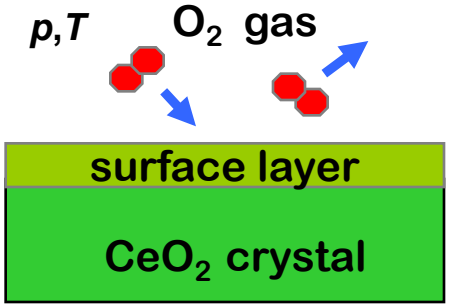


$$\tfrac{1}{2}\Delta\mu_{O_2} = \tfrac{1}{2}\mu_{O_2} - \tfrac{1}{2}E_{O_2}$$

**Oxygen chemical potential**

$$\mu_{O_2}(T,p) = \mu_{O_2}(T,p^\circ) + RT\ln(p/p^\circ)$$

# Stability of reduced $CeO_2(111)$

G. E. Murgida and M.V. Ganduglia-Pirovano, PRL 110, 246101 (2013)

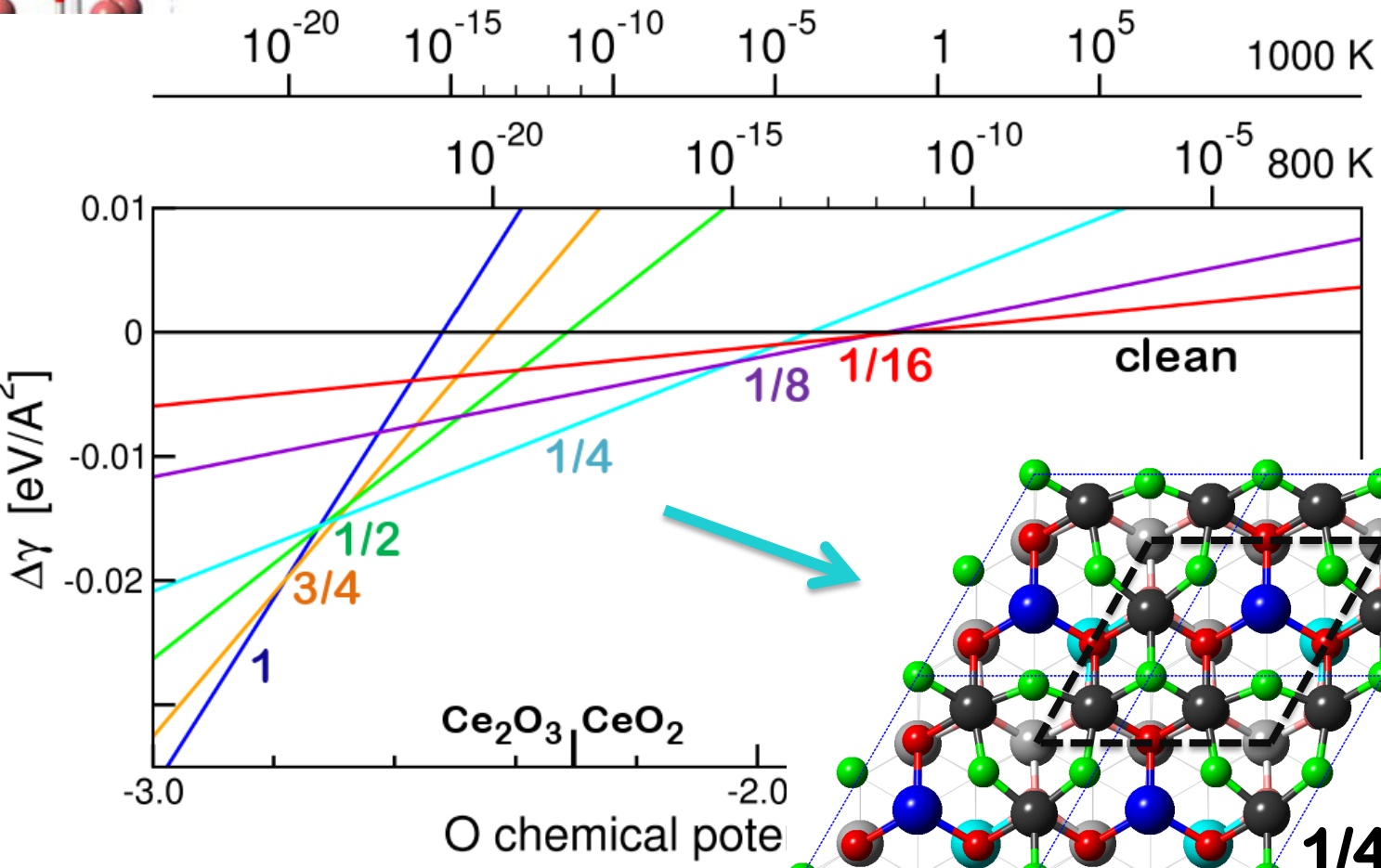




$1/4(a)_{ss}$

❑ (2×2) pattern of subsurface vacancies → third neighbors

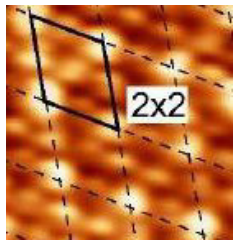


**Agreement with experiment!**

# Why subsurface vacancies do NOT agglomerate?

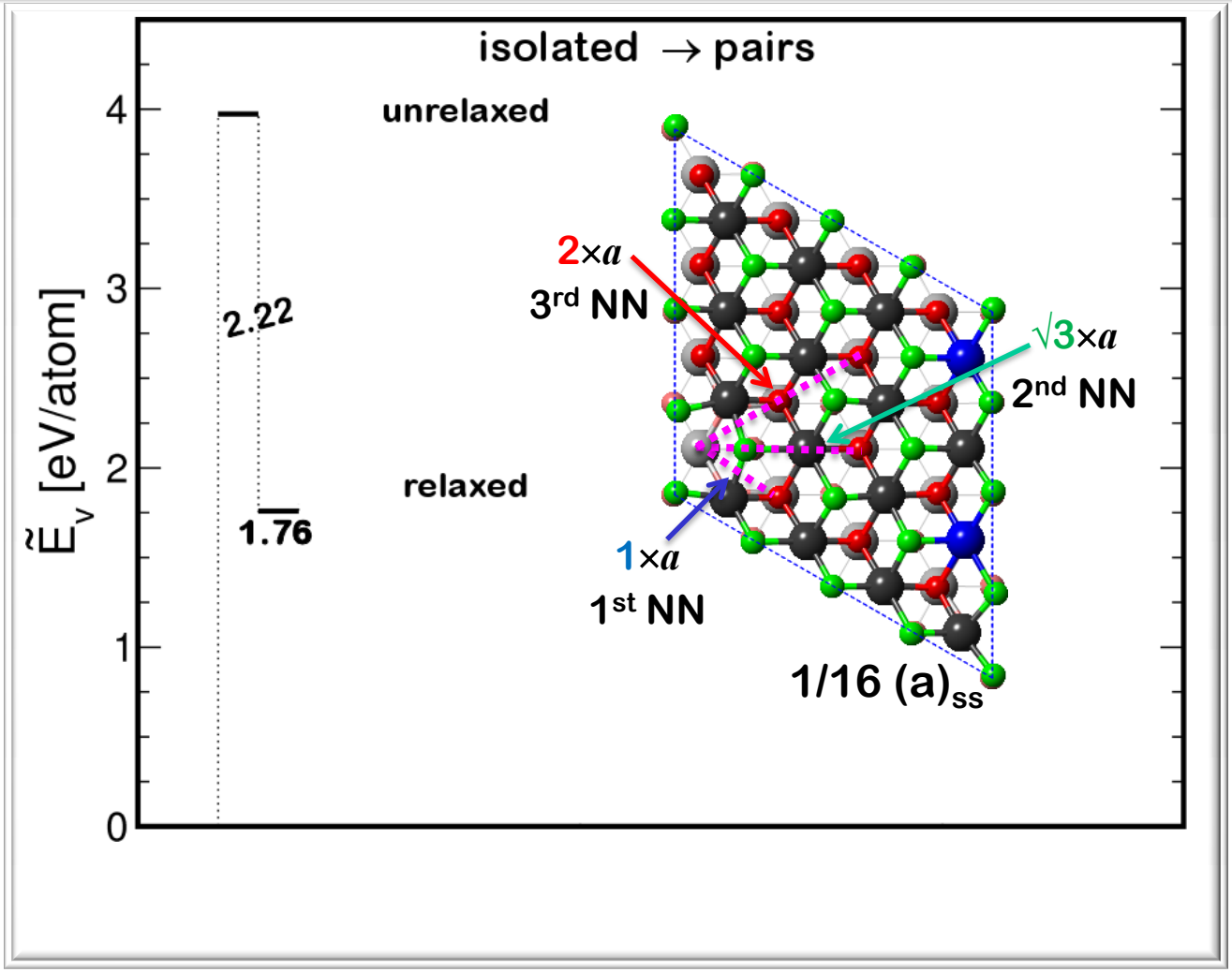

# Why subsurface vacancies do NOT agglomerate?

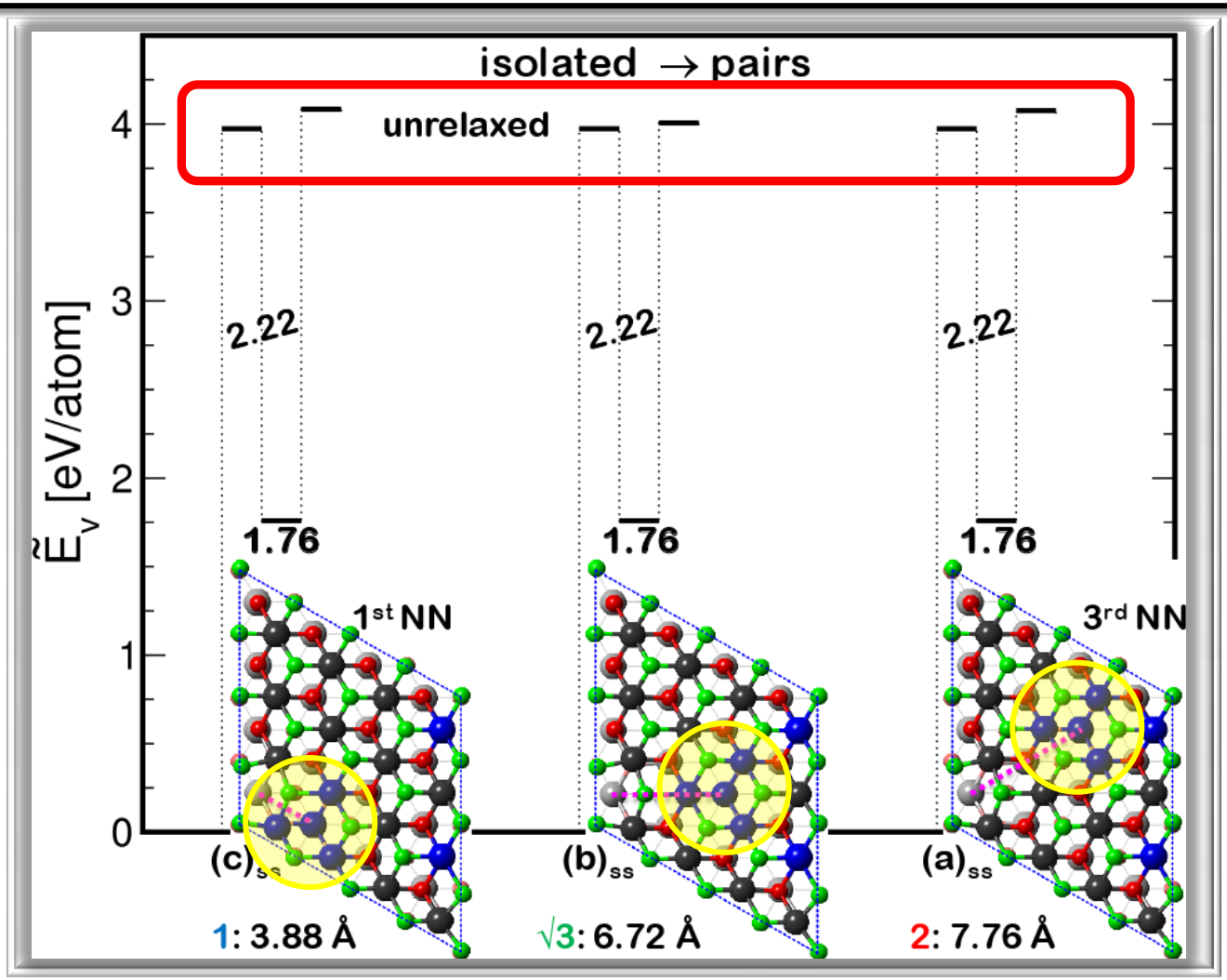


- energy for additional unrelaxed vacancy ~ constant;
  slightly larger than first vacancy (by up to ~0.1 eV)

- two additional electrons shared by the 4 Ce neighbors → $4\times Ce^{3.5+}$

# Why subsurface vacancies do NOT agglomerate?

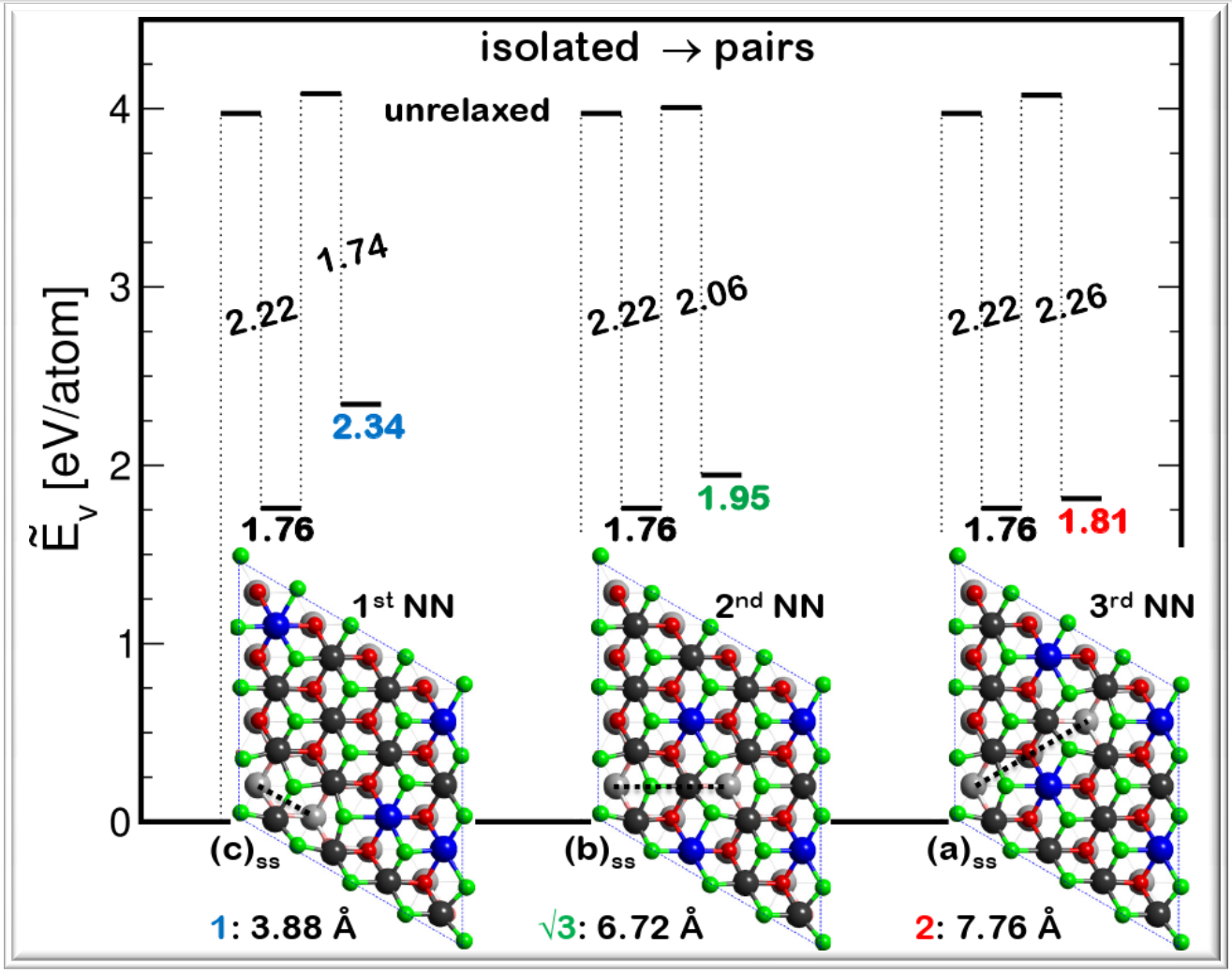


- relaxation energy gain depends on distance !!
- atomic displacements of first vacancy counteracted by second vacancy
  → net increase in the formation energy

# The repulsive interaction

$2 \times$ isolated $\rightarrow$ pair+ $CeO_2(111)$

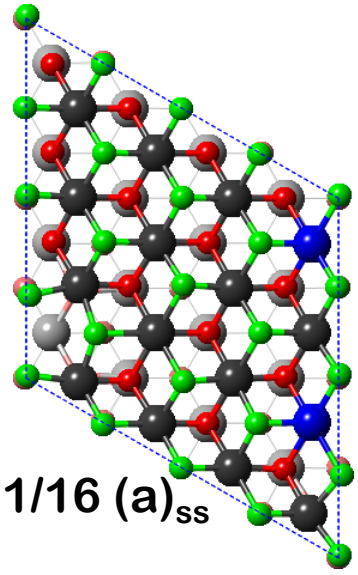


$\Delta E = +\ 0.58$ eV  1st NN

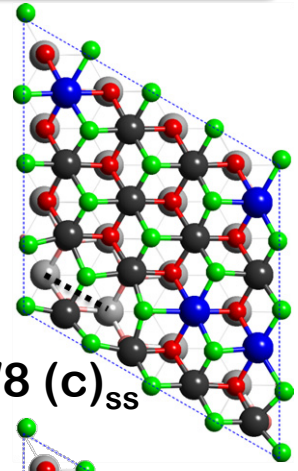


atomic displacements of first vacancy counteracted by second vacancy
$\rightarrow$ net increase in the formation energy

$\Delta E = +\ 0.19$ eV  2nd NN

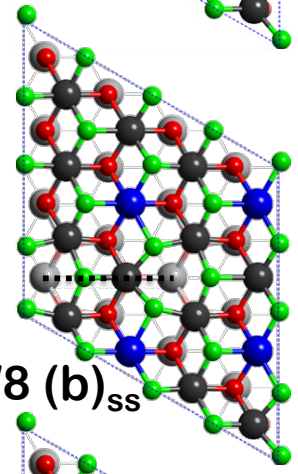


$\Delta E = +\ 0.05$ eV  3rd NN

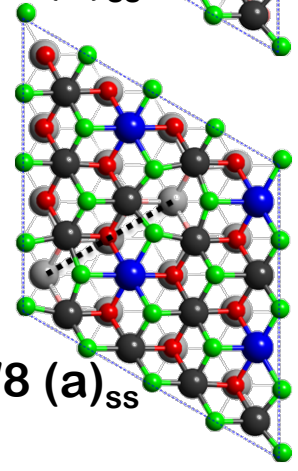


- a vacancy repels others from its immediate vicinity!!

- (2×2) structure $\rightarrow$ all 3rd NN !!

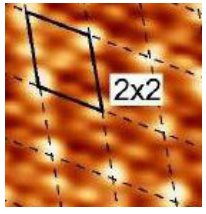


Torbrügge et al., PRL 99, 056101 (2007)

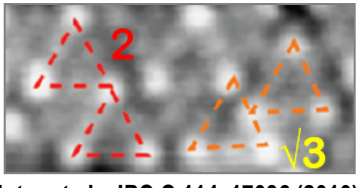


Grinter et al., JPC C 114, 17036 (2010)

# Reduced $CeO_2(111)$: Conclusions

- DFT predicts a tendency of $Ce^{3+}$ ions to be away from the defect
- STM/STS +DFT confirm the tendency of defects to bind to $Ce^{4+}$ ions
- DFT predicts a preference for subsurface O defects ($1/16 \leq \Theta \leq 1$ML)
- DFT + statistical thermodynamics predict a $(2\times2)$ subsurface vacancy structure $\rightarrow$ consistent with experiments

Explanations in terms of defect-induced lattice relaxation effects

- localization phenomenon
- proneness of defects to be bound by $Ce^{4+}$
- subsurface preference
- repulsive interactions between subsurface vacancies

We recognize the merit of DFT+U and hybrid approaches in predicting the subsurface preference and the NNN localization

# What have we learned and remaining challenges

ELSEVIER

Available online at www.sciencedirect.com
ScienceDirect

Surface Science Reports 62 (2007) 219–270

surface science reports

www.elsevier.com/locate/surfrep

## Oxygen vacancies in transition metal and rare earth oxides: Current state of understanding and remaining challenges

M. Verónica Ganduglia-Pirovano*, Alexander Hofmann, Joachim Sauer

*Humboldt-Universität zu Berlin, Institut für Chemie, Unter den Linden 6, D-10099 Berlin, Germany*

Accepted 26 March 2007

**Abstract**

Defects at transition metal (TM) and rare earth (RE) oxide surfaces, neutral oxygen vacancies in particular, play a major role in a variety of technological applications. This is the motivation of numerous studies of partially reduced oxide surfaces. We review, discuss, and compare theoretical data for structural and electronic properties and energetic quantities related to the formation of oxygen defects at TM and RE oxide surfaces using $TiO_2$, $ZrO_2$, $V_2O_5$, and $CeO_2$ as examples. Bulk defects, as far as relevant for comparison with the properties of reduced surfaces, are briefly reviewed. Special attention is given to the fate of the electrons left in the system upon vacancy formation and the ability of state-of-the-art quantum-mechanical methods to provide reliable energies and an accurate description of the electronic structure of the partially reduced oxide systems.

# What have we learned and remaining challenges

» Physics » Condensed Matter Physics

Springer Series in Surface Sciences

© 2015


## Defects at Oxide Surfaces

Editors: **Jupille**, Jacques, **Thornton**, Geoff (Eds.)

### Chapter 5
### Oxygen Defects at Reducible Oxide Surfaces: The Example of Ceria and Vanadia

**María Verónica Ganduglia-Pirovano**

**Abstract** Cerium and vanadium oxide-based systems play a major role in a variety of technological applications, with the reducibility of the systems being crucial to their functionality in the applications. The in-depth understanding and control of the type, density, and distribution of oxygen vacancies provide a means to influence the electronic structure and to tailor the systems' functionality. Hence, a great deal of experimental and theoretical work has been devoted to the study of partially reduced ceria and vanadia, both surfaces and bulk. Here, theoretical data for structural and electronic properties and energetic quantities related to the formation and interaction of neutral oxygen vacancies at the $CeO_2(111)$ and $V_2O_5(001)$ surfaces are reviewed, discussed and compared. Experimental findings on oxygen defects in ceria and vanadia are briefly reported. Special attention is given to the fate of the electrons left in the system upon vacancy formation, the vacancy-induced lattice relaxation, whether vacancies agglomerate or repel each other, and the ability of state-of-the-art quantum-mechanical methods to provide an accurate decription of the geometric and electronic structures of the partially reduced oxide systems as well as reliable oxygen defect formation energies.